FCTUC DEPARTAMENTO DE ENGENHARIA CIVIL
FACULDADE DE CIÊNCIAS E TECNOLOGIA
UNIVERSIDADE DE COIMBRA

Seismic response of steel MR-frames with friction joints

In Partial fulfilment to the requirements for the degree of Master Civil Engineering

Author
Ana Francisca Henriques Parente dos Santos

Coordinator
Prof. Luís Alberto Proença Simões da Silva (FCTUC)
Prof. Jean-Pierre Jaspart (ULG)

Coimbra, July, 2015

ACKNOWLEDGMENTS

This page is dedicated to those that, in some way, had contributed to make possible the realisation of this master dissertation.

I would like to thank to my coordinator professor Luís Simões da Silva, for giving me the opportunity to work in this project, which is integrated in the European FREEDAM project and for his support and guidance during all my dissertation work.

In addition, I am grateful to my coordinator in University of Liège, Professor Jean-Pierre Jaspart and to Professor Jean-Francois Demonceau for always be available to listen my doubts and for help me to feel welcome in a foreign University.

My special thanks to Elide Nastri of Salerno University, for all her patient, motivation and help during all the semester. Without her, concluding my master dissertation would have been much more difficult. Also, to the PhD student Antonella of Salerno University to always be available to help me when I knock at her office door, during her stay in University of Liège.

To Professor Gianvittorio Rizzano for being available to listen to my doubts and concern in his quick stay in Liège.

To my closest friends, sister and boyfriend, whose support helped me to overcome setbacks and stay focused. I am very grateful for having them always by my side.

Most importantly, none of this would have been possible without the unconditional support and love of my parents. They taught me to always fight and never give up of my objectives, even when it seems almost impossible to accomplish. This work is dedicated to them.

RESUMO

Todos os anos existem relatos de eventos sísmicos que são responsáveis pela destruição de grande parte das cidades. Por esta razão nos países industrializados, encontrar soluções estruturais capazes de fazer frente a estes terramotos sem causar danos estruturais aos edifícios, tem vindo a ser investigado pela comunidade científica.

Ao longo dos últimos anos têm vindo a ser implementadas diversas soluções que tem por base o conceito de dissipação de energia suplementar, isto é, estruturas que quando sujeitas a acções sísmicas tenham a capacidade de absorver a energia induzida pelo sismo, sem provocar danos significativos aos diferentes componentes estruturais. Uma destas soluções é a de utilização de amortecedores de fricção em edifícios, por apresentarem uma eficácia-custo elevada, para além de que são fácil instalação e manutenção.

Nesta dissertação apresenta-se uma nova tipologia de ligações viga-pilar inseridas em pórticos simples em aço estrutural, com o objectivo principal de se conseguir estruturas que, quando solicitadas por acções sísmicas de alta intensidade, não registem danos nos principais componentes estruturais. Esta nova tipologia de ligação consiste na introdução de amortecedores de fricção, de modo a dissiparem a energia induzida pela acção sísmica. O tipo de ligações referido tem vindo a ser estudado pela Universidade de Salerno e foi recentemente proposta pelo projecto Europeu FREEDAM (*Free from damage connections*), projecto no qual se insere este trabalho de dissertação.

Assim sendo, o objectivo principal desta dissertação é o estudo do comportamento de pórticos simples com esta nova tipologia de ligações, quando solicitadas por acções sísmicas de alta intensidade. O estudo será feito através de modelação numérica a partir do software de elementos finitos *SeimoStruct* tendo em conta uma análise estática não linear Pushover e uma análise dinâmica não linear, seguindo a metodologia de análise estipulada no EC8.

Com a adopção deste novo tipo de ligações, espera-se uma melhoria no comportamento da estrutura quando solicitada a acções sísmicas quando comparada com o comportamento dos pórticos simples com ligações convencionais devido à capacidade de dissipação de energia dos amortecedores de fricção.

Palavras-chave: Análise sísmica; estruturas sem danos; ligações com amortecedores de fricção

ABSTRACT

It is well known that, every year, earthquakes are responsible for the destruction of almost entire cities. For this reason, especially in countries with medium to high seismicity, has been a main concern among the scientific community find structural solutions able to withstand destructive seismic events without damage to the main structural members.

Over the past few years, several solutions with the so-called strategy of supplementary energy dissipation or passive control, where the input energy of the earthquake is dissipated by means of viscous damping or hysteretic damping by the introduction of energy absorbers, have been studied and used on buildings located in high seismicity regions. Among the different strategies within in the framework of passive control systems, are the friction dampers devices. These devices are widely used because they present high potential at a low cost and are easy to install and maintain.

In this dissertation an innovative typology of beam-to-column connections for steel moment resisting frames are proposed aiming the goal of free from damages structures under destructive seismic actions. The innovative typology is constituted by the use of friction dampers within beam-to-column connections, so that dissipative zones are constituted by friction devices at beam ends. This kind of connection has already been studied by the University of Salerno and has been proposed by the European Project FREEDAM ("Free from damage connections"), in which this dissertation is inserted.

In this view, in this dissertation work has been studied the behaviour of steel MR-frames with that new connection typology when under destructive seismic events. Numerical analysis on this innovative type of frames has been carried out with the finite elements software *SeismoStruct*, considering a seismic nonlinear static analysis (pushover analysis) and a nonlinear dynamic analysis, according to Eurocode 8-1.

It is expected a substantial improvement of the structure behaviour when comparing with steel moment resisting frames with conventional joints. The reason for this substantial behaviour improvement deals with the fact that the friction damper material dissipate all the earthquake input energy, without any damage for the steel components.

Key words: Seismic analysis; free from damages structures; friction joints

RESUMÉ

Tous les ans, les séismes provoquent la destruction d'une grande partie des villes. C'est pour cette raison que la communauté scientifique des pays industrialisés étudie des solutions structurelles qui permettent de faire face à ces tremblements de terre sans que ceux-ci ne provoquent de dommages au niveau des structures des bâtiments.
Au cours de ces dernières années, diverses solutions ont déjà été mises en place, lesquelles exploitent le principe de la dissipation d'énergie supplémentaire. Ce principe permet aux structures soumises à une activité sismique d'absorber l'énergie induite par le séisme et ce, sans que les différents éléments structuraux ne subissent de dommages significatifs. L'une de ces solutions passe notamment par l'utilisation d'amortisseurs à friction dans les bâtiments, compte tenu qu'ils présentent un rapport coût-efficacité favorable et qu'ils sont faciles à installer et à entretenir.

Cette dissertation présente un nouveau type d'assemblage poteau-poutre, encastré dans des portiques simples en acier de construction, dont le principal objectif est d'obtenir des structures qui ne subissent pas de dommages au niveau de leurs principaux éléments structuraux, quand celles-ci sont soumises à une activité sismique de grande intensité. Ce nouveau type d'assemblage consiste à utiliser des amortisseurs à friction, qui servent à dissiper l'énergie induite par l'activité sismique. Ce type d'assemblage a fait l'objet d'études de la part de l'Université de Salerno et, récemment, d'une proposition faite dans le cadre du projet européen FREEDAM (*Free from damage connections*), dont fait d'ailleurs partie ce travail de dissertation.

Cette dissertation vise donc essentiellement à étudier le comportement des portiques simples équipés de ce nouveau type d'assemblage, quand ceux-ci sont soumis à une activité sismique de grande intensité. L'étude se réalisera à travers la modélisation numérique faite à l'aide du logiciel d'éléments finis *SeimoStruct,* en tenant compte d'une analyse statique non linéaire Pushover et d'une analyse dynamique non linéaire, selon la méthodologie d'analyse stipulée dans l'EC8.

L'adoption de ce nouveau type d'assemblage devrait permettre d'améliorer le comportement des structures, quand celles-ci sont soumises à une activité sismique, par rapport au comportement des portiques simples à assemblages conventionnels et ce, du fait de la capacité de dissipation d'énergie des amortisseurs à friction.

Mots-clés : analyse sismique ; structures sans dommages ; assemblages avec amortisseurs à friction

TABLE OF CONTENTS

ABBREVIATIONS

CBF – Concentrically Braced Frames;

DST – Double Split Tee Connections;

DCH – High Ductility Class;

EC1-1 – Eurocode 1 part 1;

EC8-1 – Eurocode 8 part 1;

EBF – Eccentrically Braced Frames;

IDA – Incremental dynamic analyses;

MRF – Moment Resisting Frame;

ANNOTATIONS

A_{Ed} – design value of seismic action;

$F_{c,Cd}$ – Design Preload of the bolts;

F_k – Seismic Force applied at k-th storey;

G_k – Characteristic value of a permanent action;

$M_{bj,k}$ - Beam plastic Moment

$M_{N,Rd}$ – Design plastic moment reduced due to the axial force $N_{Ed;}$

N_{Ed} - Axial force;

P_{NCR} – Reference probability of exceedance;

PGA – peak ground acceleration;

Q_k – Characteristic value of a variable action;

S_a (T) – spectral acceleration;

S_e (T) – Elastic horizontal acceleration response spectrum;

S – Soil coefficient;

T_{NR} – reference return period of the reference seismic action for the no-collapse requirement;

T - Vibration period of a linear single degree of freedom system;

T_B – Corner period at the lower limit of the constant acceleration region of the elastic spectrum;

T_C - Corner period at the upper 1inlit of the constant acceleration region of the elastic spectrum;

T_D – value that defines the beginning of the spectrum line of constant displacement;

V_k – Total vertical load acting at k-th storey;

W_e – External work;

W_i – Internal work;

a_{gr} – peak ground acceleration on type A ground;

a_g - Design ground acceleration on type A ground;

b – Beam;

c – Column;

i – Column index;

i_m – Mechanism index;

k – Storey index;

h_{ns} - Value of h_k at the top storey;

h_k – k-th storey height with respect to the foundation level;

n – Number of friction surfaces;

n_b – Number of beams per storey;

n_c – Number of columns per storey;

n_s – Number of storeys;

q – Behaviour factor;

q_0 –Basic value of behaviour factor;

α – Horizontal forces multiplier;

$\alpha_0^{(g)}$ – Kinematic admissible multiplier of the horizontal forces for global mechanism;

$\alpha_{im}^{(t)}$ - Kinematic admissible multiplier of the horizontal forces for the -*im* mechanism;

η - Damping correction factor;

β – Lower bound factor for the horizontal design spectrum;

γ_I – Importance factor;

$\Psi_{2,i}$ – combination coefficient for the quasi-pern1anent value of a variable action i;

$\Psi_{E,i}$ - combination coefficient for a variable action *i,* to be used when determining the effects of the design seismic action;

μ- Slip factor;

δ_u – Top sway lateral displacement;

θ – Rotation;

$\gamma^{(g)}$ – Slope of the equilibrium curve for the global mechanism

$\gamma_{im}^{(t)}$ – Slope of the equilibrium curve for the –*im* mechanism

1. INTRODUCTION

1.1. General considerations

Throughout world history, there are many evidences of the destructive effects that seismic actions have on buildings. One great example was the 1775 Lisbon earthquake, known as the *Great Lisbon earthquake*, which it is estimated that reached a magnitude between 8.5 and 9.0, and was responsible for the destruction of most of the city and adjoining areas. Another example of the destructive effects of the earthquake was the 1995 Kobe earthquake in Japan, well known as the *Great Hashin Earthquake*, that reached a magnitude of 7.0 in the Richter scale, see (Figure 1.1).

Figure 1.1- Example of the destructive effects of seismic events on building (Great Hashin Earthquake - Kobe, Japan, 1995

Due to the destructive impacts of seismic events, finding new structural strategies to prevent structural damage in the buildings is gaining more relevance on the industrialized countries. In this view, in countries with medium to high level of seismicity, as Portugal and others European countries, it has been a main concern to find structural solutions able to withstand destructive seismic events without damage to the main structural elements. Within this scope, the European project FREEDAM has been proposed.

According to modern seismic codes (CEN 2010b), in case of frequent earthquakes structures in seismic zones have to be designed in order to remain safe and without suffering structural

damages. However, with regard to destructive earthquake a certain amount of damage is accepted. With reference to steel moment-resisting frames (MRFs), they can be designed in order to concentrate the input energy at the beam-ends or at the connections. The first approach is the most applicable around the world, where the behaviour of the structure depends on the energy dissipation capacity of the steel members that have to be able to develop stable hysteresis loops. This approach, however, can lead to damage to structural members. The second approach is a more recent approach that is gaining more acceptance, whereby the energy dissipation capacity of the frame depends on the ability of the connection (in this case a partial strength connection) to withstand excursions in plastic range without losing their capacity to withstand vertical loads.

In this dissertation work, a new partial strength typology of connection has been proposed and the influence of this connection on the behaviour of a steel MRF under destructive seismic events has been tested. In this approach, the dissipative zones are constituted for connections equipped with friction dampers. When a rare or very rare earthquake occurs, i.e a destructive earthquake, leads to the activation of the friction dampers, which are designed to ensure the dissipation of the seismic input energy without any damage to both the structure and the other components of the connections. Therefore, only the friction damper component needs to be substitute after the earthquake. Furthermore, the friction damper as to ensure the transmission of the beam bending moment required to fulfil the serviceability requirements and to withstand without slippage under gravity loads.

1.2. Objectives to be accomplished

The aim of this dissertation is to study the behaviour of steel MR frames equipped with friction joints on beam-column connections with the purpose of finding a solution in which the structure is able to withstand seismic events without structural damage.

Thus, the objectives of this dissertation are:

- To develop a numerical model able to simulate the behaviour of MR frames with friction pads in the connections, using the element finite software *SeismoStruct*;
- To calibrate the friction pads;
- To analyse the performance of a MR frame with friction joints on the connections under seismic events by means of a nonlinear static pushover analysis and on a nonlinear incremental dynamic analysis;

1.3. Dissertation structure

The dissertation is structured as follows:

The **Chapter 1** presents a summary of the scope of the project as well as the importance of the subject. In addition contains the objectives to be accomplished by this work and its structure.

The **Chapter 2** contains a literature review about the different strategies regarding the seismic resistance of steel structures.

The **Chapter 3** contains a description of the experimental researches that have been done on beam-to-column connections with friction dampers by the University of Salerno and a description of an experimental research regarding the influence of connections with friction dampers on steel MRF.

The **Chapter 4** contains a description of all the decisions that have been made for the structural modelling of the analysed frame, concerning the design loads, preliminary design of the elements, elements and material modelling and modelling and calibration of the connections.

The **Chapter 5** presents the parametric studies regarding static nonlinear pushover analysis and dynamic incremental nonlinear analyses of the MRF.

The **Chapter 6** provides conclusions and future work recommendations resulted from this research work.

2. An overview on the strategies for seismic resistance of steel structures

The different strategies for the design of seismic resistant structures can be made in view of energy balance. Among the different strategies for the seismic resistance, we can divide them into two main groups:

- Traditional strategies;
- Innovative strategies.

2.1. Traditional strategies

In the traditional strategy, the dissipative zones are located at the structural members. For this reason, concerning severe seismic events, most of the earthquake input energy is dissipated by hysteresis, leading to severe plastic excursions and damage of the dissipative structural members. Furthermore, the structural damage has to be compatible with the ductility and the energy dissipation capacity of the structure because collapse has to be prevented even though, structural damage is accepted.

Generically, ductility is the ability of a member to exhibit significant deformations excursions, without significant loss of strength. At global scale, it is quite clear that the level of ductility is greatly influenced by the local capacity of the materials and members of the constituting system. Modern seismic codes take into to account the possible collapse mechanisms and the ductility desired for the structures, using the behaviour factor q. This factor represents the ratio between the seismic forces that a single degree of freedom system equivalent to the real structure would experience if its response would be completely elastic (with 5% of equivalent viscous damping) and the seismic forces that may be used in the design (EC8). In accordance with the behaviour factor, seismic resistant steel buildings may belong to one of the following design concepts:

- Low-dissipative structural behaviour;
- Dissipative structural behaviour.

In structures with *low-dissipate structural behaviour*, the non-linear behaviour of the structure can be neglected and the action effects may be calculated based on an elastic analysis. In these cases, the behaviour factor is equal to 1.0.

In contrast, in structures with *dissipative structural behaviour* it is expected to have significant plastic engagement in dissipative elements. For this reason, Eurocode 8 provides specific design

rules, both at global and local scale, in order to guarantee sufficient ductility of these elements. In some cases, some of the rules are common to all the structural typologies and others are specific for each type of structural typology. One of the common requirements is the fact that the behaviour factor in these cases is always larger than 2 and its value depends on the type of seismic resistant structural scheme. In addition, depending on the behaviour factor, different cross-sectional classes for the dissipative members are required.

Among the dissipative structural schemes, there are three main structural schemes, as follows:

- Moment resisting frames (MRF);
- Concentrically braced frames (CBF);
- Eccentrically braced frames (EBF).

Moment resisting frames (MRF) (Figure 2.1) in order to achieve a ductile global collapse are designed to form plastic hinges at the beams ends rather than in the columns, with the exception to the columns bases and the top level of multi-storey buildings. In fact, the ductility of a MRF is influenced by the number of plastic hinges that the dissipative zones are able to form so, with the aim to promote the plastic engagement of the greatest number of dissipative zones, the seismic codes, requires the application of a hierarchy criteria, the so-called "weak beam/strong column", to promote, as was said before, the yielding of the beams ends rather than the columns. This requirement bring some advantages, as the development of stable hysteresis loops of the dissipative zones and the prevention of soft-storey mechanisms. However, also leads to some disadvantages as the fact that structural damage is needed to dissipate the earthquake input energy and the fact that the use of the code requirement strength on full-strength joints is not cost-effective.

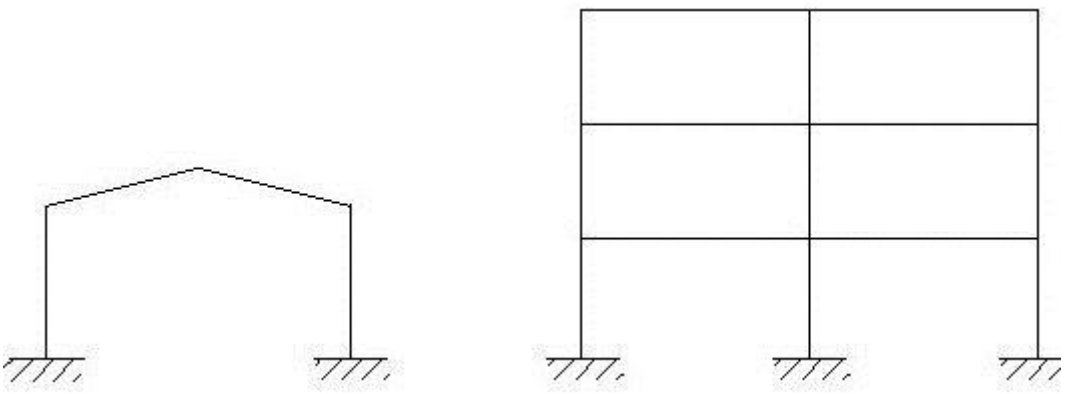

Figure 2.1- Moment resisting frames (MRF)

Concentrically braced frames (CBF) (Figure 2.2) are characterized by a truss behaviour due to axial forces developed in the bracing members. The diagonal bracings in tension constitute the dissipative zones and therefore, they have to yield in order to prevent the damage of the connected members. Thus, the response of these structures are essentially influenced by the behaviour of the bracing elements. However, the role of bracing members differs with the CBF configurations. In fact, for the X and diagonal CBFs the energy dissipation capacity of braces are assigned to tension braces only. On the contrary, in frames with V and inverted V bracings both the tension and compression diagonals participate on the dissipation of the energy.

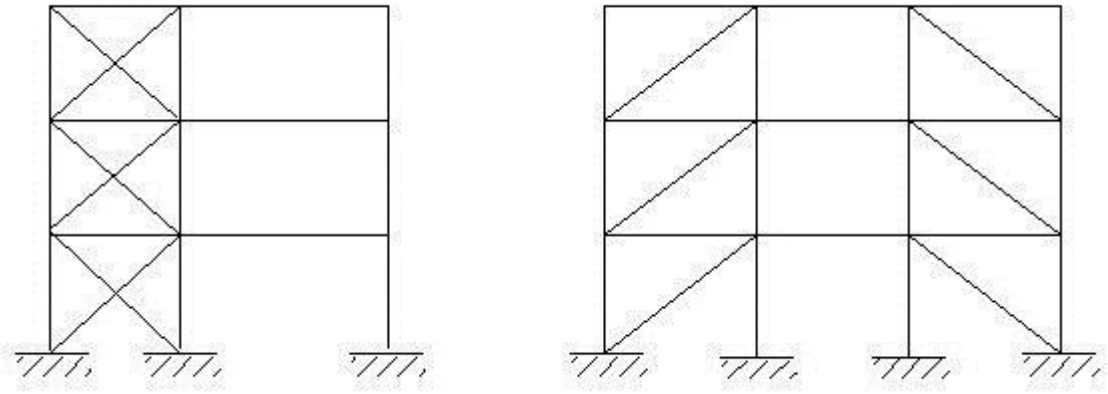

Figure 2.2- Concentrically braced frames (CBF)

Eccentrically Braced frames (EBF) (Figure 2.3) are a viable alternative to the previous structural typology. The rigidity of the system is greatly influenced by the presence of the diagonals, which are placed eccentrically with respect to the elements that make up the frame earthquake-resistant. In addition, at least one end of each brace is connected in order to isolate a segment of beam called "link", which transmits forces by shear and bending.

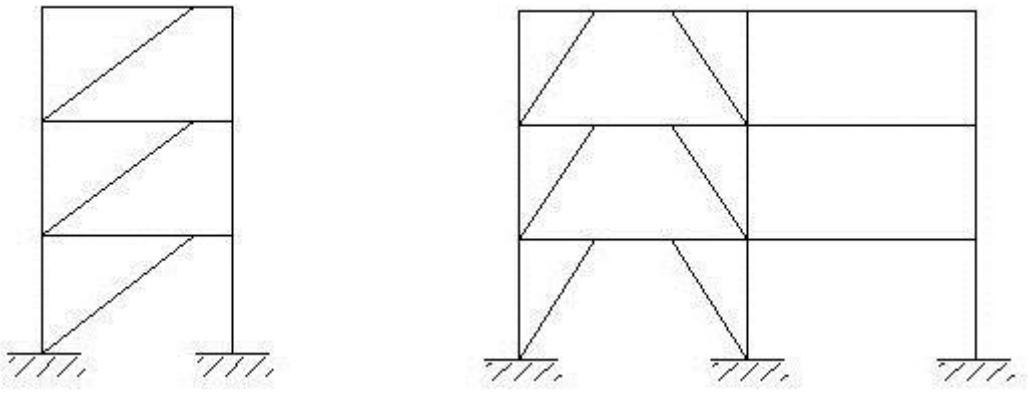

Figure 2.3- Eccentrically braced frames (EBF)

2.2. Innovative strategies

Although the traditional strategies mentioned above have a good performance under seismic events, the fact that under destructive seismic events structural damage is accepted constitutes a great disadvantage to those strategies. Thus, in the recent years, a great number of investigations with the purpose of minimizing the structural damage of steel structures under destructive seismic events have been performed. Among these investigations are the implementation of control systems in steel frames, which can be divided into three main groups(Gowda & Kiran 2013):

- Active systems;
- Semi-active systems;
- Hybrid systems;
- Passive systems.

2.2.1. Active Systems

Active Systems are composed by electronic devices such as computers, actuators and starters. The operation mechanism of this type of systems is based on providing a continuous energy from outside and it can control the acceleration, displacement or velocity of the structures. In fact, these systems changes its rigidity or the quantity of motion according to the intensity of the ground motion induce by the earthquake. Examples among active control devices include active turned mass dampers, active tuned liquid column damper and active variable stiffness damper.

2.2.2. Semi-active systems

A semi-active system is a control which usually requires a small external power source, such as a battery, and it used the motion of the structure to develop control forces which magnitude is adjusted by the external power source. Similarly to passive devices, the control forces are generated as a result of the excitation and/or the response of the structure. On the hand, like the active systems, the feedback from the structure response is measure by sensors that are responsible to generate an appropriate signal for the semi-active device. Examples of these control systems are the stiffness control devices, the electrorheological dampers, the magnetorheological dampers, the friction control devices and Tuned mass dampers and tuned liquid dampers (Symans & Constantinou 1999).

2.2.3. Hybrid systems

Hybrid control systems consists in a combination of passive and active or semi-active devices. The purpose in combine the different types of control system is to beneficiate of all the benefits derived by each system. The fact that part of the control is accomplished by the passive system implies less effort by the active system so, less power resource is required. Another benefit that came from these systems is that, in case of a power failure, the passive components still can offer some protection. Examples of hybrid control devices include hybrid mass damper and hybrid base isolation.

2.2.4. Passive systems control

Passive control systems do not need any external energy source, contrarily to the active systems. Thus, the cost of these systems when compared to the others systems mentioned above is substantially lower. Therefore, that and the fact that are composed of dampers, isolators or other devices that can be easily found and applied, are the reasons why these control systems are widely applied in buildings and other constructions all over the world.

These systems develops control forces at the location of the device which magnitude depends on the motion of the structure. Through that control forces, the passive device reduces the energy induced to the structure by the earthquake by absorbing part of it. Thus, these type of systems cannot add energy to the structural system. Passive control devices are typically applied in locations where high relative displacement are expected to occur.

Among the passive devices control systems are the base isolation, tuned mass dampers (TMD), tuned liquid dampers (TLD), metallic yield dampers, viscous fluid dampers and the friction dampers. One example of the used of these control systems is the *Millennium Bridge* in London. Tuned mass dampers were installed below the bridge deck (Figure 2.4) in order to controlling the excitation at the bridge frequencies and viscous dampers were installed at specific locations for suppressing the strong lateral movements of the bridge (Figure 2.4).

Figure 2.4- Tuner mass damper and viscous dampers installed in the London Millennium Bridge (Mualla & Nielsen n.d.)

With reference to friction dampers, they have been proposed in past researches activities to be used as passive system control as a supplementary energy dissipation devices in order to reduce the damages to the main structural elements. In particular, friction dampers present a low cost with a high capacity energy dissipation and they are easily to install and maintain. Thus, several friction dampers have been experimentally tested and used around the world, being the introduction of a bracing system which is integrated with a friction damper the most used (Mualla & Belev 2002).

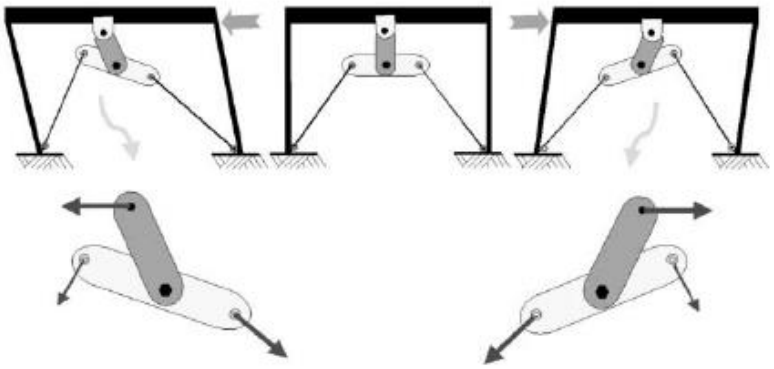

Figure 2.5- Bracing system integrated with a friction damper (Mualla & Belev 2002)

However, in the past few year, a new concept within the framework of passive control devices with friction dampers have been introduced. Instead of introducing the energy dissipaters from a bracing system, the friction dampers is integrated in the beam-to-columns connections of the frame. In this concept the connection works as a dissipative partial strength connection in which the friction dampers are the dissipative zones of the frame.

The first experimental results about this innovative concept of beam-to-column connections was made by Inoue et al. (Inoue et al. 2006b), that proposed the use of buckling Braces (BRB) connected between the beam flange and the column flange close to the member ends. The top beam flange is pin connected to the column flange, so that the bending moment is transmitted by means of BRBs axial force acting with a given lever arm (Figure 2.6-b). Similar to Inoue et al., Kishiki et al (Kishiki et al. 2006) proposed a beam-to-column connection where the top beam flange is connected to the column flange by means of a bolted T-stub with a stiffened stem, fixing the point of rotation, while the bottom beam flange is connected to the column flange with a bolted T-stub. In addition, the T-stub stem has a dog-bone shape and is restrained by an additional plate in order to prevent its buckling in compression. In fact, the bottom T-stub is designed to work as a BRB (Figure 2.6-b). Oh et al (Oh et al. 2009) have also proposed a beam-to-column connection where the top beam flange is connected to the column flange by means of a fixed bolted T-stub (Split T), while the bottom beam flange is connected to the column flange by means of a slit damper (Figure 2.6-c). The connection behaves as a partial strength joint where the slit damper is responsible to the dissipation of the seismic input energy. In a more recent research, Yeung et al. (Yeung et al. 2013) proposed a beam-to-column typology with asymmetric friction dampers as connecting elements between the beam bottom flange and the column flange, whereas the center of rotation is fixed by means of a flange plate bolted to the beam top flange and welded to the column flange(Figure 2.6-d)

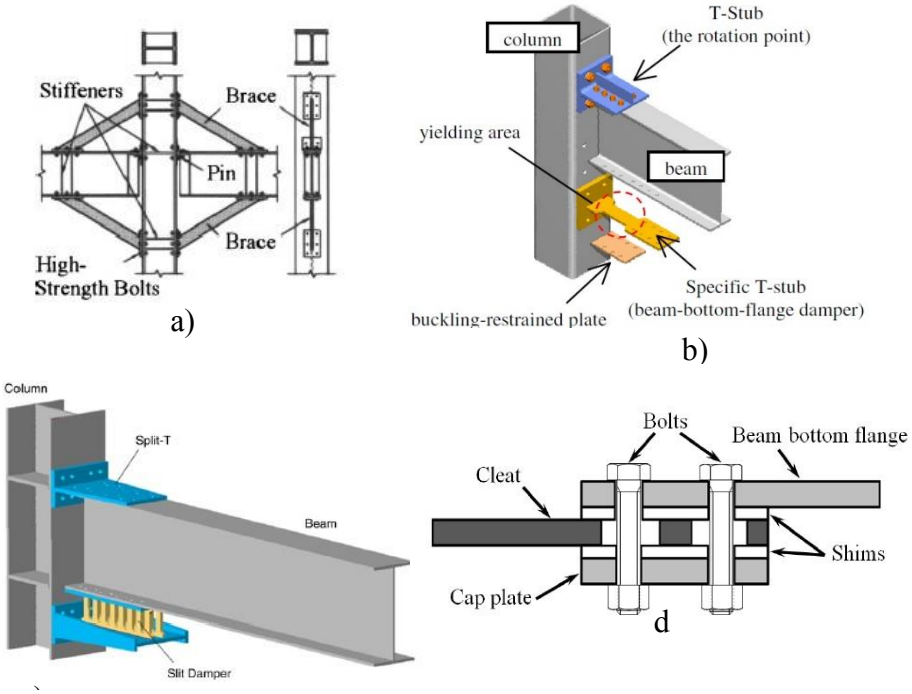

Figure 2.6- Different approach to improve the seismic performance of MRFs; a) Inoue et al (Inoue et al. 2006) connection: BRB typology; b) Kishiki et al (Kishiki et al. 2006) connection; c) Oh et al (Oh et al. 2009) connection; d) Yeung et al. (Yeung et al. 2013) connection

Another connection typologies was proposed by Latour et al. (Massimo Latour et al. 2014) (Latour et al. 2015a) . In 2014 (Figure 2.7b), the authors proposed a modification of the classical DST connections by realizing a fixed classical T-Stub at the top beam flange, preventing the concrete slab damage, and to provide a friction damper at the bottom beam flange and realizing slotted holes on the beam flange (or an additional haunch). This specimen typology is the same as the one proposed by the European project FREEDAM.

In 2015, the same authors proposed a similar connection typology but with a pair of T-stubs interposed by friction dampers, both at the top and at the bottom beam flange (Figure 2.7a).

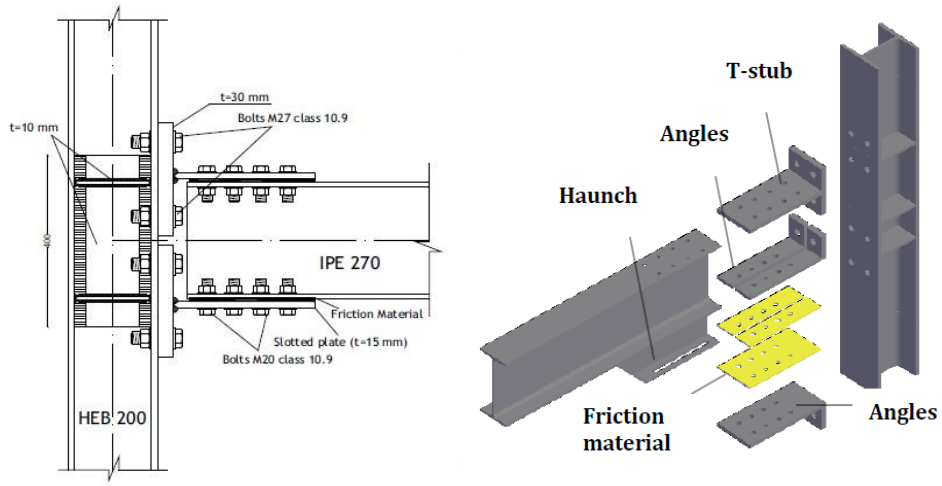

a) b)

Figure 2.7- a) Connection typology performed by Salerno University . (Latour et al. 2015a)**; b) Connection typology performed by Salerno University**(Massimo Latour et al. 2014) **and FREEDAM connection typology**

3. Experimental tests on DST connections with friction dampers and on MR-frames with frictions joints

In this chapter, the recent researches performed by the University of Salerno on DST beam-to-column connections equipped with friction dampers are described. Those researches have the following steps:

1º. **Experimental tests on the friction component**: in this stage, a several number of material that have the potentiality to be use as friction dampers have been investigated in order to obtain the friction coefficients (both static and kinematic) under different values of normal forces acting on the sliding interface, evaluate the stability of the cyclic response and the energy dissipation capacity;(M. Latour et al. 2014; Latour et al. 2015a; Massimo Latour et al. 2014)

2º. Experimental test on full-scale joints: In this part, full-scale DST beam-to-column connections equipped with the friction materials (selected from the previous step) under cyclic loads have been tested. (Latour et al. 2015a; Massimo Latour et al. 2014)

Furthermore, the influence of those connections on the response of an MRF have been investigated (Piluso et al. 2014).

3.1. Experimental tests on friction material

The main purpose of this experimental research was to obtain the friction coefficients of the different materials investigated, both static and kinematic, under different values of normal forces acting on the sliding interface and evaluate the stability of the cyclic response and the energy dissipation capacity. To achieve it, different layouts of the sub-assemblage was considered, with the variation of the following parameters:

- The interface;
- The tightening torque;
- Number of tightened bolts.

In particular, the friction characteristics of a steel-steel, a brass-steel, a Friction material (M1)-steel, a friction material (M2)-steel interfaces (Latour et al. 2015a) and a interface with a sprayed aluminium interface(Massimo Latour et al. 2014) were investigated. The different properties of these interfaces were analyse with the sub-assemblage showed in Figure 3.1a), which is constituted by a friction material placed between two steel (S275) plates. In order to allow the relative movement of the steel placed between the friction materials, one of the internal plates has been realized with slotted holes while the other inner plate and the external plates have been realized with circular holes. The clamping force has been applied by means of

16 M20 bolts 10.9 class and the holes have been drill with a 12mm drill bit. Furthermore, the analyses were carried out by varying the bolt tightening level in a range between 200Nm and 500Nm.

The tests were carried out with a testing machine Schenck Hydropuls S56 (Figure 3.1b). The cyclic tests were carried out under displacement control for different amplitudes at a frequency equal to 0.25 Hz.

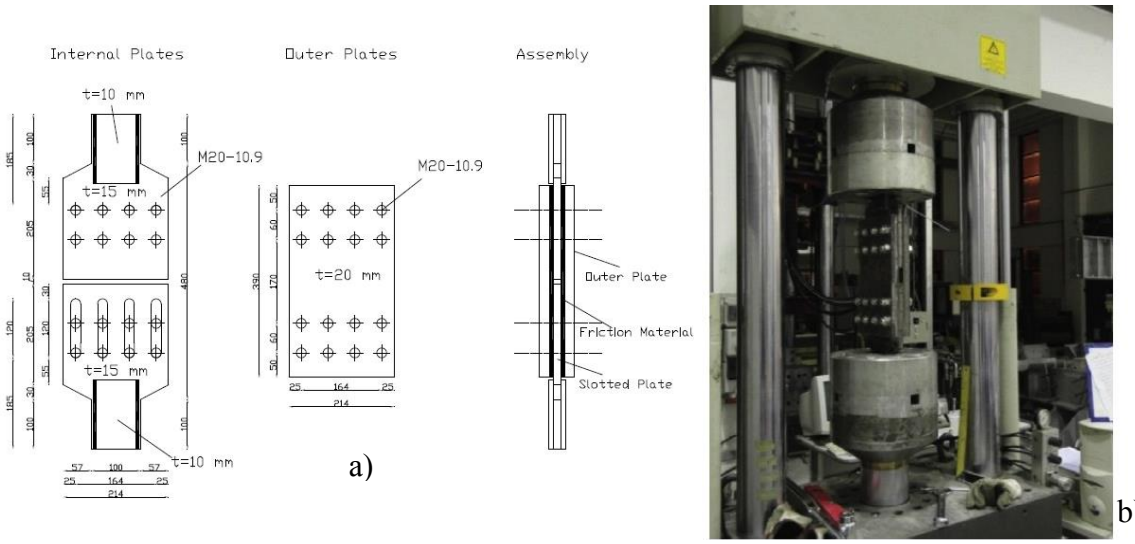

Figure 3.1-a) Scheme of the adopted sub-assemblage in the experimental research conducted by the University of Salerno (Latour, Piluso, and Rizzano 2015); b)Testing machine Schenck Hydropuls S56 (Latour, Piluso, and Rizzano 2015)

A summary of the tests carried out in the experimental program for each interface is present in the table below (Table 3-1).

Table 3-1- Summary of the tests carried out on the experimental program

Interface	Torque	Number of bolts of friction pad	Number of cycles of the sequence	Amplitude
Steel–steel	200 N m	4	10	±30 mm
	300 N m		10	
	500 N m		10	
Brass–steel	200 N m	8	30	±15 mm
	300 N m		20	
Sprayed aluminum–steel	200 N m	4	10	± 15 mm
	300 N m		10	
	400 N m		10	
M0–steel	300 N m	8	10	±7.5–±15 mm
	400 N m		10	
	400 N m		10–10	
	500 N m		10–10	
M1–steel	200 N m	8	10	±10 mm
	300 N m		10	
	400 N m		10	
	550 N m		10	
M2–steel	200 N m	8	10	±15 mm
	300 N m		10	
	400 N m		10	

All the results reported in the following sections are expressed by means of friction coefficient, which can be determinate by the following equation:

$$\mu = \frac{F}{mnN_b} \tag{3.1}$$

Where m is the number of surfaces in contact, n is the number of bolts, F is the sliding force and N_b is the bolt preloading force, which is defined starting from the knowledge of the tightening torque by the following expression:

$$N_b = \frac{T_b}{0{,}2d} \tag{3.2}$$

Where T_b is the value of the tightening torque and d is the bolt nominal diameter.

Metallic interfaces

As was said before, three metallic interfaces were investigated in this research, a steel-steel interface, a Brass-steel interface and a sprayed aluminium-steel interface. The specimens have been pre-loaded in each test with different tightening torque levels, in accordance with Table 3-1, with the aim of obtaining forces in a range compatible with structural applications.

Concerning the steel-steel interface (made of S275JR structural steel) the Figure 3.2 presents the results of the variation of the friction coefficient during the cycles. As it can be seen, the cyclic behaviour of the steel-steel interface is quite instable. In particular, during the first loading sequence (1st to 10th cycle) the friction coefficient is always increasing until reaching

the value of 0.344. Actually, this behaviour can be due two effect: ploughing and steel strain hardening. The first is when, due to the wearing of the steel in the zone under the bolts heads, the number of asperities increases and the surface become rougher and so, it leads to an increasing of the friction coefficient. The second effect is related to the strain hardening of the steel, which can influence the friction coefficient by varying the shear strength and the steel hardness. Contrarily, in the second and third loading sequence, the friction initially assumes a value between 0.35-0.4 and after that, it quickly decreases up to a value approximately equal to 0.20. In fact, the results of the 2nd and 3rd cycles point out that the friction coefficient of the steel does not depend by the increase of the pressure acting on the surface.

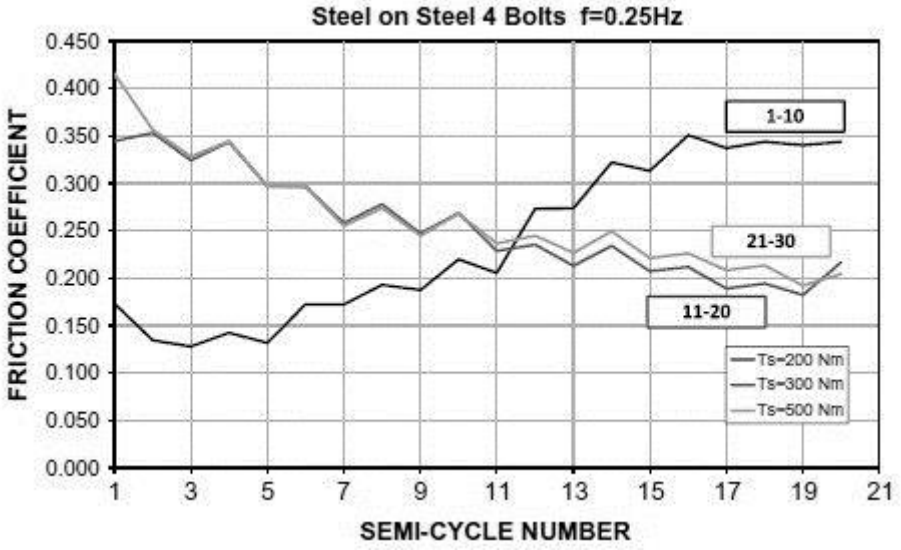

Figure 3.2- Friction coefficient of the steel-steel interface (M. Latour et al. 2014)

Regarding to the brass-steel interface, as can be observed by the Figure 3.3, the cyclic behaviour of the brass-steel interface is completely different from the cyclic behaviour of the steel –steel interface. In fact, the brass-steel interface presents a first initial friction coefficient lower when compared to steel-steel interface but as the number of cycles increases, the friction coefficient also increases, exhibiting a hardening behaviour.

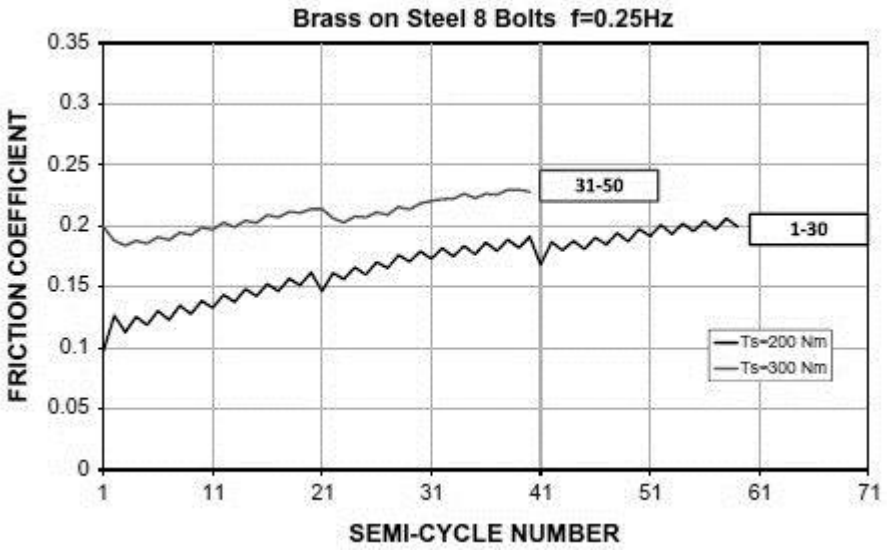

Figure 3.3-Friction coefficient of the brass-steel interface (M. Latour et al. 2014)

Finally, the third metallic pad is composed by an 8mm steel plate on which a layer of aluminium is thermally sprayed. In fact, because the thickness of the coating layer can influence significantly the friction coefficient, three values of cover thickness have been considered, namely, 50μm, 150μm and 300μm (Massimo Latour et al. 2014). The experimental results varying the coating thickness shows that for thickness between 50μm and 150μm the friction coefficient slight decrease, while for values greater than 150μm it becomes approximately constant. In the figure below (Figure 3.4) is show the variation of the friction coefficient for a coating thickness equal to 300μm. Those experimental results outline that, when comparing to the other metallic interfaces, the response of the sprayed aluminium is more stable and present a higher initial value of the friction coefficient. In addition, the material behaviour under cyclic loads only presents a slight degradation without initial hardening, contrarily to the other metallic interfaces. Furthermore, there is not a significant difference between the static and dynamic value of the friction damper. Notwithstanding, the tests also outline the fact that the preloading bolt level has a significant influence on the friction coefficient, since when the preloading bolt force increases, the friction coefficient decreases.

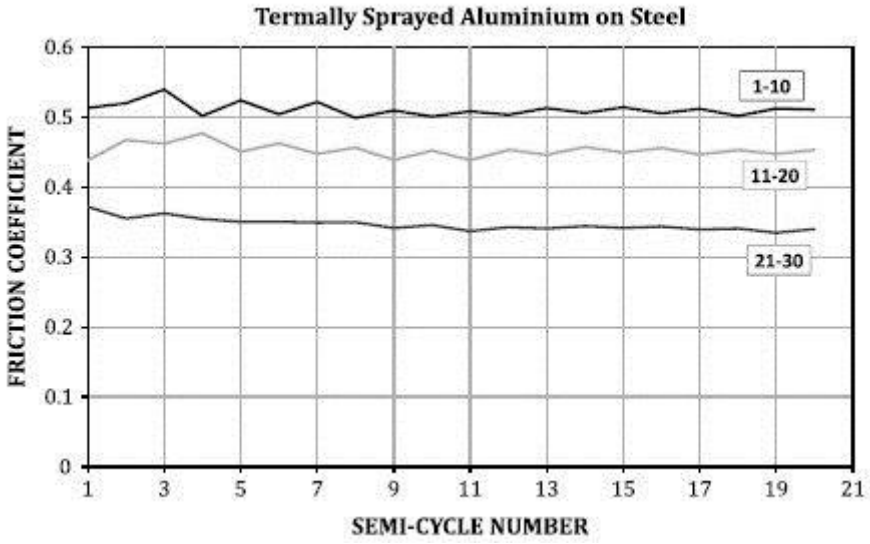

Figure 3.4-Friction coefficient of the sprayed aluminium-steel interface [coating with 300µm] (M. Latour et al. 2014)

Rubber materials

Three different rubber materials have been tested, in accordance to the Table 3-1.

The first material, called M0, is a blend of mineral and organic fibbers aggregated by means of phenolic resin, usually used for braking application. The results (Figure 3.5) shows that the material M0 has a stable cyclic behaviour leading to a high ability of dissipate energy and does not present a significant strength degradation. In fact, during the first and second loading steps (1-40th cycle) the strength degradation of the material can be ignore. It is just in the third and fourth loading sequence (41st to 60th cycle) that the interface present strength degradation which can be explained by the higher initial pressure acting on the surface. Thus, the force reached during the first cycle is the greatest of the loading history due to the wearing of the material during the sliding motion that leads to the loss of bolt preloading.

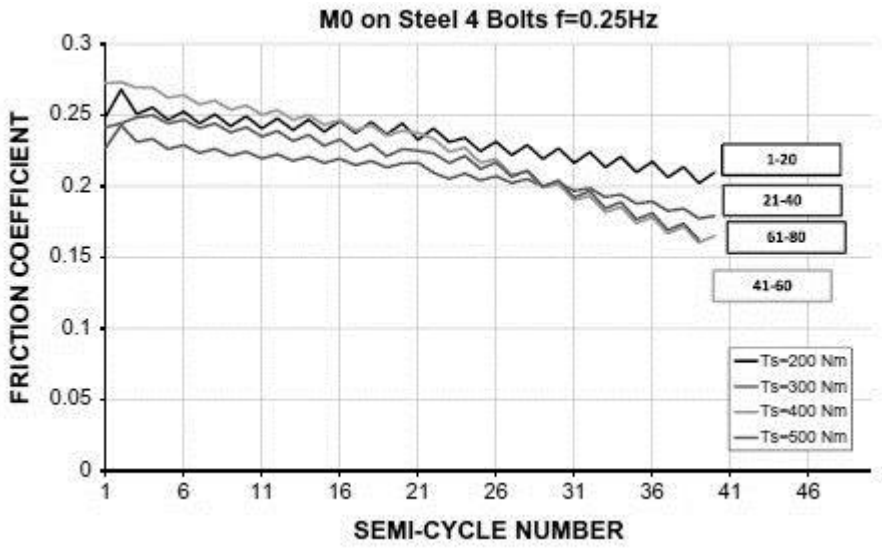

Figure 3.5- Friction coefficient of the friction material (M0)-steel interface (M. Latour et al. 2014)

The second rubber, called friction M1, is the friction material SA-21, normally used as a material for electric motors. It presents a density of 2150 g/cm2 and a superficial hardness of 75 shore D. By observing the Figure 3.6, we can see that for values of tightening torques lower than 300Nm, the friction coefficient is lower when comparing to higher tightening torques levels but it presents a stable cyclic response. However, for values higher than 300Nm, the material exhibits a degradation of stiffness and strength due to the low tensile resistance of the material.

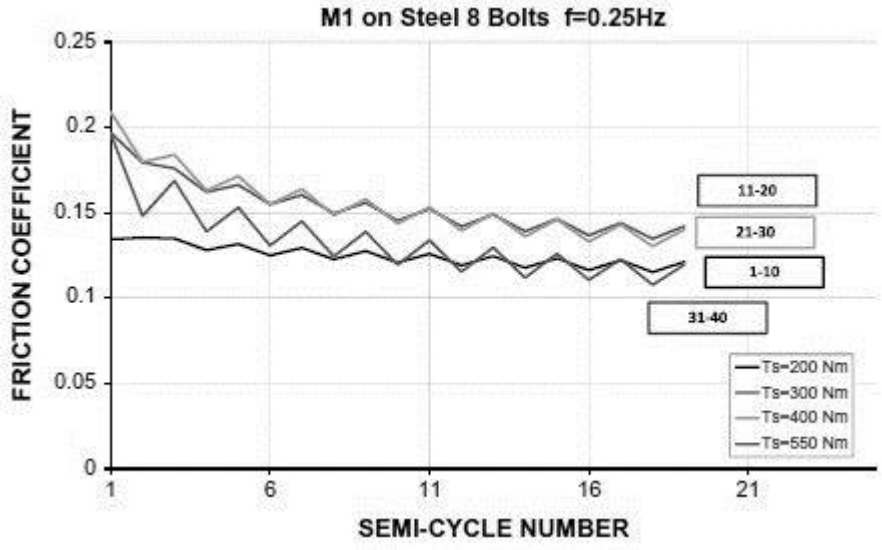

Figure 3.6-Friction coefficient of the friction material (M1)-steel interface (M. Latour et al. 2014)

The third and last material tested (M2) is a friction material STR-396 and it includes within its thickness a mesh made of copper. This material presents a high resistance to abrasion because of his high superficial hardness of 85 shore D and density equal to 1.8 g/cm^2.

Regarding to his cycle behaviour, it is a material characterised for providing a very stable response, as we can see at Figure 3.7. In the first test, after the 1st cycle the material exhibit a slight hardening behaviour. In the second test, the material present a stable behaviour. It is just in the third test, that the material presents a softening behaviour, probably due to high contact pressure.

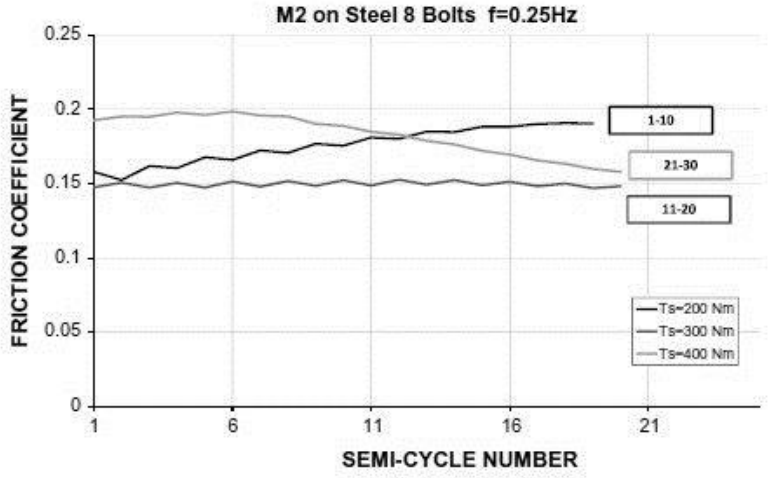

Figure 3.7- Friction coefficient of friction material M2-steel (M. Latour et al. 2014)

3.2. Experimental tests on the full-scale joint

In this part of the research, the performance of proposed innovative DST (Double split tee) connections with the friction pad under cyclic loads was tested. The beam-column coupling consist in a HEB200 column made of S275 steel and in a IPE270 beam made of S355 steel.

Design Criteria

Regarding to the framework of the component method, with reference to the proposed DST connection the following components could been identified:

- The column panel in shear;
- The column web in compression and tension;
- The T-stub;
- The friction damper.

The design goal of the connection could only be achieved if the components of the DST connection has been designed with sufficient over strength with respect to the maximum force that the friction dampers are able to transmit. Under this hierarchy, starting from the knowledge of the design bending moment, the geometry of all the elements composing the joint was defined by exploiting formulation provided by literature models, as the Kim and Engelhardt's model (Kim & Engelhardt 2002) (used for the design of the column panel in shear), or by the formulation contained in EC3(CEN 2010a).

In particular, from the several researches in the field it is possible to identify three different geometry specimens of DST connections:

- **TSJ-SA300-320-CYC 12 (**Figure 3.8**)–** Partial strength joint with a fixed classical T-stub at the top beam flange level and with a friction damper (in this case a sprayed aluminium friction damper) at the bottom flange level. Slotted holes are realised on the lower beam flange in order to allow the slippage of the friction damper. In addition, in order to assure the sufficient overstrength of the connection components, the column shear panel was reinforced with a couple of 10mm supplementary plates welded on the column web and the panel in tension and in compression have been reinforced with a continuity plate with the thickness of the beam flange. The connection was design for the resisting moment of the beam (M=133KN.m).

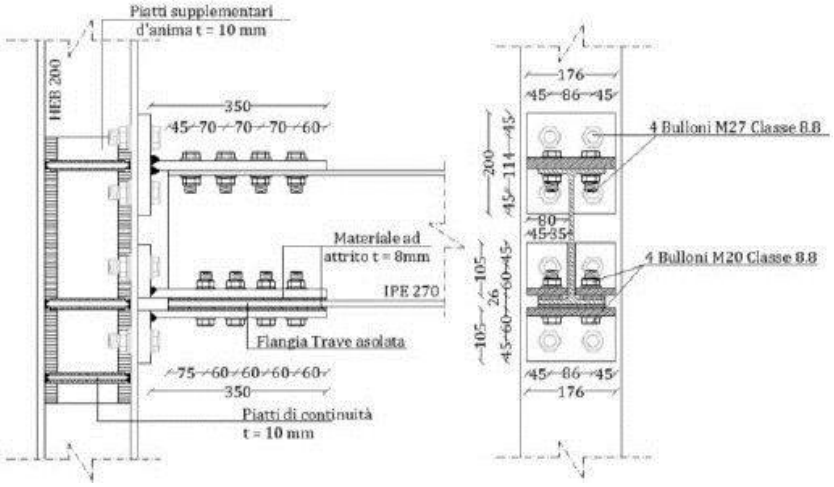

Figure 3.8- Connection typology for the specimen TSJ-SA300-320.CYC12 (Massimo Latour et al. 2014)

- **TSJ-H-SA300-260-CYC 13 (**Figure 3.9**) -** The typology of this joint is similar to the previous mentioned but the friction dampers is applied on an additional haunch welded to the beam. The joint has been design for a design moment of 166KN.m,

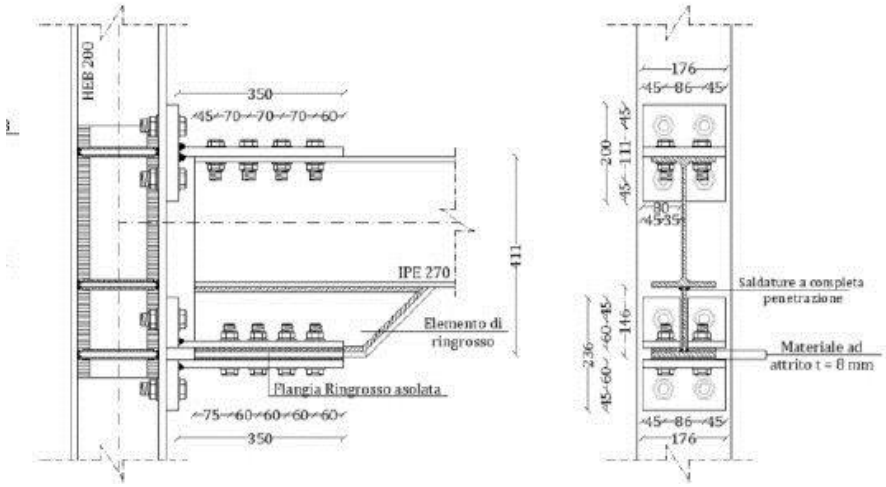

Figure 3.9-Connection typology for the specimen TSJ-H-SA300-260-CYC13(Massimo Latour et al. 2014)

- **TS-M1-460-CYC08, TS-M2-460-CYC09, TS-M2-DS-460 -CYC10** and **TS-B-460-CYC11 (**Figure 3.10**) –** Partial strength joint, similar to the ones present above, but the friction dampers are interposed between the T-stubs webs and the beam flange both at the bottom and at the lower beam flange and bolted to the beams flange and the column web. Similarly, to the previews connections typology, this one also have a couple of supplementary plates on the column web. All of these specimen have been design for a design moment equal of 100KN.m

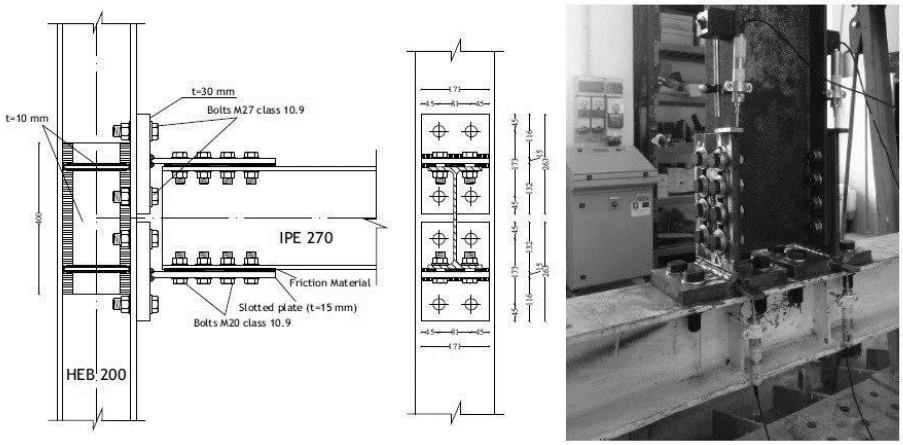

Figure 3.10- Geometry of the specimens (Latour et al. 2015a)

Description of the experimental tests

The experimental tests on joints has made considering the experimental setup present in Figure 3.11. As it can be seen, two steel hinges bolted to the carriage are connecting the specimens to the reaching system. These steel hinges were designed to resist shear forces up to 2000KN.

Two different hydraulic actuators have applied the loads. The first one, a MTS 243.6 actuator has a load capacity equal to 1000KN in compression and 650 KN in tension with a piston stroke equal to ± 125mm, was used to apply under force control, a axial load in the column equal to 30% of the squash load. The second actuator is a MTS 243.35 which has a load capacity of 250KN both in tension and in compression and a piston stroke of ± 500mm, used to apply, under displacement control, the desired displacement history at the beam end.

A horizontal frame were employed in order to avoid the lateral-torsional buckling of the beam. This frame works as a guide restraining the lateral displacement of the beam but allowing its rotations. The loading history has been defined in terms of drift angle, according to the protocol provided by AISC (2005).

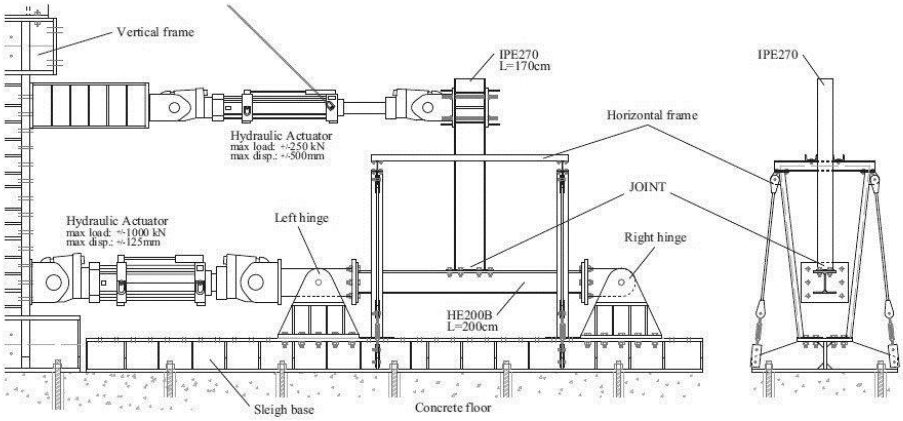

Figure 3.11- Experimental setup for tests on joints (Latour et al. 2015a; Massimo Latour et al. 2014)

All the six specimen already mentioned were evaluated, namely TSJ-M1-CYC08, TSJ-M2-CYC09, TSJ-M2-DS-CYC10, TSJ-B-CYC11, TSJ-SA300-320-CYC 12 and TSJ-H-SA300-260-CYC 13. The first three have a friction damper with a rubber material (M1 and M2), the fourth has a brass plate between the Tee stems and the beam flanges and the last two have sprayed aluminium friction dampers.

Experimental test results

In Figure 3.12 and Figure 3.13 is present the envelope of the cyclic moment-rotation and the energy dissipation for the specimens with the friction material M1 and M2 and for the brass damper and also for a typical DST joint.

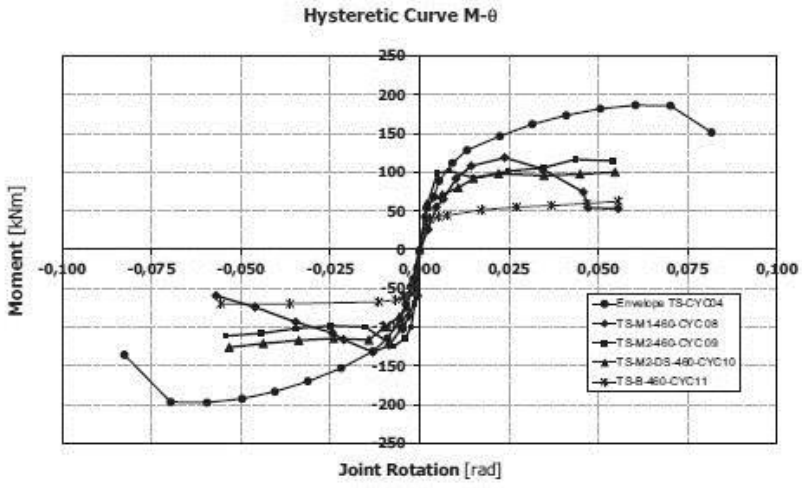

Figure 3.12- Hysteric Curves M-θ of the tested specimens (Latour et al. 2015a)

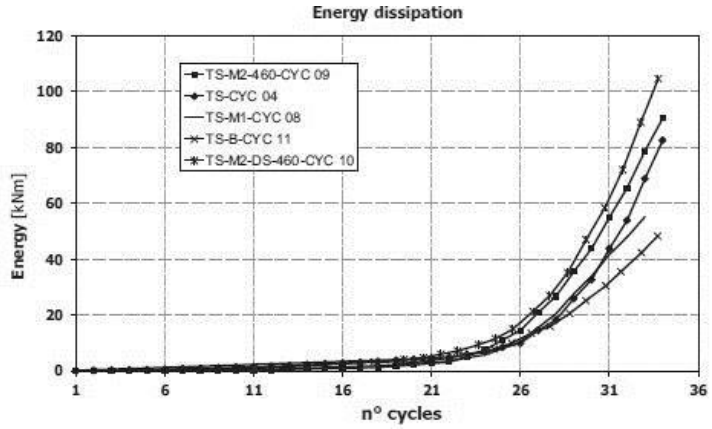

Figure 3.13- Energy dissipation of the tested specimens (Latour et al. 2015a)

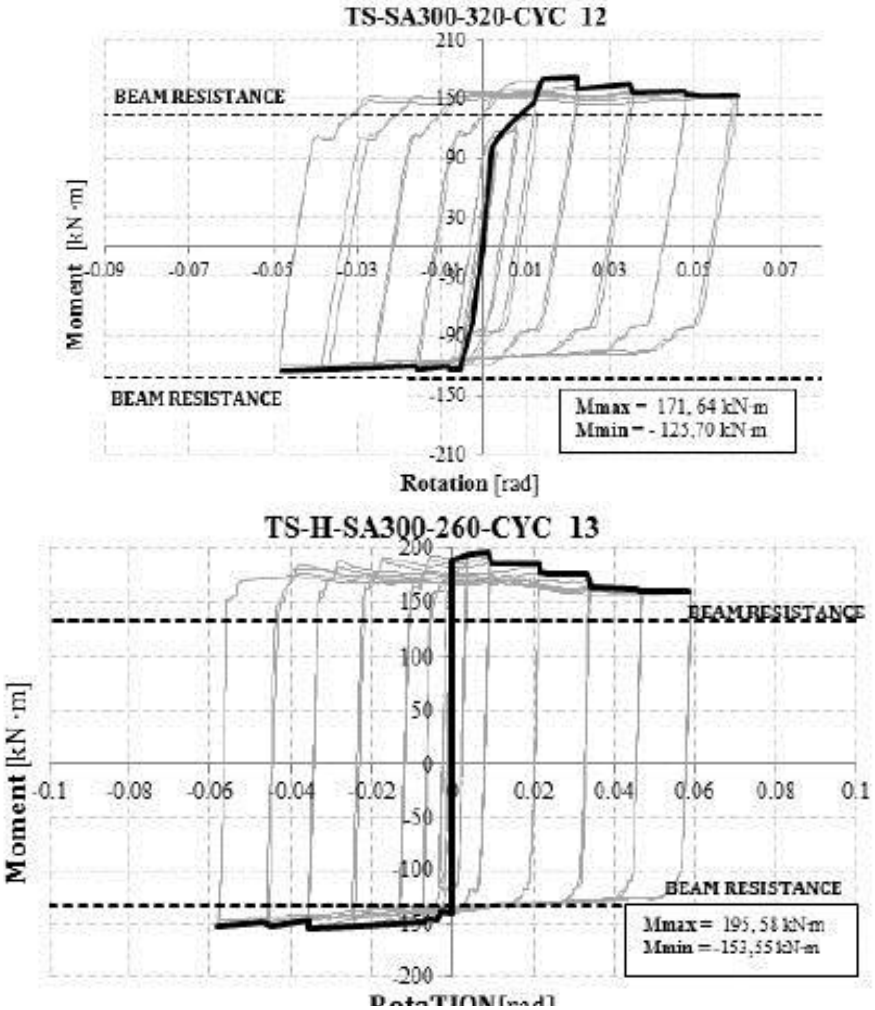

Figure 3.14- Moment-rotation curves for the specimens with sprayed aluminium dampers(Massimo Latour et al. 2014)

In view of the results exposed in the figures below, some conclusions can be made:

- In all the experimental tests, any of the joint components have been damage, just the wear of the friction pad;

- Experimental test points out that the cyclic behaviour of the joint is governed mainly by the cyclic behaviour of the friction damper;

- The specimen with the friction damper **M1** present a poor cyclic behaviour, affected by significant pinching and strengthen degradation after the slippage of the friction dampers. From these results is possible to conclude that this rubber material is not appropriate to be use as friction damper;

- The specimen **TSJ-M2-CYC09** presents wide and stable hysteretic loops during the analysis. However for high rotations amplitudes, shows a slight strength and stiffness degradation due to the consumption of the friction pads;

- The specimen **TSJ-M2-DS-CYC10** is the same connection as the one mentioned before but with disc springs interposed between the bolt head and the tee web plate in order to overcome the pinching and degradation found for the specimen **TSJ-M2-CYC09.** The results actually shows the effectiveness of those springs;

- The specimen with the brass-steel interface, **TSJ-B-CYC11**, shows a very stable cyclic behaviour even at high rotations demands. However a value for the bending moment less than the design moment was obtained, what can be explained by the fact that the static friction coefficient of the interface is lower than the dynamic one so, the bending moment obtained is lower than the expected one;

- When compare to the traditional DST connection, the tested specimen's presents a lower hardening behaviour but, on the other hand, present the ability to dissipate more energy;

- Regarding to the specimens with a friction damper interface with sprayed aluminium, both presents very stable and wide hysteretic loops with an approximately rectangular shape.

The experimental results confirms the ability of the connection to dissipate a high amount of energy without damage to the structural parts, in other words, a free-from-damage connection was achieved. Regarding to the different tested specimens, the specimens with the friction material M2 and the specimens with the sprayed aluminium material were the ones who presents a greater hysteric behaviour.

3.3. Experimental tests on MR-frames with connections with friction dampers

In this experimental work, a multi-storey steel MR-frame equipped with friction dampers on the connections, has been investigated by means of static nonlinear analysis and nonlinear dynamic analysis (Piluso et al. 2014).

The structural typology investigated was a Steel MRF with DST with friction dampers beam-to-column connections as well as column base connections integrated with friction dampers. The purpose of integrate the friction dampers on beam-to-column connection is to develop an energy dissipation mechanism that only involve the friction dampers, while all the structure members remain in elastic range. On the other hand, these devices on column base connections assure the damage prevention even when a global mechanism is completely developed. The column-base connections are constituted by a pin-joint hinge, transmitting the axial force and the shear force, while the friction dampers transmits the bending moment.

Furthermore, a rigorous design procedure has been adopted, assuring that all the columns remain in elastic range during the analysis, i.e., a design procedure that assure a global collapse mechanism type. In this view, the collapse mechanism control described by Mazzolini and Piluso (Mazzolani & Piluso 1997) was used. This theory is based on rigid-plastic analysis and on the kinematic theorem of plastic collapse extended to the concept of mechanism equilibrium curve.

The steel Mr-frame investigated was the three bay six-storey frame present in Figure 3.15.

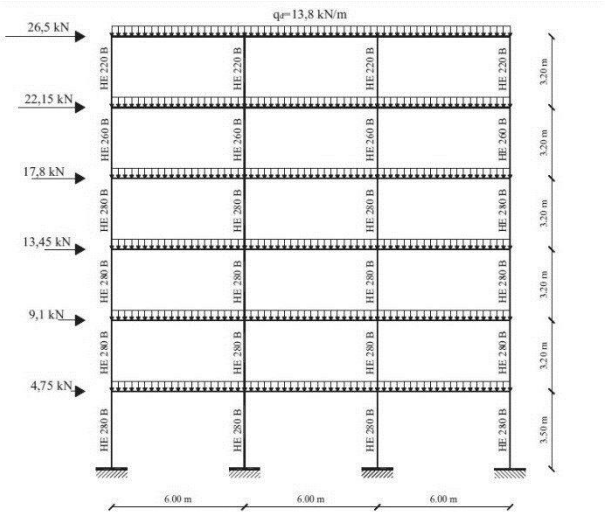

Figure 3.15- Structural scheme investigated(Piluso et al. 2014)

Regarding the design loads, was considered a uniform dead load (G_k) equal to 12KN/m and a uniform live load (Q_k) equal to 6KN/m. According to Eurocode 0 (En 2009), the design vertical load is equal to $q_= 1.35G_k+1.5Q_k = 25.20$KN/m. According to Eurocode 8 (CEN 2010b), the seismic load combination is $Gk+\psi_2 Qk + E_{d,}$ where ψ_2 is the coefficient for quasi-permanent value of variable actions, equal to 0,3 for residential buildings, so the vertical seismic load is equal to 13.8KN/m, as can be seen in Figure 3.15.

The preliminary design of the beams has been made for the design vertical load and assuming a design value of the beam plastic moment approximately equal to $qL^2/8$, what has led to IPE270 profiles made of S275 steel grade.

The design seismic horizontal forces have been determined according to Eurocode 8 (CEN 2010b), assuming a peak ground motion of 0.35g and a behaviour factor equal to 6. A horizontal distribution according to the first vibration mode was assumed, see Figure 3.15.

As was said above, both beam-to-column and base column connections are equipped with friction dampers. The beam-to-column connection is the DST connection integrated with friction pads designed investigated in the first experimental research described in this section(Latour et al. 2015a). The base column connection is a column-base hinged connection, conceived as a pin-joined connection and designed to transmit the shear force and the axial force, while the friction dampers, located with a lever arm, transmits the desire bending moment. For this reason the friction dampers has been calibrated for the desired bending moment of the column base connections. The structural scheme of the connections is present in Figure 3.16.

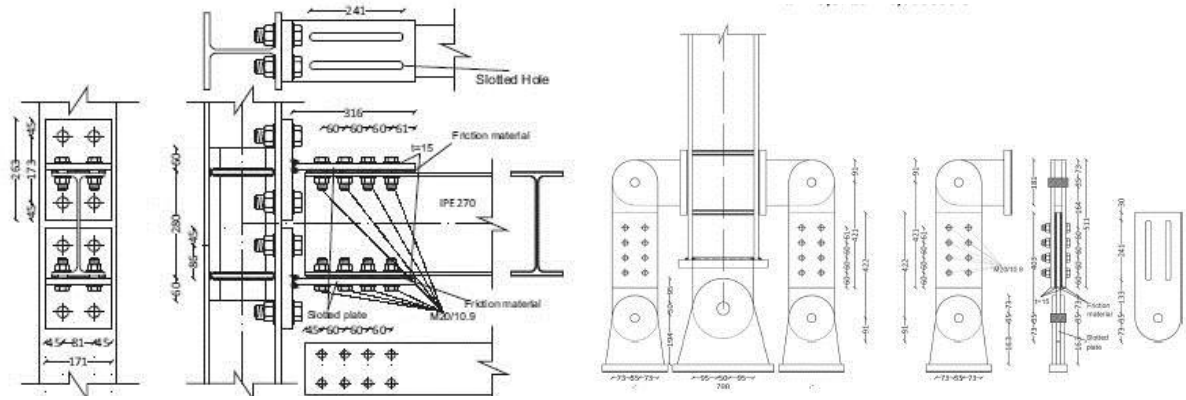

Figure 3.16-Structural scheme of the connections; beam-to-column connection (left);base column connection (right) (Piluso, Montuori, and Troisi 2014)

The slip resistance is given by the ratio between the bending moment and the lever arm of the friction damper, which depends on design pre-loaded force, $F_{p,cd}$, of the bolts given by the Eurocode 3 (En 2010).

Moreover, the stroke of the friction dampers can be calibrated depending on the design ultimate displacement (top sway displacement) for which global collapse mechanism has to be assure. With respect to the case study, the value of 0.04rad has been assumed for the maximum rotation of the columns (θ_p), so that the top sway displacement is equal to 0.78m ($H\theta_p$). The stroke of the friction dampers on the beam-to-column connections has to accommodate a displacement of 10.8mm (0.04x270), while the column base connection has to accommodate a displacement of 28mm (0.04x700), obtained considering the lever arm of the friction dampers, see Figure 3.16.

Validation of the design procedure and main results

The validation of the design procedure presented above, has been made by means of a static nonlinear analysis (pushover) and dynamic nonlinear analyses both carried out with the computer program SAP2000. These analyses had the purpose to check the actual energy dissipation, i.e. the development of global collapse mechanism and testing the accuracy of the design methodology.

Regarding the static nonlinear analysis, the members were modelled by means of beam-columns elements, whose non-linearity has been modelled by spring elements at their ends. The friction devices located at the beam ends has been modelled by means of plastic hinges accounting only for the bending moment and characterized by a rigid hardening moment rotation curve representing the monotonic envelope of the cyclic response point out by the experimental tests (Latour et al. 2015a; Latour 2011). The column-base connections equipped with friction dampers have been modelled by means of plastic hinges in pure bending with a rigid perfectly plastic behaviour.

The pushover analysis has been carried out under displacement control taking into account both geometric and mechanical nonlinearity. The result provided by this analysis is reported in Figure 3.17(a), where both pushover curve and the global mechanism equilibrium curve are depicted. In addition, the distribution of the "equivalent plastic hinges" are showed in Figure 3.17 (b), which point out the activation of the friction dampers at the design displacement. These results shows that the pattern of the energy dissipation are in agreement with the global mechanism and the softening branch of the push over curve agrees with the global mechanism curve obtain from second order rigid plastic analysis.

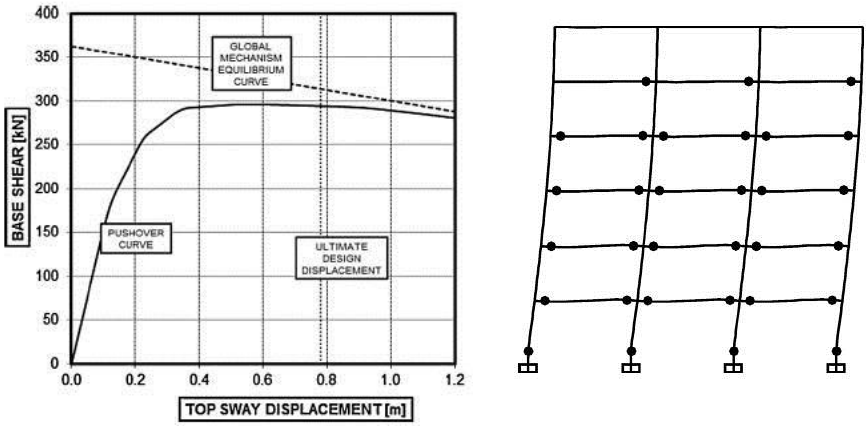

Figure 3.17- a) Pushover curve ; b) Activation of the friction dampers at the design displacement (Piluso et al. 2014)

A further validation of the procedure were carried out by means of incremental dynamic nonlinear analyses. Such analyses require modelling of the cyclic response of the connections with the friction dampers, reported in the chapter 3.

The seismic performance of the MR-frame were carried out by the program SAP2000 for increasing levels of seismic intensity, assuming a critical damper equal to 3%. Record-to-record variability is accounting for considering ten earthquake records selected from PET database.

In order to perform an incremental dynamic nonlinear analysis, all the records have been scaled to provided increasing values of the spectral acceleration Sa (T_1) corresponding to the fundamental period of vibration (T_1 =1.6s). Specifically, the analyses have been repeated by increasing the spectral acceleration until achieve the connection rotation demand (0.04rad).

The Figure 3.18 and in Figure 3.19 provides the IDA curves giving the maximum stroke, required by the friction dampers, versus the spectral acceleration for beam-to-column and column-base connections and the maximum interstorey drift ratio and the maximum roof drift versus spectral acceleration.

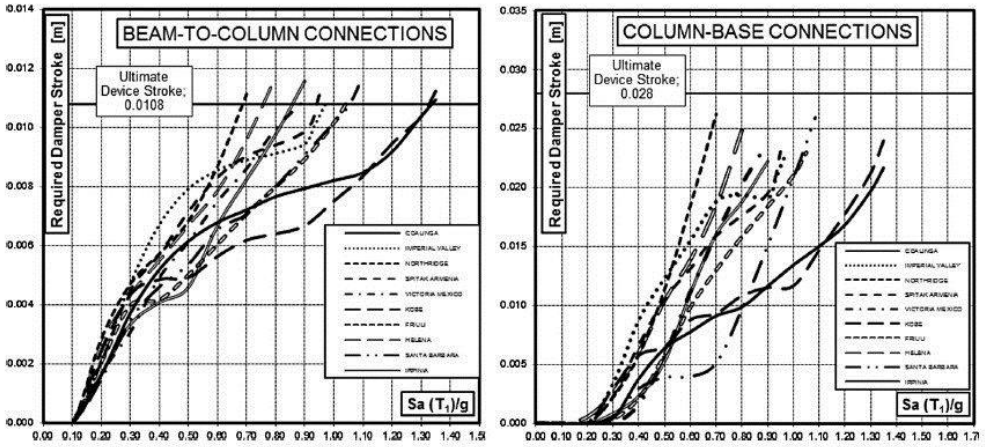

Figure 3.18- Damper required stroke versus spectral acceleration for friction dampers of Beam-to-column and column-base connections (Piluso et al. 2014)

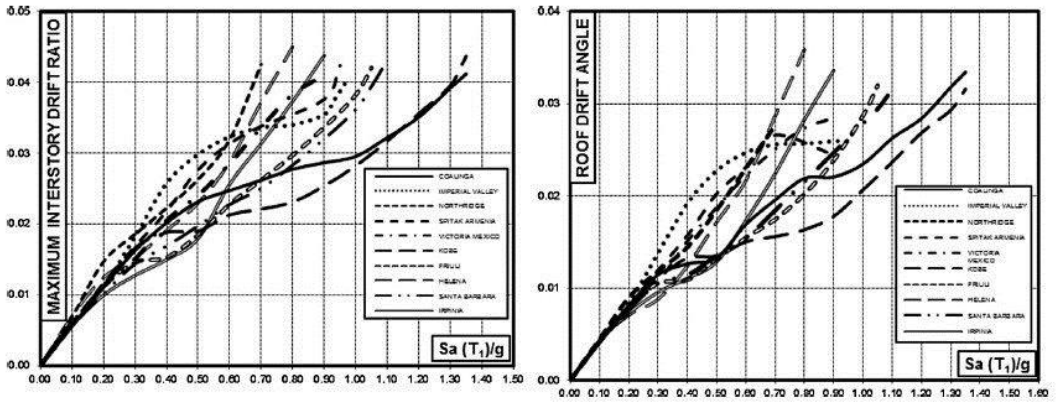

Figure 3.19- Maximum interstorey drift and maximum roof drift angle versus spectral acceleration (Piluso et al. 2014)

The above graphical representations lead to few conclusions. In the Figure 3.18, the curve concerning the column base connection shows that when the ultimate stroke of the friction dampers located in beam-to-column connections are reached, column base connections are still safe. In addition, it shows that the calibration of the friction damper allows withstanding spectra acceleration from 0.70g to 1.35g, depending on the ground motion. In Figure 3.19 shows that the maximum interstorey drift ratio and the roof drift angle is achieved also for high spectral acceleration, what confirms the effectiveness of the friction damper in the dissipation of the seismic input energy.

4. Structural modelling of the steel MRF

The study of the steel MRF with the innovative dissipate typology of connections has been made by means of nonlinear analyses, both static pushover and incremental dynamic analyses using the software *SeismoStruct*. In addition, the same analyses have been done for a steel MRF with a traditional approach, i.e with strength connection in order have a reference behaviour for the seismic response of these type of buildings.

4.1. Description of the analysed frame

The frame geometry adopted was obtained by the Salerno investigations (Piluso et al. 2014) and is a three bay, six storey steel frame Figure 4.1. The frame has a total height of 19,5m with interstorey heights of 3.5m in the first storey and 3.2m in the remaining storeys. The bay span are equal to 6m.

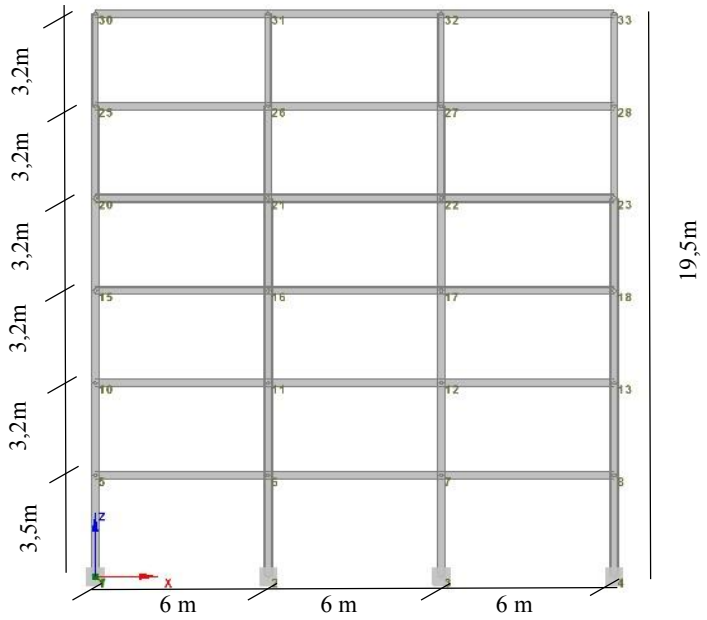

Figure 4.1- Frame geometry adopted

The dissipative zones are constitute by friction dampers that are located at the beam-to-column connections at the bottom flange of the beams. These friction devices have to assure the dissipation of the seismic input energy and, furthermore, assure that all the frame elements remain in elastic range.

4.2. Frame design

4.2.1. Seismic Action

The building frame is assumed to be located in the South of Portugal, specifically where the Seismic zone is classified as 1.1 by the National Annex, which correspond a peak ground acceleration of 0,255g (2,5m/s^2). The soil was considered as a soil type A, which according to EC8-1 has the following description: *"Rock or other rock-like geological formation, including at most 5m weaker material at the surface"*, to which correspond the followings soil parameters for a seismic action of type 1: S equal to 1.0, T_B=0.1s, T_C = 0,6s and a T_D equal to 2s. Since the building is classified as a residential building, the importance factor was admitted equal to 1.0.

Furthermore, as the purpose of the MRF is to dissipate the seismic input energy and remain safe after the event without structural damage, it was classified as having a dissipative structural behaviour, specifically as belonging to a high ductility class (DCH). For that reason, according to Figure 4.2 and Table 4-1 below of the EC8-1, for MRF with high ductility the reference value of the behaviour factor, q_0, is equal to 5, while α_u/α_1 can have a value between 1.1 and 1.3. The behaviour factor adopted was equal to 6.

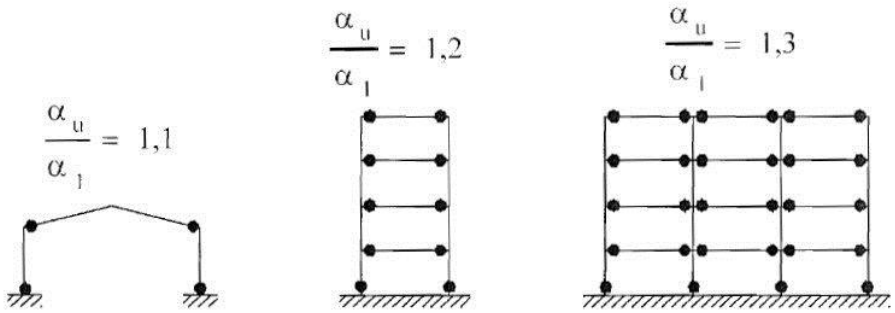

Figure 4.2-Values of α_u/α_1 for MRF (figure 6.1 of EC8-1(CEN 2010b))

Table 4-1-Upper limits of reference values of the behaviour factors (table 6.2 of EC8-1(CEN 2010b))

STRUCTURAL TYPE	Ductility Class	
	DCM	DCH
a) Moment resisting frames	4	$5\alpha_u/\alpha_1$
b) Frame with concentric bracings		
Diagonal bracings	4	4
V-bracings	2	2,5
c) Frame with eccentric bracings	4	$5\alpha_u/\alpha_1$
d) Inverted pendulum	2	$2\alpha_u/\alpha_1$
e) Structures with concrete cores or concrete walls	See section **5**	
f) Moment resisting frame with concentric bracing	4	$4\alpha_u/\alpha_1$
g) Moment resisting frames with infills		
Unconnected concrete or masonry infills, in contact with the frame	2	2
Connected reinforced concrete infills	See section **7**	
Infills isolated from moment frame (see moment frames)	4	$5\alpha_u/\alpha_1$

Applying all the parameters referred above on the equation (3.2) to (3.5) and (3.13) to (3.16) of the EC8-1, for a damper coefficient of 3%, it was possible to define the elastic response spectra (Figure 4.3) and the design response spectra (Figure 4.4), respectively.

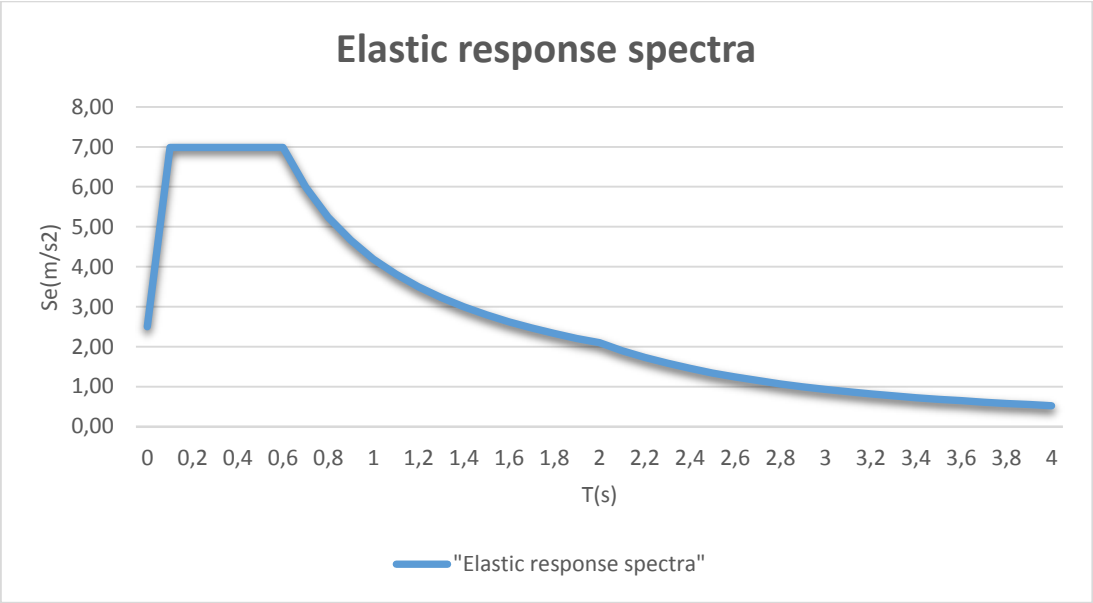

Figure 4.3- Elastic response spectra

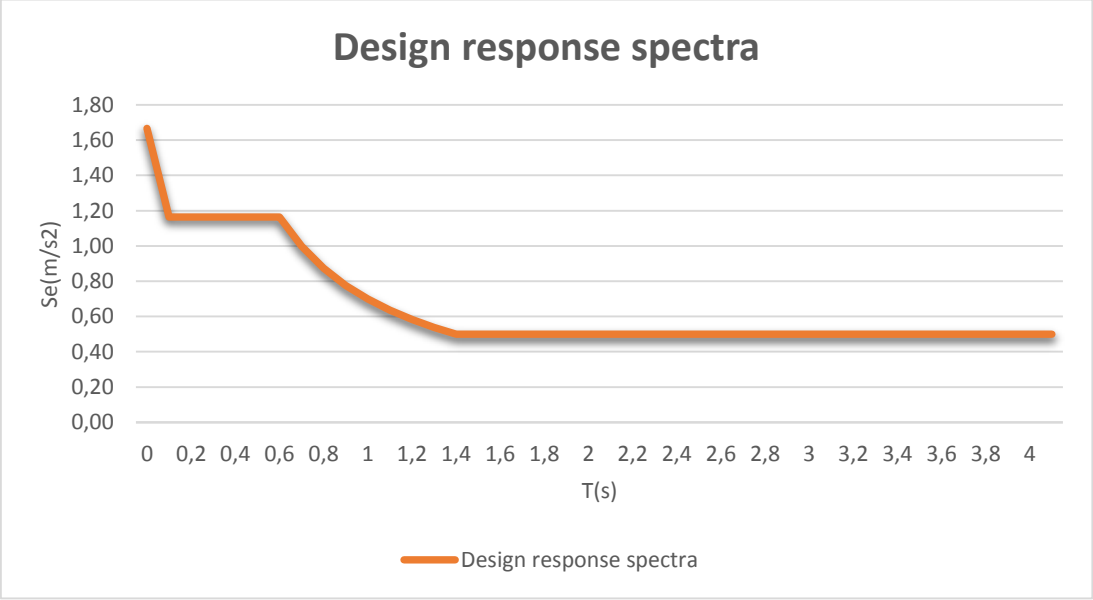

Figure 4.4- Design response spectra

4.2.2. Design loads

1. Live loads

The following live loads have been considered in the design of the frame, taking into account what is stated by the EC1-1 (CEN 2009) for residential building (Category A) :

- A live load equal to 2 KN/m^2 for each floor;
- A live load equal to 0.8 KN/m^2 to take into account the partition walls.

2. Permanent loads

Regarding permanent loads have been considered a steel-concrete slab for each floor. Furthermore, has been considered a screed material with 7cm thickness for the pavement coating with a load value equal to 2 KN/m^2.

The characteristics of the steel-concrete slab was taken from the catalogue "***O FELIZ***", considering the slab works in the perpendicular direction to the secondary beams so, the distance between supports has considered equal to 1.5m. Therefore, the slab **H60x0.7x100,** to which correspond a weight equal to 1.68 KN/m^2 was admitted.

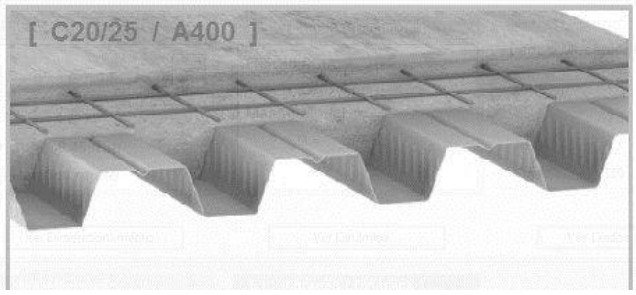

Figure 4.5- Steel-concrete slab from the catalogue O FELIZ

Table 4-2- Principal characteristics of the slab

H60x0.7x100mm	
Hslab [mm]	100
$thickness_{steelshet}$ [mm]	0,7
$pp_{steelshet}$ [kg/mm^2]	8,38
pp_{slab} [KN/m^2]	1,68

4.2.3. Preliminary design of beam/column elements

In the field of seismic engineering, structures has to be design in order to assure that columns remain in elastic range during the seismic event. In order to accomplish that, a rigorous design procedure that not only prevent the soft-storey mechanisms but also assuring a global collapse mechanism has to be adopted. Regarding steel MRF, most recent seismic codes, suggest an application of a member hierarchy criterion, which prevent the development of soft storey mechanisms but cannot assure the formation of a global collapse mechanism type. Therefore, the theory of plastic mechanism control described by *Mazzolani and Piluso* (Mazzolani & Piluso 1997) and improved in 2004 by *Mountori et al*.(Mountori et al. 2015) has been applied. This method is based on rigid-plastic analysis and on the kinematic theorem of plastic collapse extend to the concept of mechanism equilibrium curve. The global mechanism is achieved with

the application of rigorous design conditions that are derived by imposing that the mechanism equilibrium curve corresponding to the global mechanism has to be located bellow those corresponding to all the undesired mechanisms up to a top sway displacement level compatible with the local ductility supply of dissipative zones.

Energy dissipation mechanisms

According to the theory limit analysis, there are three main collapse mechanism typologies that the structure can exhibit (Figure 4.6). All the typologies of mechanisms depicted in the Figure 4.6, excepting the global mechanism, are undesired mechanisms because they do not involve all the dissipative zones.

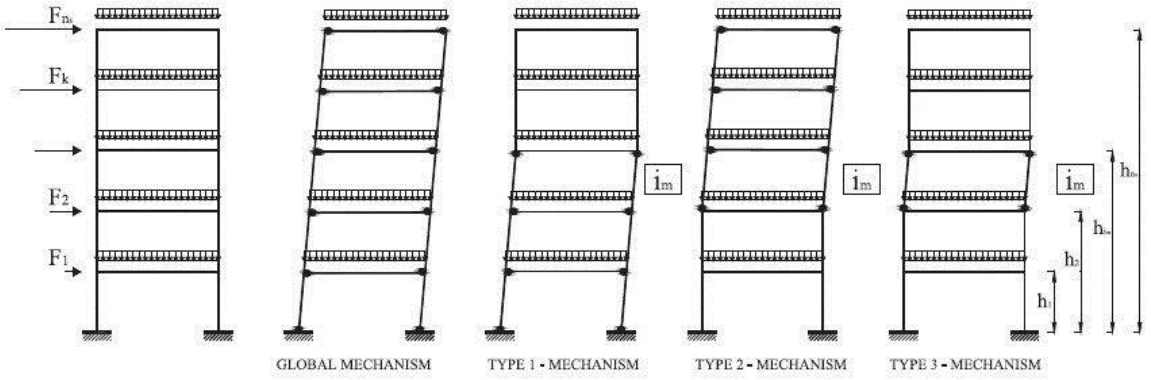

Figure 4.6- Collapse mechanisms typologies

Concerning the fact that this theory is based on the kinematic theorem of plastic collapse, the equilibrium curve, for any of the collapse mechanism mentioned, can be derived by equating the external work to the external work due to the plastic hinges involved in the collapse mechanism. In addition, the external second-order work due to vertical loads is also evaluated. The external work for the global mechanism due to the virtual rotation dθ of the plastic hinges is given by:

$$W_e = \alpha \sum_{k=1}^{ns} F_k h_k d\theta + \frac{\delta}{h_{ns}} \sum_{k=1}^{ns} V_k h_k d\theta \quad (4.1)$$

In the other hand, the internal work due to the virtual rotation dθ of the plastic hinges is:

$$W_i = \left(\sum_{k=1}^{nc} Mc_{i,1} + 2 \sum_{k=1}^{ns} \sum_{j=1}^{nb} Mb_{j,k}\right) d\theta \quad (4.2)$$

Equating the external work to the internal work is possible to obtain the horizontal force multiplier, α and therefore, the mechanism curve equation:

$$\alpha = \frac{\sum_{k=1}^{nc} Mc_{i,1} + 2 \sum_{k=1}^{ns} \sum_{j=1}^{nb} Mb_{j,k}}{\sum_{K=1}^{ns} F_k h_k} - \frac{\sum_{k=1}^{ns} V_k h_k}{h_{ns} \sum_{k=1}^{ns} F_k h_k} \delta \quad (4.3)$$

As can easily be seen the equation above (4.3) is linear and is generally expressed in the form:

$$\alpha = \alpha_0 - \gamma\delta \tag{4.4}$$

So in case of a global collapse mechanism, the kinematic admissible multiplier of the horizontal forces is:

$$\alpha_0^{(g)} = \frac{\sum_{k=1}^{nc} Mc_{i,1} + 2\sum_{k=1}^{ns}\sum_{j=1}^{nb} Mb_{j,k}}{\sum_{K=1}^{ns} F_k h_k} \tag{4.5}$$

The slope of the equilibrium mechanism curve is given by:

$$\gamma^{(g)} = \frac{\sum_{k=1}^{ns} V_k h_k}{h_{ns}\sum_{k=1}^{ns} F_k h_k} \tag{4.6}$$

The parameters obtain with the equation (4.5) and (4.6) for the mechanisms type 1, 2 and 3 are obtain in a similar way. For the i_m th mechanism of type-1, 2 and 3 the admissible multiplier are, respectively:

$$\alpha_{im}^{(1)} = \frac{\sum_{i=1}^{nc} Mc_{i,1} + 2\sum_{k=1}^{im-1}\sum_{j=1}^{nb} Mb_{j,k} + \sum_{i=1}^{nc} Mc_{i,im}}{\sum_{k=1}^{im} F_k h_k + h_{im}\sum_{k=im+1}^{ns} F_k} \tag{4.7}$$

$$\alpha_{im}^{(2)} = \frac{\sum_{i=1}^{nc} Mc_{i,1} + 2\sum_{k=im}^{ns}\sum_{j=1}^{nb} Mb_{j,k}}{\sum_{k=im}^{ns} F_k (h_k - h_{im})} \tag{4.8}$$

$$\alpha_{im}^{(3)} = \frac{\sum_{i=1}^{nc} Mc_{i,1}}{h_1\sum_{k=1}^{ns} F_k}, i_m = 1 \tag{4.9}$$

$$\alpha_{im}^{(3)} = \frac{2\sum_{i=1}^{nc} Mc_{i,im}}{(h_{im} - h_{im-1})\sum_{k=im}^{ns} F_k}, i_m > 1 \tag{4.10}$$

And the slope of the equilibrium curve, are given by:

$$\gamma_{im}^{(1)} = \frac{\sum_{k=1}^{im} V_k h_k + h_{im}\sum_{k=im+1}^{ns} V_k}{h_{im}\sum_{k=1}^{im} F_k h_k + h_{im}\sum_{k=im+1}^{ns} F_k} \tag{4.11}$$

$$\gamma_{im}^{(2)} = \frac{\sum_{k=im}^{ns} V_k (h_k - h_{im-1})}{h_{ns} - h_{im-1}\sum_{k=im}^{ns} F_k (h_k - h_{im-1})} \tag{4.12}$$

$$\gamma_{im}^{(3)} = \frac{\sum_{k=im}^{ns} V_k}{h_{im} - h_{im-1}\sum_{k=im}^{ns} F_k} \tag{4.13}$$

Design conditions for plastic mechanism control

Considering what were mentioned above, the equilibrium curve for each of the collapse mechanism typologies can be obtained. As was mentioned before, according to the kinematic theorem of plastic collapse a global mechanism is achieved when its equilibrium curve is above off all the equilibrium curves corresponding to each of the undesired mechanisms within a top sway displacement range compatible with the ductility supply of structural members (Figure 4.7).

$$\alpha_0^{(g)} - \gamma^{(g)}\delta_u \leq \alpha_{im}^{(t)} - \gamma_{im}^{(t)}\delta_u, im = 1,2,..,ns\ , t = 1,2,3 \tag{4.14}$$

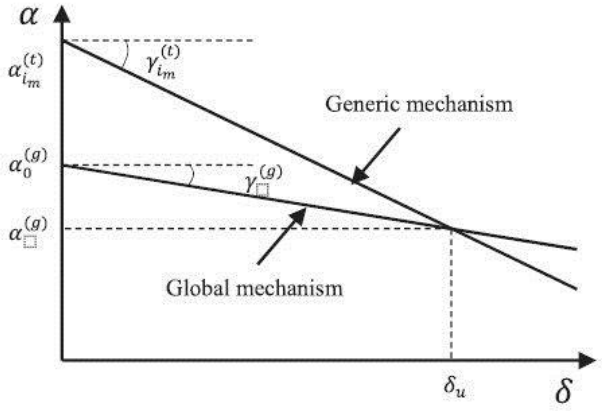

Figure 4.7- Design conditions (Mountori et al. 2015)

4.2.3.1. Design algorithm

The results of the design procedure resulting from the method present above, can be obtain by the following steps:

I. Selection of the top sway displacement, δ_u, compatible to the ductility supply of the structural members;

II. Computation of the slopes of mechanism equilibrium curves $\gamma_{im}^{(t)}$ by means of the equations (4.11),(4,12) and (4.13). The slope of the global mechanism equilibrium curve, $\gamma^{(g)}$, provided by the equation (4.6) it is the minimum among the $\gamma_{im}^{(t)}$ values;

III. Design of the beams sections and the first storey columns. The beams were designed for the maximum value of the plastic moment resistance between the one required resisting the design vertical loads, and the yield moment of the beam-to-column connections. The required sum of plastic moment of the columns, which is reduce for taking into account the contemporary action of the axial force, at the first storey is computed by means of the following relation:

$$\sum_{i=1}^{nc} Mc_{i.1} \geq \frac{2\sum_{k=1}^{ns}\sum_{j=1}^{nb} M_{b.j,k}+(\gamma_1^{(3)}-\gamma_1^{(g)})\delta_u \sum_{k=1}^{ns} F_k h_k}{2\frac{\sum_{k=1}^{ns} F_k h_k}{h_1 \sum_{k=1}^{ns} F_k}-1} \quad (4.15)$$

The equation above (4.15) is derived from the design conditions (4.14) for i_m=1 and t=1 or t=3, since for i_m=1 the type-1 and the type-3 mechanism are coincident. In addition, for i_m=1 the type-2 mechanism is coincident with the global mechanism, what means that equation (4.14) for i_m=1, type 2 mechanism becomes an identity.

IV. Computation of the axial load acting in the columns at a collapse state, when a collapse mechanism of global type is completely developed.

V. The sum of the required plastic moment of the columns at the first storey (obtained in the point III) is distributed among the columns proportionally to the axial load acting at the collapse state (point IV), so that the design of the internal actions can be derived and columns sections of the first storey can be obtained.

In addition, the required plastic moment was reduced by taking into account the influence of the axial forces according to EC3-1-1(CEN 2010a), by means of the following relationship:

$$M_{N,yRd} = minimum\begin{cases} M_{pl,y,Rd}(1-n)/(1-0{,}5a) \\ M_{pl,y,Rd} \end{cases} \quad (4.16)$$

$$n = {N_{Ed}}\Big/{N_{pl,Rd}}\,; a = \frac{A-2btf}{A} \leq 0{,}5 \quad (4.17)$$

Then, when the column sections are selected from standard shapes, the value obtained for the required plastic moment of the columns at the first storey, $\sum_{i=1}^{nc} Mc_{i,1}^{*}$, is generally greater than the one obtained from the equation (4.15). For that reason, the equilibrium mechanism curve has to be evaluated by means of the equation (4.3) by replacing $\sum_{i=1}^{nc} Mc_{i,1}$ for $\sum_{i=1}^{nc} Mc_{i,1}^{*}$.

VI. Computed of the required sum of plastic moment of columns, reduced due to the contemporary action axial force, $\sum_{i=1}^{nc} Mc_{i,im}^{(t)}$ for i_m>1 and t=1,2 and 3 by means of the following relations

For avoiding type-1 mechanism:

$$\sum_{i=1}^{nc} Mc_{i,im}^{(1)} \geq \left(\alpha^{(g)} - \gamma_{im}^{(1)}\delta_u\right)\left(\sum_{k=1}^{im} F_k h_k + h_{im}\sum_{k=im+1}^{ns} F_k\right) - \sum_{i=1}^{nc} Mc_{i,1}^{*} - 2\sum_{k=1}^{im-1}\sum_{j=1}^{nb} Mb_{j,k} \quad (4.18)$$

For avoiding type-2 mechanism:

$$\sum_{i=1}^{nc} Mc_{i,im}^{(2)} \geq \left(\alpha^{(g)} - \gamma_{im}^{(2)}\delta_u\right) \sum_{k=im}^{ns} F_k(h_k - h_{im}) - 2\sum_{k=1}^{ns}\sum_{j=1}^{nb} Mb_{j,k} \quad (4.19)$$

For avoiding type-3 mechanism:

$$\sum_{i=1}^{nc} Mc_{i,im}^{(3)} \geq \left(\alpha^{(g)} - \gamma_{im}^{(3)}\delta_u\right) \frac{(h_{im} - h_{im-1})}{2} \sum_{k=im}^{ns} F_k \quad (4.20)$$

The required sum of the reduced plastic moment of the columns for each storey is the maximum value of each obtain from the equation above:

$$\sum_{i=1}^{nc} Mc_{i,im} = max\left\{\sum_{i=1}^{nc} Mc_{i,im}^{(1)}; \sum_{i=1}^{nc} Mc_{i,im}^{(2)}; \sum_{i=1}^{nc} Mc_{i,im}^{(3)}\right\} \quad (4.21)$$

VII. The sum of the required plastic moment of the columns at each storey obtained from the point VII, is distributed among all the storey columns, proportionally to the axial force acting at the collapse state (point IV), allows the design of column sections from standard shapes.

VIII. A technological condition can be imposed by requiring, starting from the base, that the column sections cannot increase along the building height. If this condition requires the change of the column sections at the first storey then the procedure needs to be repeated from the point V.

Application to the study case

The procedure mentioned above was applied to the frame present in Figure 4.1 and for the design loads and the seismic action referred in the subchapter 4.2.

1. Definition of the lateral load pattern

According to EC8-1, the fundamental period of vibration that can be used for a preliminary design is:

$$T_1 = 0{,}085H^{3/4} = 0{,}085 \times 19.5^{3/4} = 0{,}79s \quad (4.20)$$

Applying the lateral forces method of EC8-1, the following lateral seismic forces distribution were found (Table 4-3):

Table 4-3- Lateral seismic forces for the preliminary design of the columns

Storey	Seismic force [KN]	h_k [m]
1	5,49	3,5
2	10,51	6,7
3	15,53	9,9
4	20,55	13,1
5	25,57	16,3
6	30,59	19,5

2. Design procedure

I. Selection of the top sway displacement, δ_u

The choice of the top sway displacement is very important due to the fact the value of this displacement governs the magnitude of second-order effects accounted in the design procedure. This displacement has to be the ultimate displacement and therefore, it can be considered as:

$$\delta_u = \theta_p H \quad (4.21)$$

Where θp is the plastic rotation supply of the beam-to-column connections. According to EC8-1, for structures with high ductility this plastic rotation supply can not be less than 0,035rad. Thus, the rotation supply considered was 0,04rad and the top sway displacement is equal to 0,78m.

II. Computation of the slopes of the mechanism equilibrium curve $\gamma_{im}^{(t)}$

By means of the equations (4.11), (4.12) and (4.13), the slopes of the equilibrium curves were computed (Table 4-4).

Table 4-4- Slopes of the mechanism equilibrium curves

Parameters of the equilibrium Curves			
Storey im	Yim(1)	Yim(2)	Yim(3)
1	0,0387	0,0057	0,038658
2	0,0190	0,0064	0,037118
3	0,0122	0,0075	0,033078
4	0,0089	0,0093	0,029831
5	0,0069	0,0132	0,027165
6	0,0057	0,0249	0,024936

The slope corresponding to the global mechanism is the minimum among all the $\gamma_{im}^{(t)}$ values.

$$\gamma^{(g)} = 0{,}0057\ cm^{-1} \quad (4.22)$$

III. Design of the beams sections and overall flexural resistance of the first storey columns

As was said above, the beams were designed for the maximum value of the plastic moment resistance between the one required resisting the design vertical loads, and the yield moment of the beam-to-column connections. In the Table 4-5 is evident that the design of the beams has been influenced by the resistance of the connections, specifically, of the specimen with the sprayed aluminium friction damper and with a Haunch. As a result, a profile section IPE300 has assumed for the beams.

Table 4-5- Design of the beams

q_{ULS} (KN/m)	27,504		
fy (Mpa)	275	→	IPE330
Mplreq (KN.m)	123,768	$Wpl_{adop.}(cm^3)$	804
$Mpl_{connectionSAD}$ (KN.m)	170	The beam design is influenced by the resistance of the connection	
$Mpl_{connectionM2}$(KN.m)	120		
$Mpl_{connectionM1}$ (KN.m)	105		
$Mpl_{connectionSAD\_H}$ (KN.m)	195		
Wplreq (cm3)	709,09		

The overall flexural resistance of the first storey columns was computed by means of the equation (4.15), leading to a value equal to 1684.76 KN.m.

IV. Computation of the axial loads at the collapse state in the columns

With reference to global mechanism, the total axial load forces in the columns is the sum of two contributions. The first, N_q, is related to the vertical loads acting in the seismic combination, and the second, N_f, is related to the shear actions due to the plastic hinges develop on the beams end (Figure 4.8).

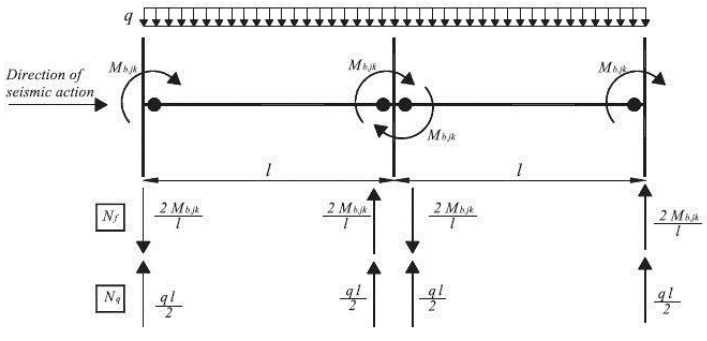

Figure 4.8- Axial loads acting in the columns at the collapse state

In the following table, the two contributions, N_q and N_f, and the total axial force N_{tot} for each storey and both for internal and external columns is reported.

Table 4-6- Axial forces in the columns at the collapse state

Storey	External Columns			Internal Columns		
	Nq (KN)	*Nf (KN)*	*Ntot(KN)*	*Nq (KN)*	*Nf (KN)*	*Ntot(KN)*
1	244,08	442,20	686,28	488,16	0	488,16
2	203,4	368,50	571,90	406,8	0	406,8
3	162,72	294,80	457,52	325,44	0	325,44
4	122,04	221,10	343,14	244,08	0	244,08
5	81,36	147,40	228,76	162,72	0	162,72
6	40,68	73,70	114,38	81,36	0	81,36

V. Design of first storey columns

As already said, the overall resistance of the first storey obtained in the step III has to be distributed among the columns proportionally to the axial forces obtained in the step IV.

In the table below (Table 4-7), are reported the total axial force, $N_{tot,}$ and the sum of the required bending moment $\sum Mc_{i1,req}$ for both external and internal columns, the $M_{ci1,req}$ for each column, the plastic modulus required, $W_{pl.req}$, the plastic modulus adopted, $W_{pl.adop}$, the profile selected and finally, the bending resistance obtained for the external and internal columns, $Mc_{i1,obt}$.

Table 4-7- Design of the column at the first storey

	N_{tot} (KN)	$\sum M_{ci1,req}$ (KN.m)	$Mci1,req$ (KN.m)	Profile	M_{ci1obt} (KN.m)
External Columns	686,28	984,4843	492,242	HEB320	566,8
Internal Columns	488,16	700,28	350,138	HEB280	412,9

After that, the sum of column plastic moment at the first storey and the multiplier of the seismic horizontal forces corresponding to the ultimate displacement state by applying the equation (4.3), are:

$$\sum_{i=1}^{nc} Mc_{i.1}^{*} = 1959{,}96KN.m \tag{4.23}$$

$$\alpha^{(g)} = 6{,}059 \tag{4.24}$$

VI. Computation of the sum of plastic moment of the columns, reduced due to the action of the axial load, at each storey

The sum of the plastic moment of the columns, $\sum_{i=1}^{nc} Mc_{i.im}^{(t)}$, for each storey was computed by means of the equations 4.18-4.21. The obtained values are reported in the table below (Table 4-8).

Table 4-8- Sum of the plastic moment of the columns, at each storey

Storey	$\sum M_{ci.1}(1)$ (KN.m)	$\sum M_{ci.1}(2)$ (KN.m)	$\sum M_{ci.1}(3)$ (KN.m)	$\sum M_{cim}$ (KN.m)
1	1959,6	1959,6	1959,6	1959,6
2	2052,9	888,2	1472,1	2052,9
3	2421,1	127,4	1275,0	2421,1
4	2487,4	-429,7	1029,2	2487,4
5	2158,7	-685,6	734,8	2158,7
6	1326,6	-543,1	391,7	1326,6

VII. Design of each column at each storey

The required sum of column plastic moments reduced due to the contemporary action of the axial load $\sum M_{req,c,i:im}$, the plastic modulus adopted $W_{pl,adop,}$ the standard shapes selected and the plastic moment adopted $M_{obt,c.i:im}$ are given in Table 4-9.

Table 4-9- Design of the columns at each storey

		N_{tot} (KN)	$\sum M_{cil,req}$ (KN.m)	$M_{cil,req}$ (KN.m)	Profile	$M_{cil,adop}$ (KN.m)	$W_{pl,adop}$ (cm3)
2	*External*	571,90	1199,6	599,8032	HEB360	737,83	2683
	Internal	406,8	853,3	426,6479	HEB320	590,98	2149
3	*External*	457,52	1414,7	707,374	HEB360	737,83	2683
	Internal	325,44	1006,3	503,1644	HEB320	590,98	2149
4	*External*	343,14	1453,5	726,751	HEB360	737,83	2683
	Internal	244,08	1033,9	516,9475	HEB320	590,98	2149
5	*External*	228,76	1261,4	630,7241	HEB340	1766,88	6425
	Internal	162,72	897,3	448,6424	HEB300	513,98	1869
6	*External*	114,38	775,2	387,5971	HEB280	421,85	1534
	Internal	81,36	551,4	275,7029	HEB240	289,58	1053

Analysing the results of the design of the columns for each columns it is clear that the sections selected for the first storey are lower than the ones obtained for the upper floors. Applying the technological condition, the first columns sections were updated for a HEB360 and a HEB320 for the external and the inner columns, respectively. As a consequence the sum of column plastic moment at the first storey and the multiplier of the seismic horizontal forces corresponding to the ultimate displacement state has to be updated, being in this point equal to 2657.44KN.m and 6.5, respectively.

VIII. Final design of the columns at each storey

After applying the technological condition, the design of the columns sections have been redo. The final design of the columns sections are present in the Table 4-10 and in Figure 4.9.

Table 4-10- Final design of the columns at each storey

		N_{tot} (KN)	$\sum M_{cil,req}$ (KN.m)	$M_{cil,req}$ (KN.m)	Profile	$M_{cil,adop}$ (KN.m)	Wpladop (cm3)
2	*External*	571,90	987,2	493,5968	HEB360	688,31	2683
	Internal	406,80	702,2	351,1019	HEB300	513,98	1869
3	*External*	457,52	1279,0	639,4801	HEB360	706,22	2683
	Internal	325,44	909,7	454,8706	HEB300	513,98	1869
4	*External*	343,14	1381,4	690,719	HEB360	724,14	2683
	Internal	244,08	982,6	491,3175	HEB300	513,98	1869
5	*External*	228,76	1236,0	618,0184	HEB340	662,20	2408
	Internal	162,72	879,2	439,6047	HEB300	513,98	1869
6	*External*	114,38	775,2	387,5971	HEB280	421,85	1534
	Internal	81,36	551,4	275,7029	HEB240	289,58	1053

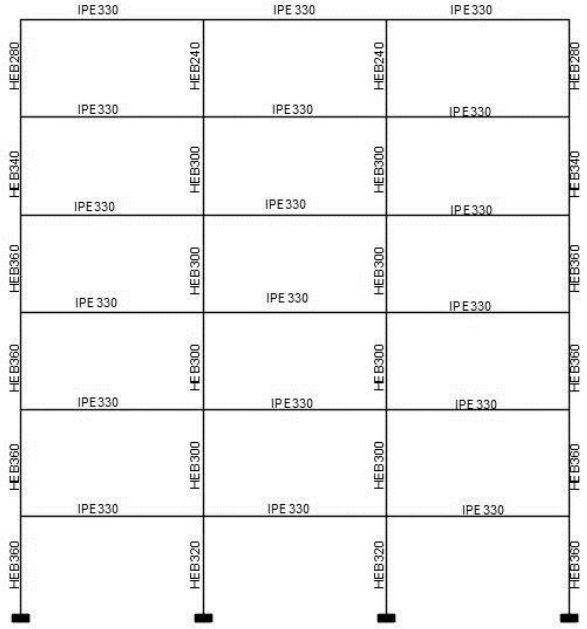

Figure 4.9- Final design of the frame elements

Damage limitation

After the preliminary design, a static elastic analysis has been carried out to check the serviceability requirements according to EC8-1(4.4.3)(CEN 2010b). This analysis has been done for a behaviour factor equal to 1.0, i.e the lateral loads have been multiplied by the behaviour factor assumed (q=6). The results of the analysis (Table 4-11) point out that the structure fulfils the drifts limitations requirements of EC8-1-1.

Table 4-11- Serviceability requirements - interstorey drifts

Storey	Displ [m]	drv	h [m]	0,0075h	drv<0,0075h
6	0,312	0,003	3,2	0,024	**OK**
5	0,286	0,005	3,2	0,024	**OK**
4	0,243	0,008	3,2	0,024	**OK**
3	0,18	0,009	3,2	0,024	**OK**
2	0,106	0,009	3,2	0,024	**OK**
1	0,035	0,004	3,5	0,02625	**OK**

4.3. Modelling for nonlinear analyses

4.3.1. Elements mechanical and geometrical nonlinearities

Mechanical nonlinearities of beams/columns elements has been modelled in *SeismoStruct.* In *SeismoStruct* the material nonlinearity is taking into account by considered distributed inelasticity elements, using the so-called fibre approach to represent the cross section behaviour. Each fibre is associated with a uniaxial stress-strain relationship and the sectional stress-strain state of beam-column elements is obtained by the integration of the nonlinear uniaxial stress-strain response of the individual fibres in which the section has been subdivided. Such approach bring some advantages, as the fact that does not require a prior moment-curvature analysis of members and it is not necessary to introduce any element hysteric curve because it is already implicitly define by the material constitutive models. Furthermore, a direct modelling of axial load bearing moment interaction, both strength and stiffness is defined and a straightforward representation of biaxial loading and interaction between flexural strength in orthogonal directions.

Distributed inelasticity elements can be implemented with two different finite elements formulation, namely *force-based* or *displacement-base* formulations. With reference to the frame adopted, an inelastic displacement-base formulation has been adopted for the beams and columns elements in which each element has been discretized into 5 integration sections. In addition both beams and columns elements has been subdivided into 4 elements in order to have more accurate results.

Regarding the geometrical nonlinearities, the *SeismoStruct* software have automatically into account the P-Delts effects of the beam-columns elements, through the employment of a total co-rotational formulation. This formulation is based on an exact description of the kinematic transformations associated with large displacements and 3D rotations of the beam-column elements and therefore, permits a correct definition of the element´s independent deformations and forces and of the effects of geometrical nonlinearities on the stiffness matrix.

At the local chord system of the element, six basic displacement degrees of freedom and the corresponding element internal forces are defined (see Figure 4.10).

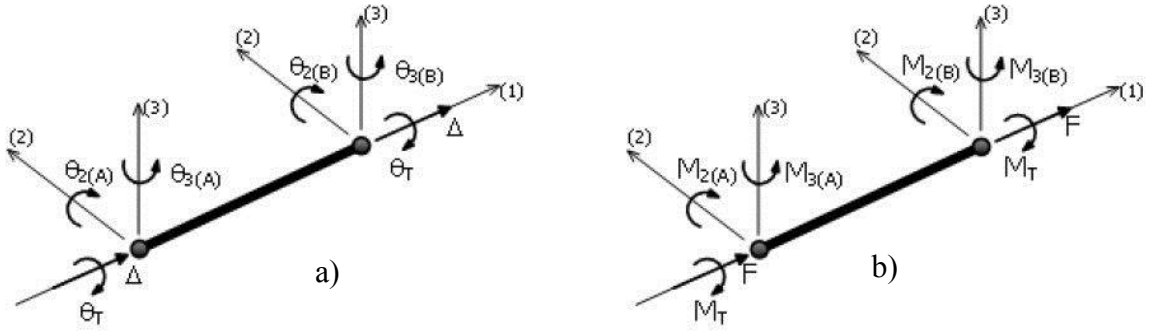

Figure 4.10-Local chord system of beam/column elements; a) displacement degrees of freedom; b) internal forces

4.3.2. Material

All the frame elements were designed with structural S275 steel (f_y=275Mpa). For the columns, a bilinear steel model has been employed for defining the steel material, with the properties present in the Table 4-12.

Table 4-12- Steel properties inserted in the model

Element	Steel	E [Gpa]	fy [Mpa]	εult	μ	γ [kN/m3]
Columns	S275	210	275	0,1	0	78
Beams			-	-	-	

As it can be seen by the strain hardening parameter adopted, the material has been modelling without hardening, i.e the behaviour of the material exhibits an elastic-perfectly plastic behaviour. Although the real behaviour of the steel exhibit hardening, the equilibrium curve is not affected by hardening so, in order to compare the pushover curve with the equilibrium curve, the material has been modelling with an elastic-perfectly plastic behaviour.

In order to assure that the yielding of the beams do not occur, the behaviour of the material has been modelling as elastic, with modulus of elasticity, *E*, equal to 210 Gpa.

4.4. Modelling and calibration of the beam-to-column connections

In view of what was reported in the **chapter 3**, four beam-to-column connection specimen have been selected in order to evaluate their influence on the seismic response of the MRF. Specifically, the TS-M2-460-CYC09, *TS-M1-460-CYC 08*, *TSJ-SA300-320-CYC 12* and the

TSJ-H-SA300-260-CYC 13 specimen have been selected. In addition, a full-strength connection has been selected in order to compare the two different approaches, i.e. dissipative zones at the beams end or in the beam-to-column connections, in this case, in the friction dampers. The specimen selected is the *EEP-DB-CYC03*, investigated by Salerno (Latour & Rizzano 2014), which is a full strength extended end-plate designed in order to develop plastic hinges in the beam by cutting the beam flanges (RBS), called also "dog bone".

Furthermore, a study of the influence on the resistance of the connection by changing the elements beam/column section is presented in this chapter for one of the friction joints.

4.4.1. Calibration of the hysteretic behaviour of the connections

In order to calibrate the hysteric behaviour of the analysed connections a simple frame has been adopted. The adopted frame has 1m height and the beam has a length of 1m as well. For the columns a HEB200 profile has been adopted and an IPE270 for the beams since those were the ones that have been used for the experimental analyses on the connections. Also, a higher yield strength was given to the frame elements in order to has no influence on the hysteretic behaviour of the connection.

The beam-to-column connections have been modelled in the software *SeismoStruct* by means of link elements. A link element is a 3D element connected to two initially coincident structural nodes and require the definition of an force-displacement or moment-rotation response curve for each of its local six degrees of freedom (F_1,F_2,F_3,M_1,M_2,M_3) (Figure 4.11)

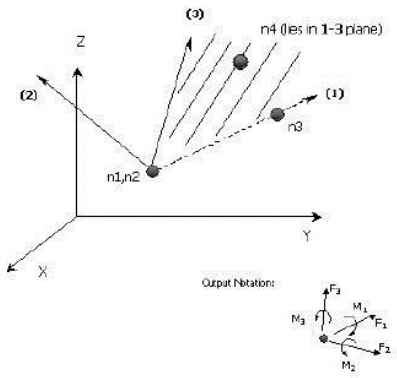

Figure 4.11- Definition of SeismoStruct link

For the degrees of freedom F_1, F_2, F_3, M_1 and M_3, was used a linear symmetrical behaviour with an initial stiffness K_0 = 1,000E+10. For the M_2 degree of freedom was used a *smooth curve* representing the cyclic behaviour of the connections obtained with the experimental tests.

The smooth curve, Figure 4.12, is a hysteric loop curve that has been formulated with rules for strength and stiffness degradation and pinching by Sivaselvan and Reinhorn (Sivaselvan &

Reinhorn 2000). It needs the definition of twenty-two parameters, eleven related to the backbone curve and eleven parameters related to the strength, stiffness and pinching rules.

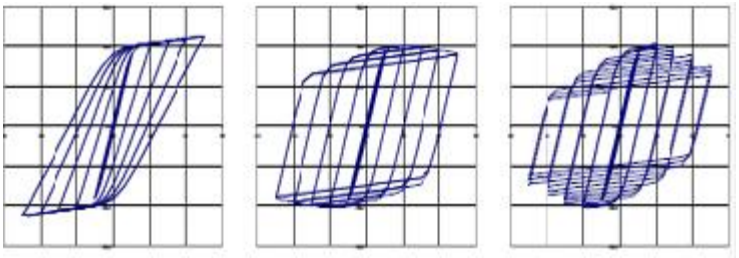

Figure 4.12-Hysteretic M- θ curve for a smooth curve (examples) (Seismosoft 2014)

The frame was analysed by means of a static time-history analysis with the same loading history of the experimental tests on the connections. As an example, in the Figure 4.13 the loading history using for the experimental analysis on the connection with the friction damper M2 is showed. Comparing the moment-rotation curves and the amount of energy dissipation in each cycle provided by the *SeismoStruct* software with those obtain with the experimental results allowed to calibrate the joint model parameters.

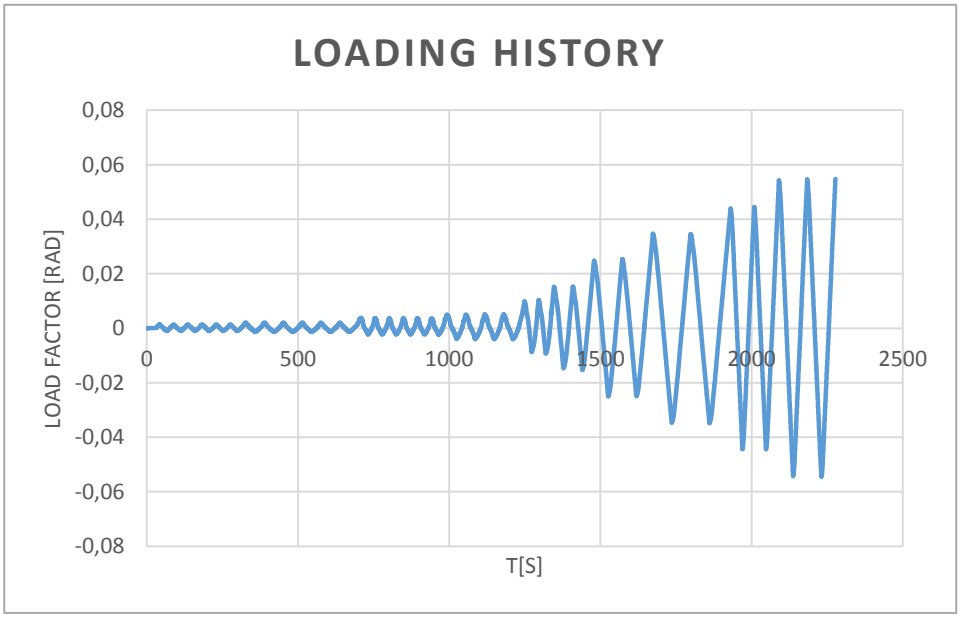

Figure 4.13- Cyclic loading history for the connection with the friction damper M2

1. Calibration of the specimen TS-M1-460-CYC08

In Table 4-13 is reported the parameters adopted for the smooth curve of the specimen *TS-M1-460-CYC08*. Furthermore, in Figure 4.14 and Figure 4.15 is reported the hysteretic curves and the energy dissipation of the specimen for the experimental tests and for the *SeismoStruct*

model. As can be seen, the model hysteretic curve is in a good agreement with the experimental hysteretic curve and the energy dissipation in the last cycles has an energy dissipation equal to around 80%-96% of the energy dissipation found in the experimental tests.

Table 4-13-Smooth curve parameters for the specimen TS-M1-460-CYC 08

Smooth Curve Parameters	Specimen TS-M1-460-CYC 08
Initial Flexural Rigidity ,EI	11763,66
Cracking Moment Positive (KNm)	54,97
Yield Moment Positive (My*+) (KNm)	118,64
Yield Curvature Positive (φmax+)	0,024
Ultimate Curvature Positve (φu+)	0,2
Post yield stiffness positve as %3IEP	0,0041
Cracking Moment Negative (KNm)	-58,16
Yield Moment Negative (My*-) (KNm)	-132,50
Yield Curvature Negative (φmax-)	-0,013
Ultimate Curvature Negative(φu-)	-0,2
Post yield stiffness negative as %3IEN	0,0027
Stiffness Degrading Parameter α	10
Ductility- based strength Decay Parameter β1	0,9
Hysteretic energy based-strength decay parameter β2	0,6
Smoothness parameter for elastic-yield transition N	0,5
Parameter for shape of unloading η	0,5
Slip length parameter s	0,1
Slip Sharpeness parameter	100
Parameter for mean moment of slip λ	0,4
Exponent of gap closing spring Ngap	2
Gap closing curvature parameter φgap	1000
Gap stiffness coefficient Kgap-closing	2

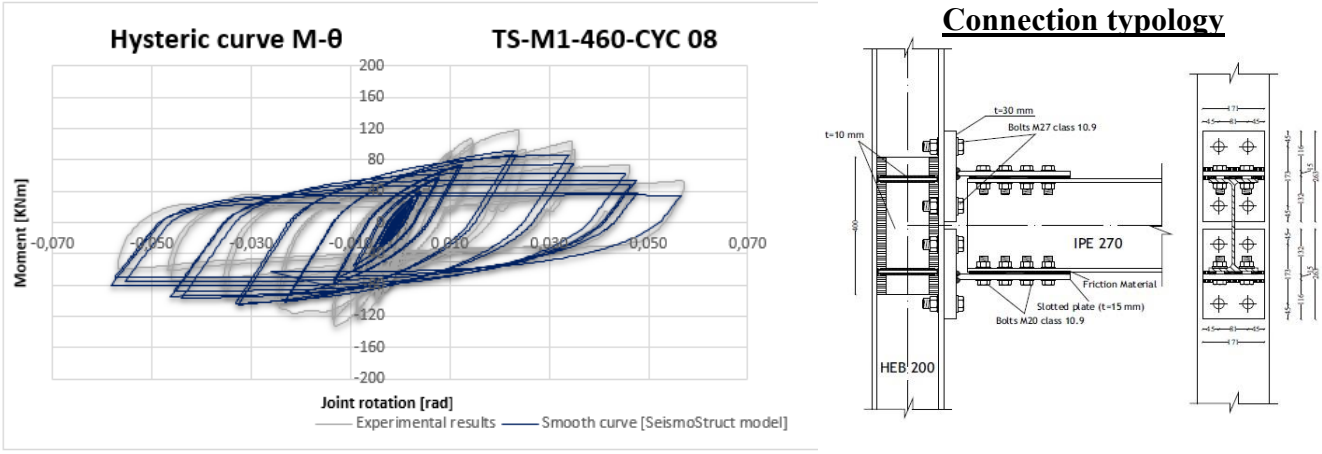

Figure 4.14-Calibration of the hysteretic curve for the specimen TS-M1-460-CYC08

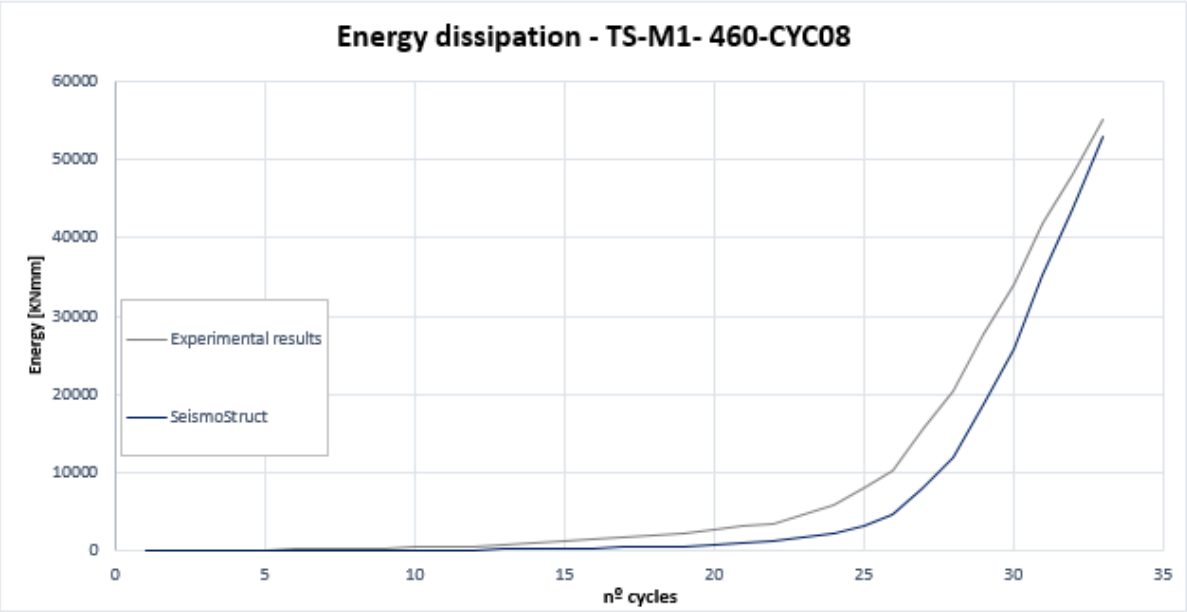

Figure 4.15-Energy dissipation of the specimen TS-M1-460-CYC08 for the SeismoStruct model vs experimental tests

2. Calibration of the specimen TS-M2-460-CYC09

The connection *TS-M2-460-CYC09* has been modelled with the parameters reported in the Table 4-14, in which results the hysteretic and energy dissipation curve reported in Figure 4.16 and Figure 4.17, respectively. The curves represent by the model is in agreement with the curve found for the experimental tests and in particular, regarding the energy dissipation curve, in the last 8 cycles, the model is able to dissipate values between 80%%-93% of the energy found in the experimental cycles for the same cycles.

Table 4-14-Smooth parameters for the specimen TS-M2-460-CYC09

Smooth Curve Parameters	Specimen TS-M2-460-CYC 09
Initial Flexural Rigidity ,EI	30000
Cracking Moment Positive (KNm)	90
Yield Moment Positive (My*+) (KNm)	100
Yield Curvature Positive (φmax+)	0,013
Ultimate Curvature Positve (φu+)	0,2
Post yield stiffness positve as %3IEP	0,03
Cracking Moment Negative (KNm)	-90
Yield Moment Negative (My*-) (KNm)	-120
Yield Curvature Negative (φmax-)	-0,015
Ultimate Curvature Negative(φu-)	-0,2
Post yield stiffness negative as %3IEN	0,03
Stiffness Degrading Parameter α	75
Ductility- based strength Decay Parameter β1	0,7
Hysteretic energy based-strength decay parameter β2	0,45
Smootheness parameter for elastic-yield transition N	5
Parameter for shape of unloading η	0,5
Slip length parameter s	0,25
Slip Sharpeness parameter	100
Parameter for mean moment of slip λ	0,4
Exponent of gap closing spring Ngap	2
Gap closing curvature parameter φgap	1000
Gap stiffness coefficient Kgap-closing	2

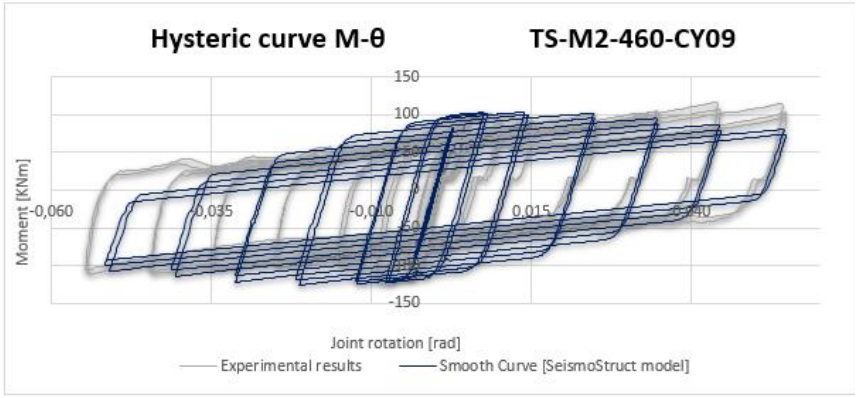

Connection typology

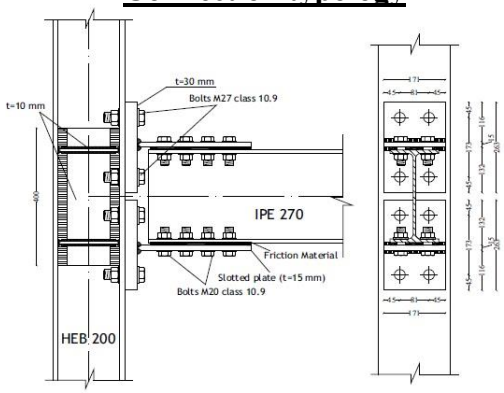

Figure 4.16-Calibration of the hysteretic curve for the specimen TS-M2-460-CYC09

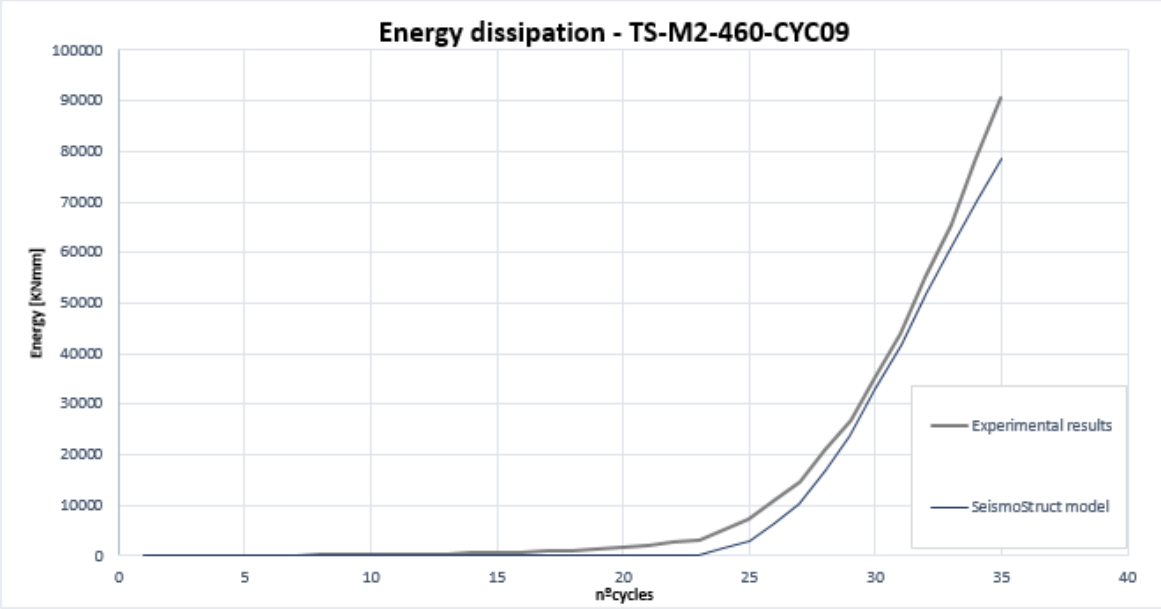

Figure 4.17-Energy dissipation of the specimen TS-M2-460-CYC09 for the SeismoStruct model vs experimental tests

3. Calibration of the specimen TSJ-SA300-320-CYC12

The analysed specimen has been calibrated by adopting the parameters in Table 4-15. In Figure 4.18 and Figure 4.19 is reported the hysteretic curves of the specimen and the energy dissipation for the considered cycles.

Table 4-15- Smooth curve parameters for the specimen TSJ-SA300-320-CYC12

Smooth Curve Parameters	Specimen TSJ-SA300-320-CYC 12
Initial Flexural Rigidity ,EI	24762,4
Cracking Moment Positive (KNm)	116,271042
Yield Moment Positive (My*+) (KNm)	169,37
Yield Curvature Positive (φmax+)	0,014
Ultimate Curvature Positve (φu+)	0,8
Post yield stiffness positve as %3IEP	0,0031
Cracking Moment Negative (KNm)	-74,55
Yield Moment Negative (My*-) (KNm)	-122,93
Yield Curvature Negative (φmax-)	-0,006
Ultimate Curvature Negative(φu-)	-0,8
Post yield stiffness negative as %3IEN	0,0032
Stiffness Degrading Parameter α	200
Ductility- based strength Decay Parameter β1	0,2
Hysteretic energy based-strength decay parameter β2	0,3
Smootheness parameter for elastic-yield transition N	5
Parameter for shape of unloading η	0,5
Slip length parameter s	0
Slip Sharpeness parameter	100
Parameter for mean moment of slip λ	0
Exponent of gap closing spring Ngap	2
Gap closing curvature parameter φgap	1000
Gap stiffness coefficient Kgap-closing	2

By observing both curves, it can be seen that the modelled curve presents a good estimation of the real behaviour of the connection, even if not perfect.

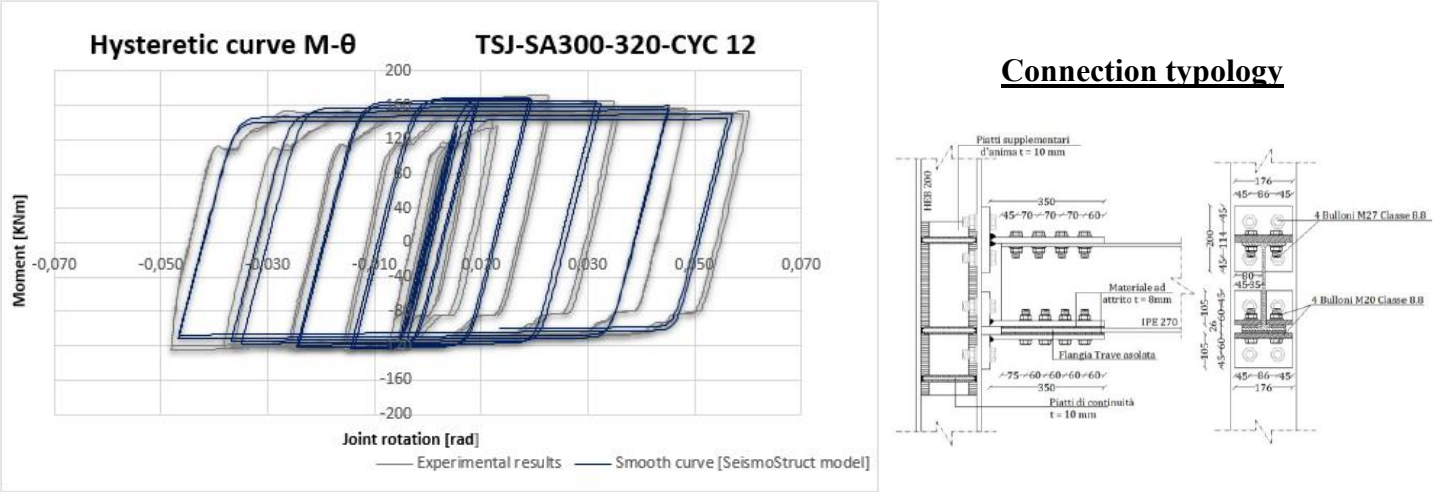

Figure 4.18-Calibration of the hysteretic curve for the specimen TSJ-SA300-CYC12

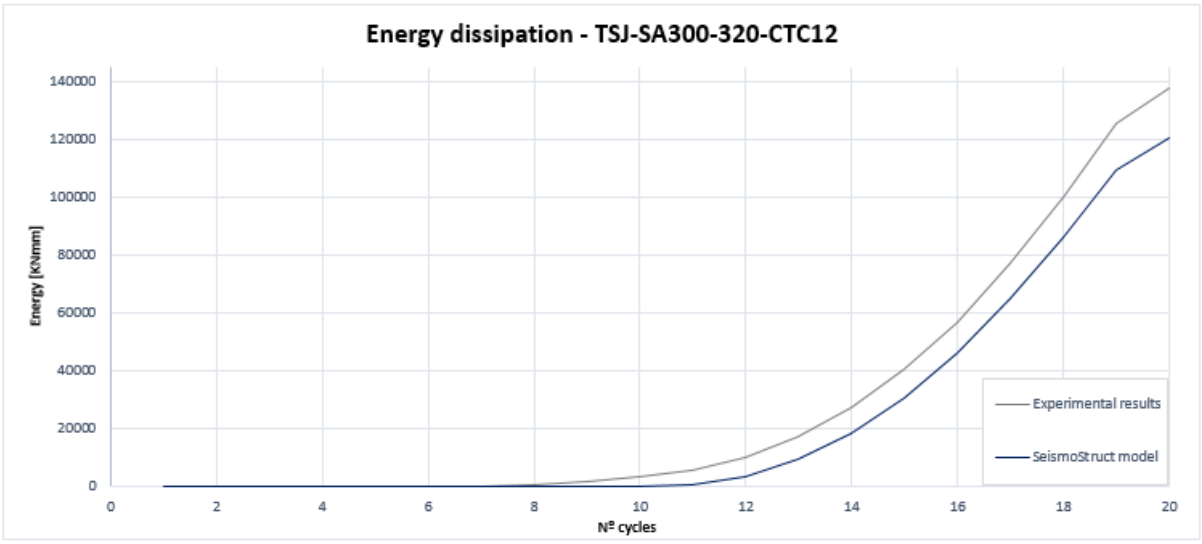

Figure 4.19- Energy dissipation of the specimen TSJ-SA300-320-CYC12 for the SeismoStruct model vs experimental tests

4. Calibration of the specimen TSJ-H-SA300-260-CYC13

The experimental results for the specimen *TSJ-H-SA300-260-CYC13* have been calibrated for the parameters reported in Table 4-16, resulting in the hysteretic and energy dissipation curves reported in Figure 4.20 and Figure 4.21, respectively.

Table 4-16- Smooth curve parameters for the specimen TSJ-H-SA300-260-CYC13

Smooth Curve Parameters	Specimen TSJ-H-SA300-260-CYC 13
Initial Flexural Rigidity ,EI	95000
Cracking Moment Positive (KNm)	188,29
Yield Moment Positive (My*+) (KNm)	194,55
Yield Curvature Positive (φmax+)	0,00000001
Ultimate Curvature Positve (φu+)	0,5
Post yield stiffness positve as %3IEP	0,000000911
Cracking Moment Negative (KNm)	-140,65
Yield Moment Negative (My*-) (KNm)	-146,57
Yield Curvature Negative (φmax-)	-0,00000001
Ultimate Curvature Negative(φu-)	-0,5
Post yield stiffness negative as %3IEN	0,000000874
Stiffness Degrading Parameter α	200
Ductility- based strength Decay Parameter β1	0,2
Hysteretic energy based-strength decay parameter β2	0,3
Smoothness parameter for elastic-yield transition N	5
Parameter for shape of unloading η	0,5
Slip length parameter s	0,25
Slip Sharpeness parameter	100
Parameter for mean moment of slip λ	0,4
Exponent of gap closing spring Ngap	2
Gap closing curvature parameter φgap	1000
Gap stiffness coefficient Kgap-closing	2

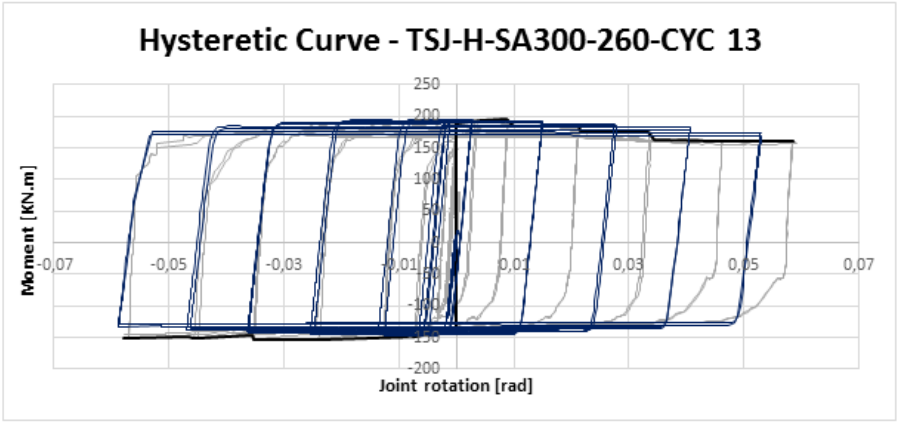

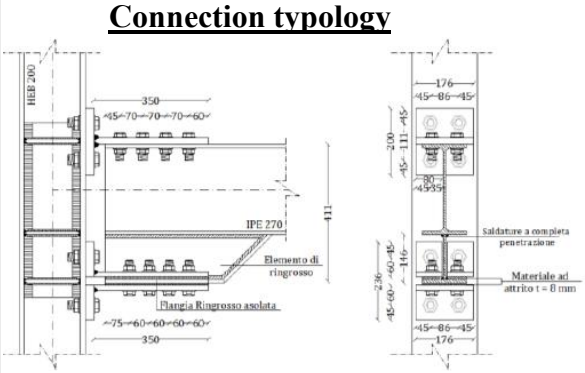

Figure 4.20-Calibration of the hysteretic curve for the specimen TSJ-H-SA300-CYC13

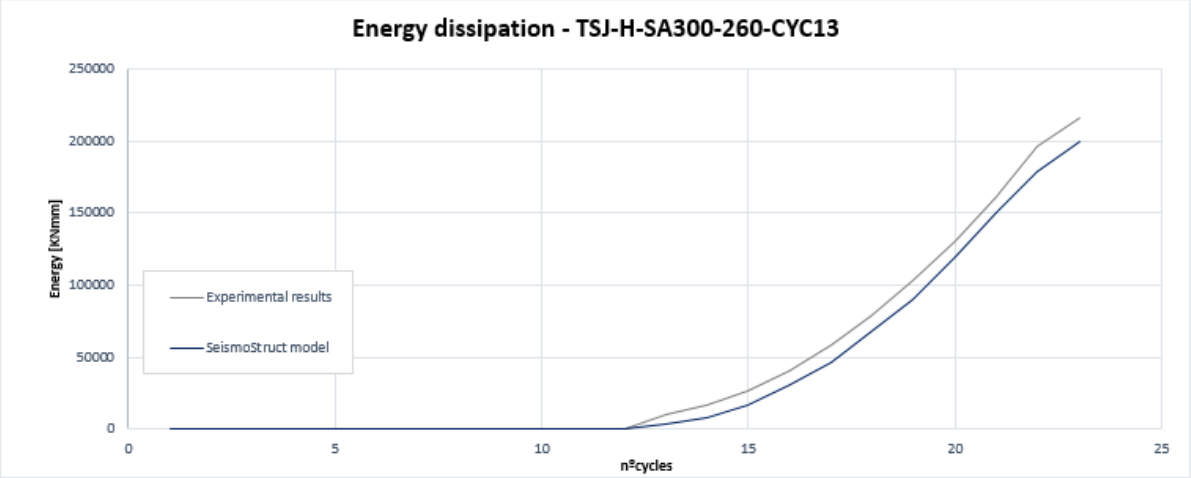

Figure 4.21-Energy dissipation of the specimen TSJ-H-SA300-260-CYC13 for the SeismoStruct model vs experimental tests

5. Calibration of the specimen EEP-DB-CYC03

The Table 4-17 report the smooth curve parameters adopted for the analysed specimen and in Figure 4.22 and Figure 4.23 is showed the hysteretic and energy dissipation for both experimental tests and smooth model. As can be seen, those curves are in perfect agreement with the experimental results.

Table 4-17- Smooth curve parameters for the specimen EEP-DB-CYC03

Smooth Curve Parameters	Specimen EEP-DB-CYC03
Initial Flexural Rigidity ,EI	47238,74
Cracking Moment Positive (KNm)	140
Yield Moment Positive (My*+) (KNm)	190
Yield Curvature Positive (φmax+)	0,013
Ultimate Curvature Positve (φu+)	0,2
Post yield stiffness positve as %3IEP	0,01
Cracking Moment Negative (KNm)	-140
Yield Moment Negative (My*-) (KNm)	-200
Yield Curvature Negative (φmax-)	-0,0107
Ultimate Curvature Negative(φu-)	-0,2
Post yield stiffness negative as %3IEN	0,0001
Stiffness Degrading Parameter α	10
Ductility- based strength Decay Parameter β1	0,5
Hysteretic energy based-strength decay parameter β2	0,01
Smootheness parameter for elastic-yield transition N	1
Parameter for shape of unloading η	0,5
Slip length parameter s	0,25
Slip Sharpeness parameter	10
Parameter for mean moment of slip λ	1
Exponent of gap closing spring Ngap	0,2
Gap closing curvature parameter φgap	0,2
Gap stiffness coefficient Kgap-closing	0,2

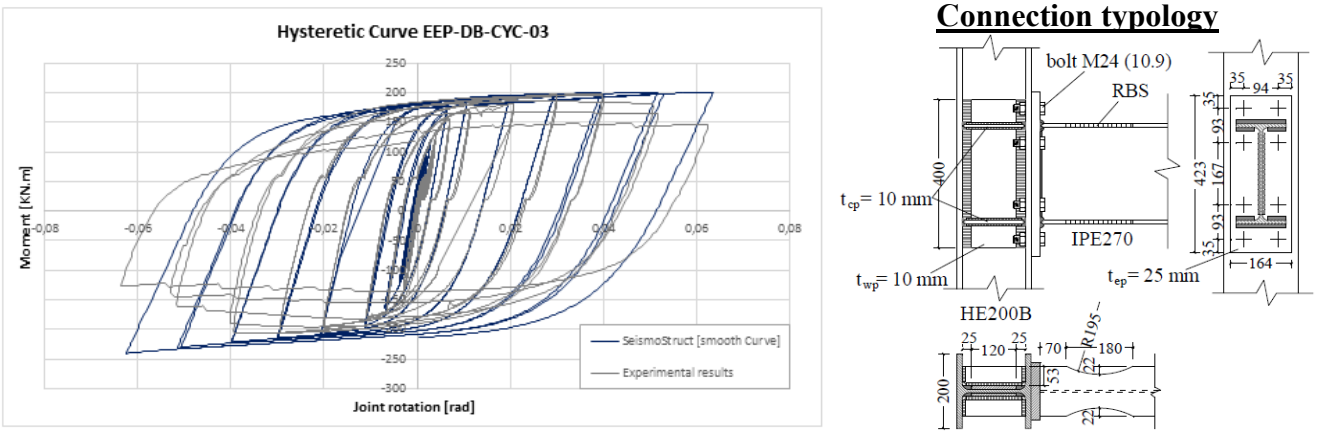

Figure 4.22-Calibration of the hysteretic curve for the specimen EEP-CYC03

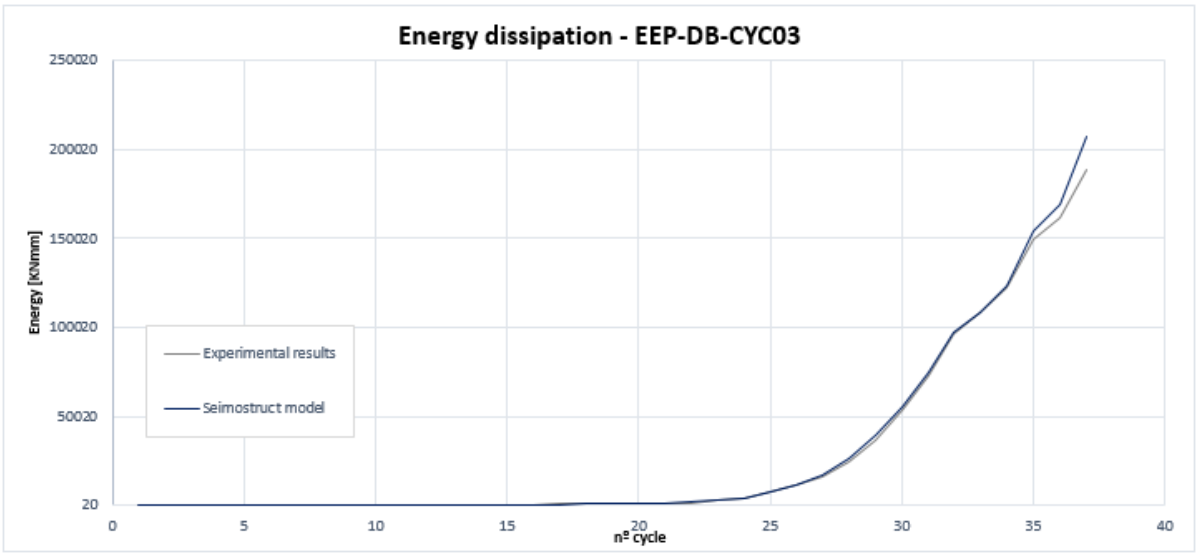

Figure 4.23-Energy dissipation of the specimen EEP-DB-CYC03 for the SeismoStruct model vs experimental tests

4.4.2. Influence of the beam/column sections on the resistance of the connections

As the experimental studies and the calibration of the connections were made for an IPE270 for the beam and a HEB200 for the column and since, the elements of the analysed MRF have higher sections, a study of the influence of elements section on the resistance of the connections has been made.

This study has been made with a software for steel connections and for the connection reported in Figure 4.24. The connection adopted is a simplified model of the friction joints reported in the chapter 3 since it does not have the friction damper component.

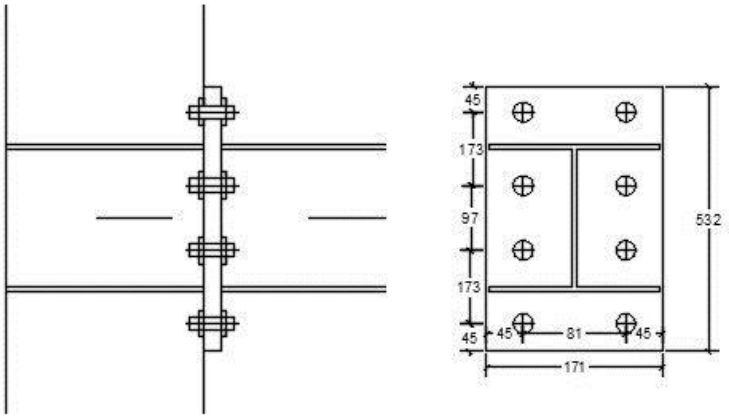

Figure 4.24- Connection typology adopted for the study of the influence of the elements section on the resistance of the connection

First, the moment resistance M_{jrd} and the initial stiffness S_{jini} for the reported connection with an IPE270 for the beams and a HEB200 for the columns were determined with the software, obtaining a resistance moment equal to 117 KNm and an initial stiffness of approximately 37000 KNm/rad. Then, comparing these results to the ones obtained for the analysed friction joints it can be observed that those results are very closed to the ones obtained for the friction joint with the rubber M_2 (about 97%) and, for that reason, the influence of varying the elements section on the resistance this connection could be made with the simplified model.

The study has been divided in two parts: first changing the column sections, keeping the beam section and then, changing the beam section (from an IPE270 to an IPE330) keeping the column section. The first part showed that the column section does not have a greater influence on the resistance of the connection. On contrary, by increasing the beam section the analysis showed an improvement of about 20% on the resistance of the connection (Table 4-18).

Table 4-18 - Study of the influence on the resistance of the connection by increasing the beam section

	Moment Resistance, M_{jrd} [KNm]		
	IPE 270	*IPE 330*	*IPE270 vs IPE330*
HEB 200	116,72	128,25	8,99%
HEB220	127,72	140,54	9,12%
HEB 240	139	154	9,74%
HEB 280	139,99	169	17,17%
HEB 300	133,22	167	20,23%
HEB 340	137,05	173	20,78%
HEB360	138,12	175	21,07%

After this study, it is clear that by increasing the section of the beam, the resistance and stiffness of the connection is significantly improved. In this view, and keeping the approximation found between the friction joint with the damper M_2 and the approximate model (about 97%), the yield moment and the initial stiffness adopted on the calibration of the model (point 4.2.1 of

this chapter) have been change for a yield moment equal to 170KNm and an initial stiffness equal to 50000 KNm/rad.

Calibrating again the connection, the following hysteretic curve was obtained (Figure 4.25). It is important to say that only the above parameters have been changed on the definition of the curve of the hysteretic behaviour of the connection.

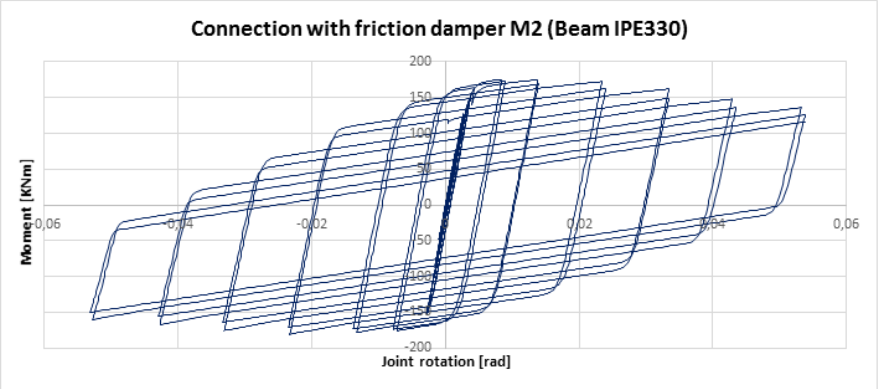

Figure 4.25 - Hysteretic curve for the friction connection with the damper M2 with the increase of the beam section

5. Seismic Response of the frame

5.1. Nonlinear Static Analysis

The pushover analysis has been lead under control displacement and taking into account both mechanical and geometrical nonlinearities, as described in the subchapter 4.3. The target displacement assumed has the same assumed for the preliminary design, i.e a rotation supply of 0.04rad and so, a target top sway displacement of 0.78m.

The aim of a pushover analysis is to check the design procedure, i.e the development of the global collapse mechanism and the localization of the plastic hinges in the end of the analysis. It also important to underline that the role of the friction dampers in the pushover analysis is to prevent the yielding of the beams.

Furthermore, the friction joints were modelling by means of link elements with a rigid-perfectly plastic behaviour in order to provide a better comparison between the capacity curve of the structure and the equilibrium mechanism curve derived by the plastic design procedure. The moment resistance of the link element was assumed equal to the moment resistance of the beam so that, the maximum moment achieved by the damper is always lower than the one achieved by the beams and, for that reason, the yield occurs in the friction dampers rather than the beams end.

The results of the pushover curve are mainly the base shear-displacement curve or the capacity curve. According to EC8-1(CEN 2010b), this curve has to be done for values of displacements between 0 and 150% of the target displacement, so, in this case, the curve has been made for a displacement range between 0 and 1.17m (150%x0.78m).

In Figure 5.1 is present the capacity curve of the frame, which is compare to the capacity curve of the same frame with a traditional approach, i.e strength connections and to the mechanism equilibrium curve derived by the design procedure described in 4.2.3. The results shows that the capacity curve is in total agreement with the softening branch of the equilibrium mechanism curve, which means that a global mechanism is developed. In addition, the Figure 5.2 provides a further confirmation of the fulfilment of the design objective, since the pattern of yielding developed at the design ultimate top sway displacement, point outs the yielding of the friction dampers rather than the beams or the columns which is in perfect agreement with the global mechanism. Furthermore, at the design ultimate displacement the collapse mode is not fully developed because the plastic hinges in the friction dampers of the top storey are still not formed, which means that even after the design displacement the structure remains safe.
Concerning the capacity curve of the frame with strength joints, it shows that this frame has a higher lateral stiffness, because for achieving the same displacement than the frame with

friction joints it needs a higher shear base force. This result was expected because one of the disadvantages of using partial joints is larger lateral displacements, i.e the reduction of the lateral stiffness when comparing to the traditional strength joints.

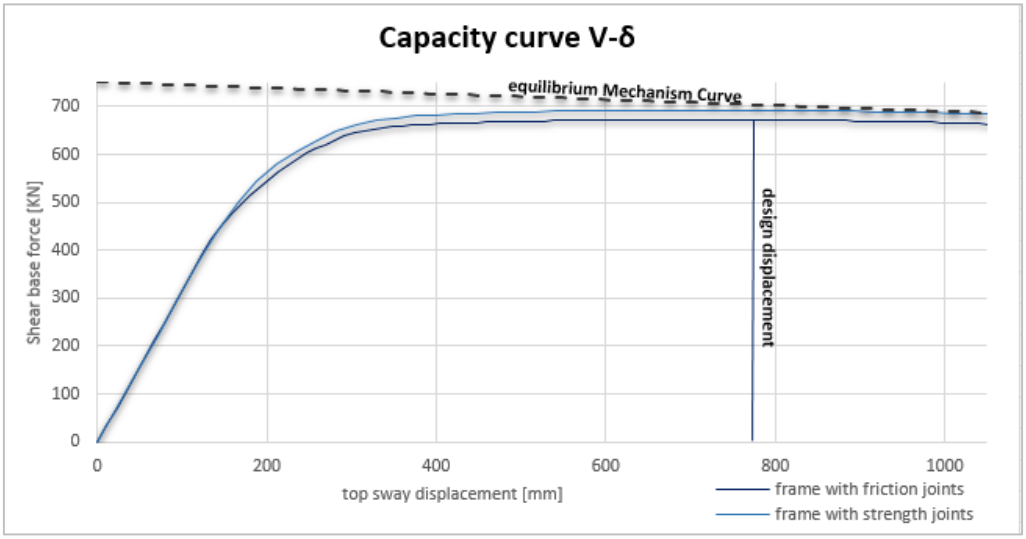

Figure 5.1-Capcity Curve V-δ

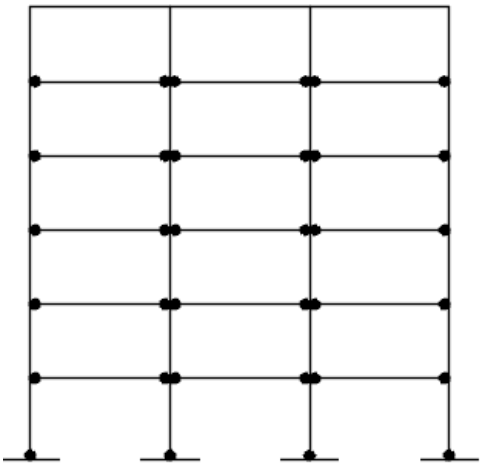

Figure 5.2- Activation of the friction dampers at the design displacement

In addition, the stability of the columns in compression has been performed at each step of the non-linear analysis.

5.2. Nonlinear incremental dynamic analysis

A further validation of the procedure have been made by means of incremental dynamic analyses (*IDA*) by testing the frame under different accelerograms. According to the seismic Eurocode(CEN 2010b), a nonlinear dynamic analysis should be done at least for seven different accelerograms with similar characteristics (in magnitude or/and duration). In particular, nine different earthquakes from the PEER ("*Pacific Earthquake Engineering Research Centre*") database have been chosen.

Each of the assumed earthquakes have been linearly scaled in order to provide increasing values of the spectral acceleration *Sa(T1)* corresponding to the fundamental period of the structure. The scale factor used is the relationship between the spectral acceleration corresponding to the fundamental period and the peak ground acceleration motion *PGA* of each one of the accelerograms. In particular, the analyses have been repeated by increasing the spectral acceleration until at least one of the connections reached the design rotation equal to 0.04rad. In fact, the seismic code (CEN 2010b) only permits the use of recorded accelerograms if they were scaled in order to the a_gS value of the region where the structure is inserted. In addition, it helps to ensure that the spectrum of the individual accelerograms are similar to the spectrum of reference, at least around the fundamental period of the structure, reducing the variability of the seismic response of the structure from record to another.

The purpose in doing several incremental dynamic analyses is to verify the design goal of free from damage structures under destructive seismic events. In particular, the results are presented in terms of:

- **Maximum required damper stroke / ultimate plastic rotation (in the full strength joint):** maximum damper stroke required to the friction damper or the ultimate plastic rotation of the connection (in the case of full strength joint) for a certain spectral acceleration;

- **Maximum interstorey drift ratio (MIDR):** maximum interstorey drift ratio in all storey for a certain spectral acceleration.

Each one of the beam-to-columns specimens have been introduced in the MRF by means of link elements with the behaviour and parameters reported in the subchapter 4.4.

5.2.1. IDA analyses for the MRF with the specimen TSJ-H-SA300-260-CYC13

For the specimen the MRF with the specimen TSJ-H-SA300-260-CYC13, an eigenvalue analysis carried out by the SeismoStruct showed that the fundamental period of the MRF equipped with this connection is 1,2s. In the Table 5-1 is reported the main data for the selected accelerograms. As was said above, the selected accelerograms have been scaled in order to have a similar behaviour around the fundamental period of the structure. In Figure 5.3 can be observed that the ordinate of the average spectrum as well as it shape is compatible with the elastic spectrum given by EC8 in a wide range of periods between the fundamental one. In fact,

in the fundamental period of the structure (T1=1,17s), all the considered spectrums have the same spectral acceleration equal to 3.49 m/s^2.

Table 5-1- Accelerograms data [for the specimen TSJ-H-SA300-260-CYC13]

Earthquake	Date	Component	PGA (g)	Length [s]	Sa (T_1=1,2s)
Helena	31-10-1935	N-S	0,15	39,99	0,03
Friuli	15-09-1976	N-S	0,11	26,39	0,09
Imperial Valley	15-10-1979	N-S	0,37	28,35	0,44
Irpinia	23-11-1980	N-S	0,13	35,80	0,22
Victoria Mexico	09-06-1980	N-S	0,15	26,91	0,30
Coalinga	02-05-1983	N-S	0,17	29,99	0,20
Spitak America	12-07-1988	N-S	0,20	19,89	0,29
Northridge	17-01-1994	N-S	0,23	39,90	0,22
Kobe	16-01-1995	N-S	0,25	40,95	0,21

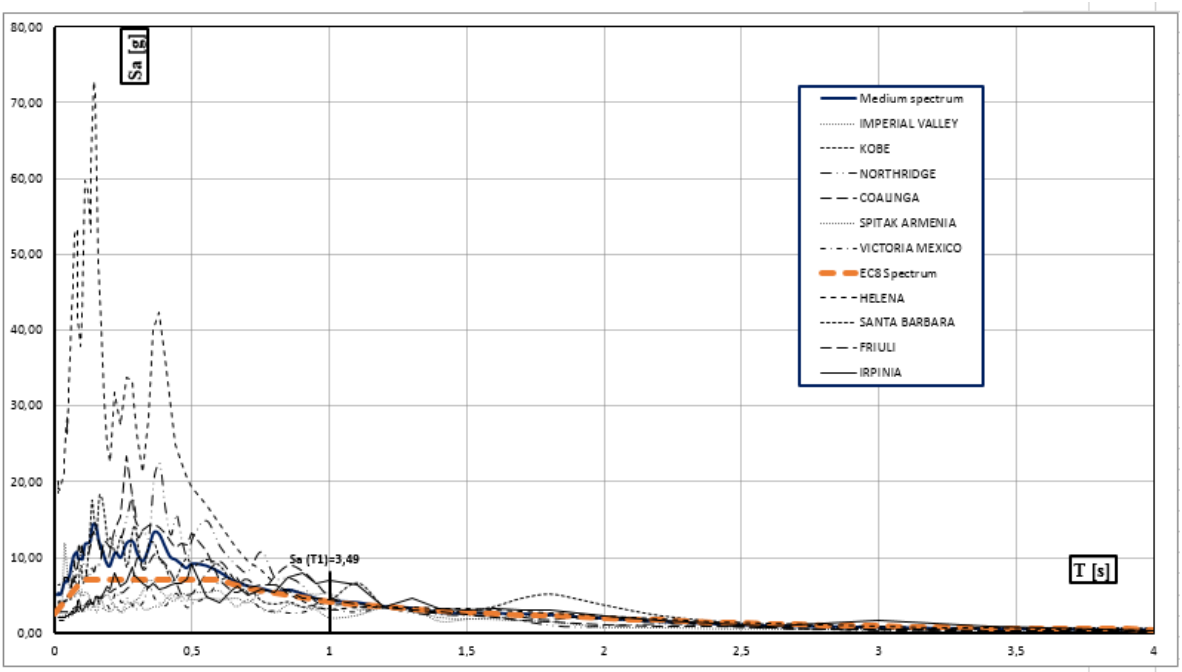

Figure 5.3- Response spectra for the considered ground motion [for the specimen TSJ-H-SA300-260-CYC13]

The typology of this specimen is the one that have been reported in the Figure 3.9 of the sub-chapter 3.2. Concerning its typology, the design ultimate stroke has been assumed equal to 0,019m, since the design rotation is 0.04rad and lever arm of the beam and the haunch is equal to 471mm (330mm+141mm= 471mm). The hysteric behaviour of this specimen is the one present in Figure 4.20 of the subchapter 4.4. In Figure 5.4 is reported the required damper stroke versus the spectral acceleration for the friction dampers in the beam-to-column connection.

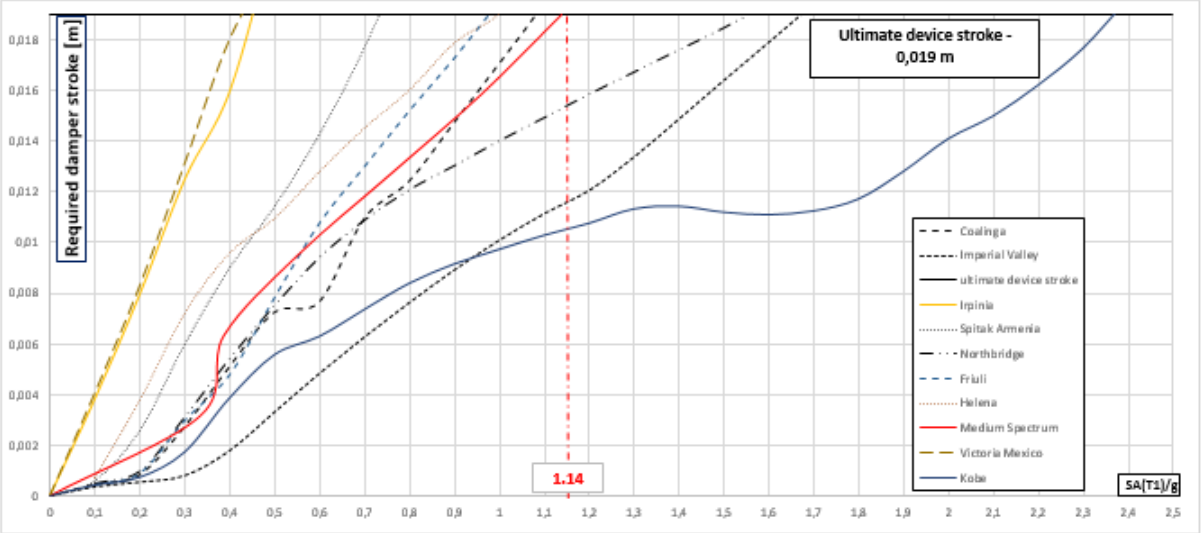

Figure 5.4- Required damper stroke vs spectral acceleration for the friction damper in beam-to-column connections [for the specimen TSJ-H-SA300-260-CYC13]

These IDA curves shows that the calibration of the friction damper allows to withstand spectral acceleration in a range between 0.43g and 2.4g, depending on the ground motion. In addition, for the medium spectrum the structure reach the ultimate device stroke for a spectral acceleration equal to 1.14g, which represents a spectral acceleration with a value approximately 3.2 times more than the spectral acceleration given by the seismic code(CEN 2010b) for the fundamental period of the structure (0.356g = 3.49 m/s^2). From these observations, is evident that the considered frame has a superior capacity to that required by the current design seismic codes.

In Figure 5.5 is reported the maximum interstorey drift ration versus the spectral acceleration. In particular, these curves shows that the structure can withstand high spectral acceleration and remaining safe since the design drift ratio (0.04 rad) is reached for an average value of 1.23g. Moreover, these curves also confirms that the structure can reach greater drift ratio values than the maximum drift ratio required by the seismic code (0.0075h) and remain free from damage because all of the input seismic energy is dissipated by the friction dampers.

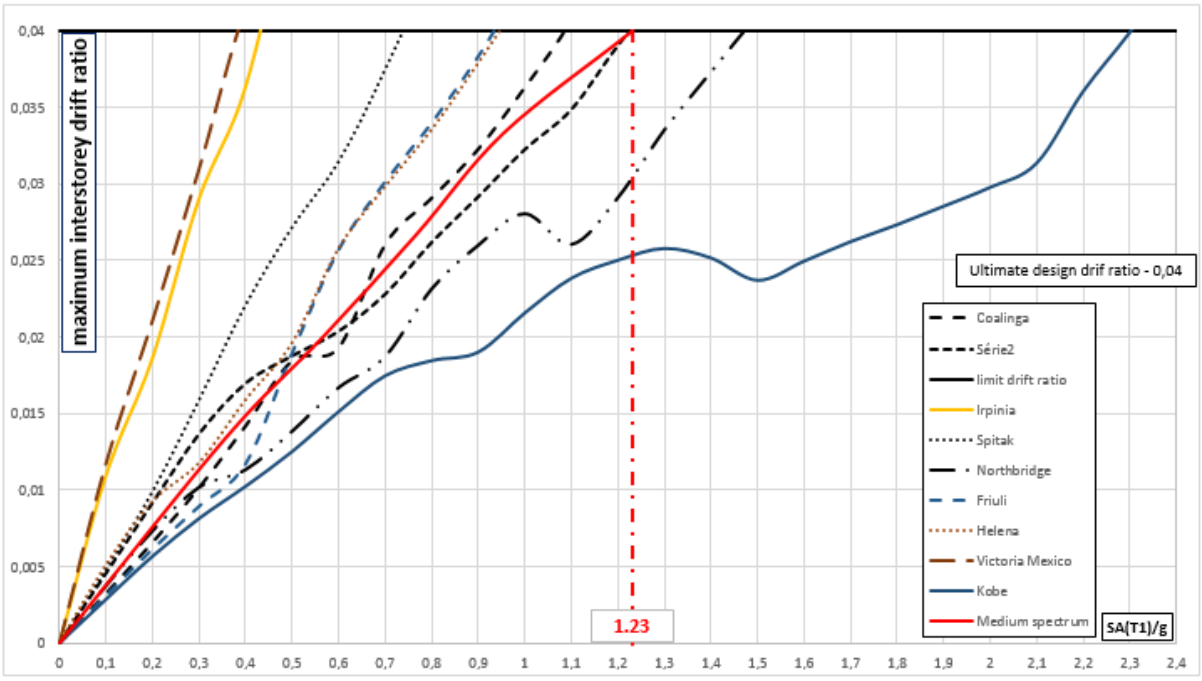

Figure 5.5- Maximum interstorey drift ratio vs spectral acceleration [for the specimen TSJ-H-SA300-260-CYC13]

5.2.2. IDA analyses for the MRF with the specimen TSJ-SA300-320-CYC12

Similarly to the MRF with the specimen TSJ-SA300-260-CYC13, the eigenvalue analysis carried out by the *SeismoStruct* showed that the fundamental period of the structure is 1.37s. In Table 5-2 is reported the main data for the accelerograms selected. In Figure 5.6 is showed the response spectra of the considered earthquakes. Once again, it can be observed that the different spectra have the same spectral acceleration [$Sa(T_1)=3m/s^2$] at the fundamental period of the structure.

The typology of this specimen is the one that have been reported in the Figure 3.8 of the sub-chapter 3.2. Concerning its typology, the design ultimate stroke has been assumed equal to 0.013m, since the design rotation is 0.04rad and lever arm of the beam is equal to 330mm. The hysteric behaviour of this specimen is the one present in Figure 4.18 of the subchapter 4.4.

Table 5-2-Accelerograms data [for the specimen TSJ-SA300-320-CYC12]

Earthquake	Date	Component	PGA (g)	Length [s]	Sa (T1=1,4s)
Helena	31-10-1935	N-S	0,15	39,99	0,028
Friuli	15-09-1976	N-S	0,11	26,39	0,103
Imperial Valley	15-10-1979	N-S	0,37	28,35	0,268
Irpinia	23-11-1980	N-S	0,13	35,80	0,212
Victoria Mexico	09-06-1980	N-S	0,15	26,91	0,237
Coalinga	02-05-1983	N-S	0,17	29,99	0,154
Spitak America	12-07-1988	N-S	0,20	19,89	0,136
Northridge	17-01-1994	N-S	0,23	39,99	0,159
Kobe	16-01-1995	N-S	0,25	40,95	0,185

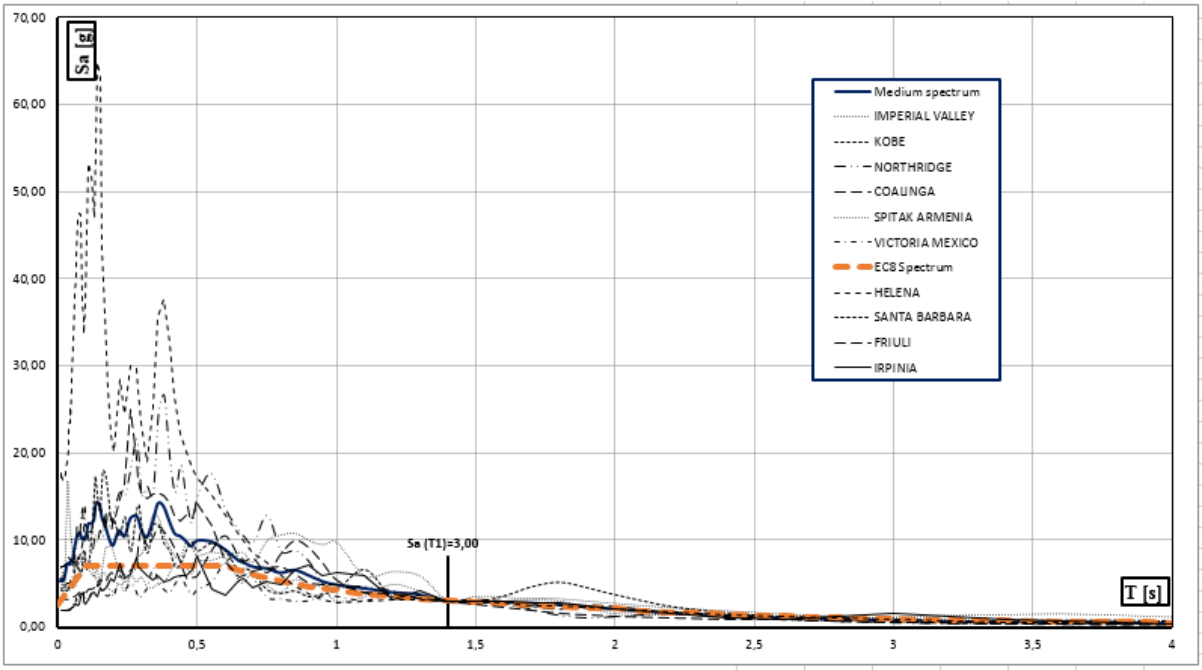

Figure 5.6-Response spectra for the considered ground motion [for the specimen TSJ- SA300-320-CYC12]

In Figure 5.7 is reported the required damper stroke versus the spectral acceleration for the friction dampers in the beam-to-column connections. In this case, the calibration of the friction dampers allows the structure to withstand spectral acceleration with ranging values between 0.4g to 2.4g, depending on the ground motion. In addition, for the average spectrum the friction damper stroke is reached for a spectral acceleration of 1.27g, i.e, approximately 4.15 times greater than the spectral acceleration given by the seismic code for the fundamental period (T_1 =3m/s^2).

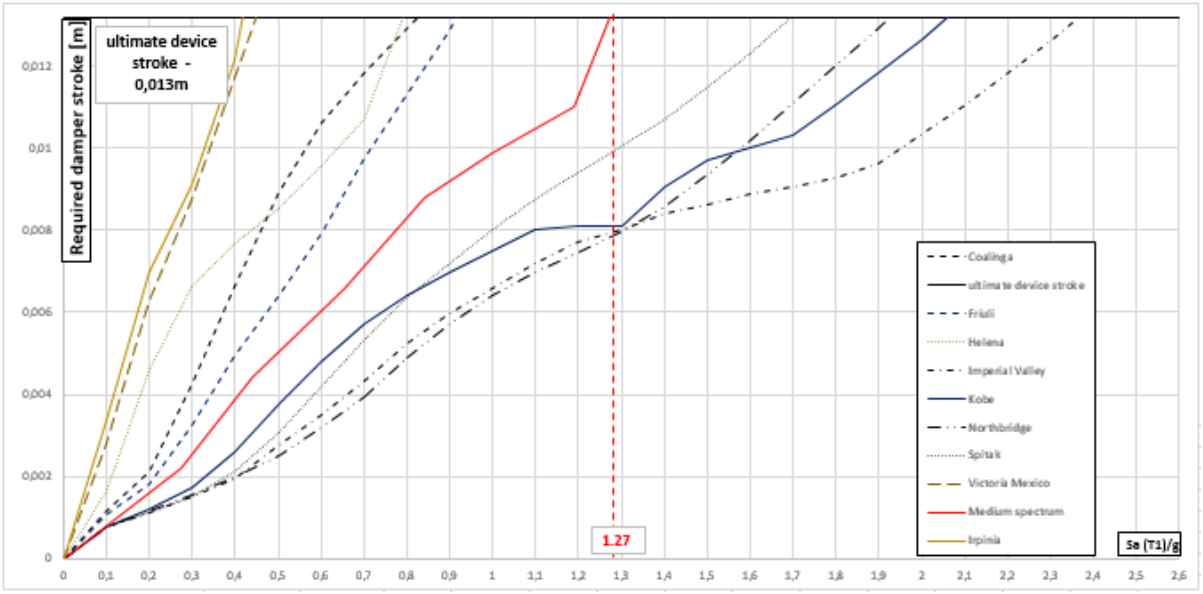

Figure 5.7-Required damper stroke vs spectral acceleration for the friction damper in beam-to-column connections [for the specimen TSJ- SA300-320-CYC12]

In Figure 5.8 is reported the maximum interstorey drift ratio versus the spectral acceleration, for the structure with the adopted specimen. From the graph, it can be seen that the ultimate design drift ratio (0.04 rad) is achieved for a spectral acceleration equal to 1.23g.

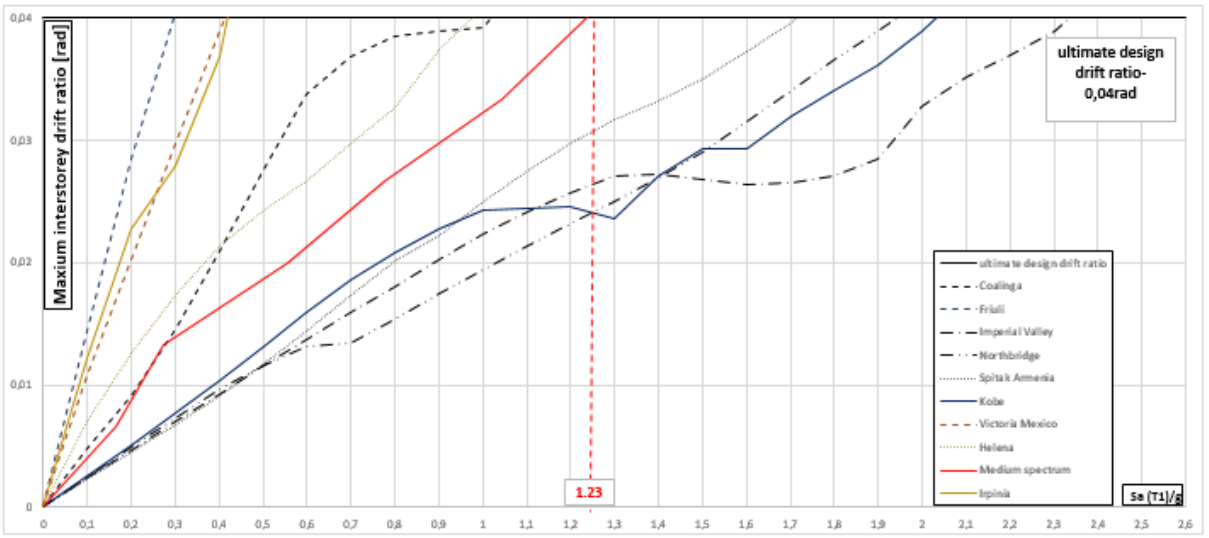

Figure 5.8-Maximum interstorey drift ratio vs spectral acceleration [for the specimen TSJ-SA300-320-CYC12]

From the results showed in Figure 5.7 and Figure 5.8, it is clear that the adopted structure have a good behaviour under high spectral accelerations due to the friction dampers dissipated all the seismic input energy, protecting the structure from collapsing. Moreover, in view of the requirements of seismic code (CEN 2010b) concerning the drift limits and spectral acceleration required, it is plain that the analysed structure has a higher capacity than the required by the seismic code.

5.2.3. IDA analyses for the MRF with the specimen TS-M2-460-CYC09

An eigenvalue analysis has been carried out with the *SeismoStruct* on the MRF with the analysed specimen. This analysis showed that the fundamental period of the structure is equal to 1.3s. In the Table 5-3and Figure 5.9 is reported the main data of the selected accelerograms and its response spectra as well as the response spectra of the medium spectrum and the elastic spectrum given by EC8. In Figure 5.9 is also possible to observed that, in the same as for the other specimens, the response spectra of the considered ground motion have been scale in order to present a similar behaviour than the spectra given by the EC8 around the fundamental period of the structure.

Table 5-3-Accelerograms data [for the specimen TS-M2-460-CYC09]

Earthquake	Date	Component	PGA (g)	Length [s]	Sa (T1=1,3s)
Helena	31-10-1935	N-S	0,15	39,99	0,028
Friuli	15-09-1976	N-S	0,11	26,39	0,093
Santa Barbara	08/13/1978	N-S	0,10	12,57	0,104
Imperial Valley	15-10-1979	N-S	0,37	28,35	0,367
Irpinia	23-11-1980	N-S	0,13	35,8	0,298
Victoria Mexico	09-06-1980	N-S	0,15	26,91	0,288
Coalinga	02-05-1983	N-S	0,17	29,99	0,171
Spitak America	12-07-1988	N-S	0,20	19,89	0,265
Northridge	17-01-1994	N-S	0,23	39,9	0,172
Kobe	16-01-1995	N-S	0,25	40,95	0,179

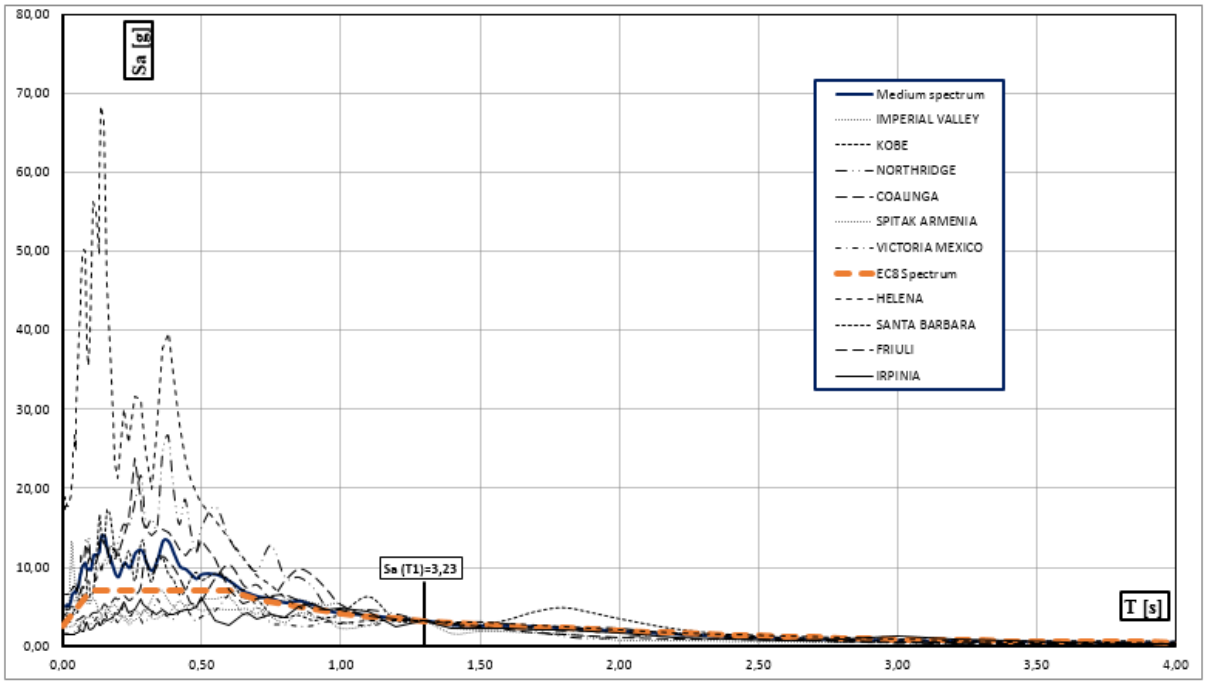

Figure 5.9-Response spectra for the considered ground motion [for the specimen TS-M2-460-CYC09]

The typology of the beam-to-column connection is the one described in the sub-chapter 3.2 in Figure 3.10, so the ultimate design stroke in this case is 0.013m (0.04x330mm). Concerning the hysteretic behaviour of the specimen, is the one reported in of the sub-chapter 4.4.

In Figure 5.10 is reported the required damper stroke versus the spectral acceleration for the friction damper in the beam-to-columns connections. As can been seen, the structure has the ability to withstand spectral acceleration in a range between 0.3g and 1.85g, depending on the ground motion, without collapsing due to the calibration of the friction dampers. Furthermore, for the medium spectrum the ultimate device stroke of the friction damper is achieved for a spectral acceleration of 1.13g, approximately 3.4 times greater than the spectral acceleration given by the EC8-1 for the fundamental period.

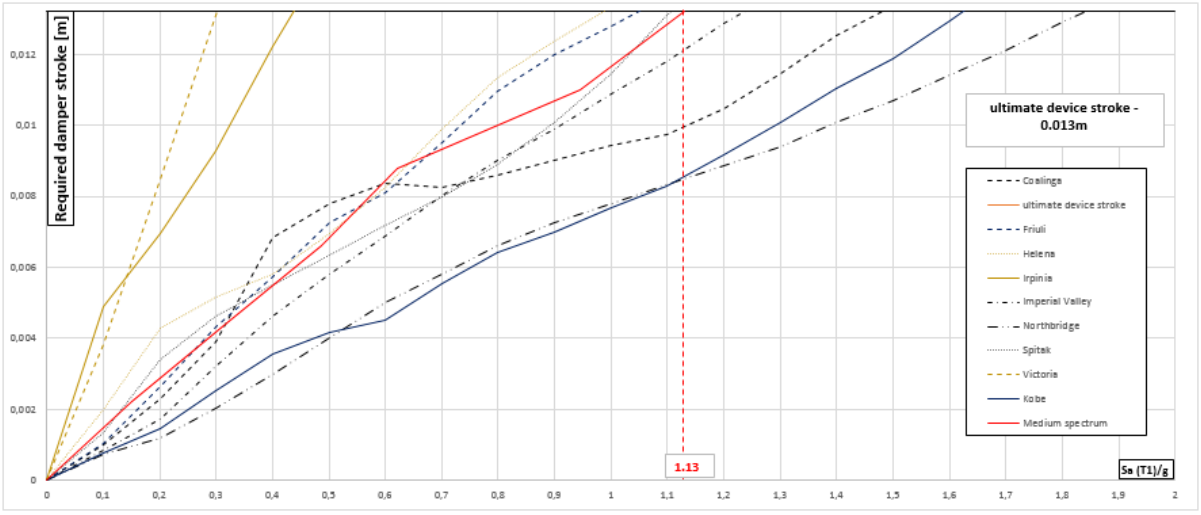

Figure 5.10-Required damper stroke vs spectral acceleration for the friction damper in beam-to-column connections [for the specimen TS-M2-460-CYC09]

Concerning the maximum interstorey drift ratio, reported in Figure 5.11, is achieved in the medium spectrum for a spectral acceleration equal to 1.19g.

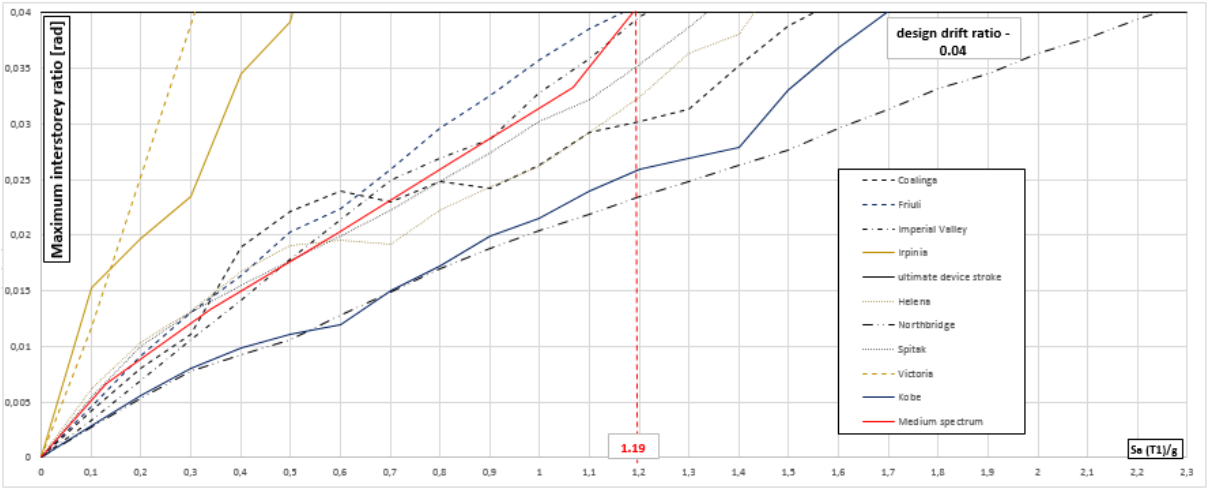

Figure 5.11-Maximum interstorey drift ratio vs spectral acceleration [for the specimen TS-M2-460-CYC09]

Both graphs shows that the structure has the ability to withstand high spectral accelerations without collapsing due to the dissipation of the seismic input energy by the friction dampers. In addition, similarly to the MRF with the other connections specimen, the structure shows a higher capacity when compared to the one required by the EC8-1 (CEN 2010b).

In addition, in view of what has been study on the subchapter 4.4.2, IDA analyses on the MRF with the modified friction joint with the M_2 damper were made for three of the earthquakes considered, *Irpinia*, *Victoria Mexico* and *Northbridge* earthquakes. Moreover, since the fundamental period of the MRF decreases from 1.3s to 1.2s, the response spectrums are no longer the one represented above in Figure 5.9 but the one reported in Figure 5.3.

In Table 5-4 is reported the results of the IDA analyses made for MRF with the considered specimen with the IPE270 and with an IPE 330.

Table 5-4- IDA results for the MRF with the specimen TS-M2-460-CYC09 with an IPE270 and an IPE330 for Irpinia, Victoria Mexico and Northbridge earthquakes

Earthquake	SA (T1)/g			
	damper stroke		*interstorey drift ratio*	
	TS-M2-460-CYC09	TS-M2-460-CYC09 [aprox. c/ IPE330]	TS-M2-460-CYC09	TS-M2-460-CYC09 [aprox. c/ IPE330]
Irpinia	0,44	0,74	0,5	0,76
Victoria Mexico	0,3	0,36	0,31	0,33
Northridge	1,83	1,84	2,24	1,87

First, concerning the achievement of the required damper stroke it is evident that for an increasing of the beam section the MRF can achieved higher spectral acceleration in particular, for the most conditioning earthquakes, the *Irpinia* and *Victoria Mexico*. In addition, the same happens for the achievement of the limit interstorey drift ratio. However, for the Northbridge earthquake the same does not happen what is explained by the fact that, by changing the fundamental period of the structure, in this case in particular, the spectral acceleration that the MRF are subjected have an increase around the 20% leading to an earlier achievement of the limit interstorey drift ratio. Furthermore, these results point out the dependence of results on the considered earthquakes and so, the importance of considered a various range of earthquakes in order to obtain more accurately results.

5.2.4. IDA analyses for the MRF with the specimen TS-M1-460-CYC 08

By carrying out an eigenvalue analysis on *SeismoStruct* on the MRF with the TS-M1-460-CYC 08 specimen, it has showed that the MRF presents a fundamental period equal to 1.6s. In Table 5-5 is reported the main data of the considered accelerograms.

Table 5-5 - Main data of the considered accelerograms [for the specimen TS-M1-460-CYC 08]

Earthquake	Date	Component	PGA (g)	Length [s]	Sa (T1=1,6s)
Helena	31-10-1935	N-S	0,15	39,99	0,02
Friuli	15-09-1976	N-S	0,11	26,39	0,14
Imperial Valley	15-10-1979	N-S	0,37	28,35	0,27
Irpinia	23-11-1980	N-S	0,13	35,80	0,21
Victoria Mexico	09-06-1980	N-S	0,15	26,91	0,22
Coalinga	02-05-1983	N-S	0,17	29,99	0,16
Spitak America	12-07-1988	N-S	0,20	19,89	0,16
Northridge	17-01-1994	N-S	0,23	39,90	0,14
Kobe	16-01-1995	N-S	0,25	40,95	0,22

Moreover, in Figure 5.12 is reported the spectrums of the considered accelerograms, the elastic spectrum given by the EC8-1 and the medium spectrum. It can also be observed that the response spectra of the considered ground motion present a similar behaviour than the spectra given by EC8 around the fundamental period of the structure.

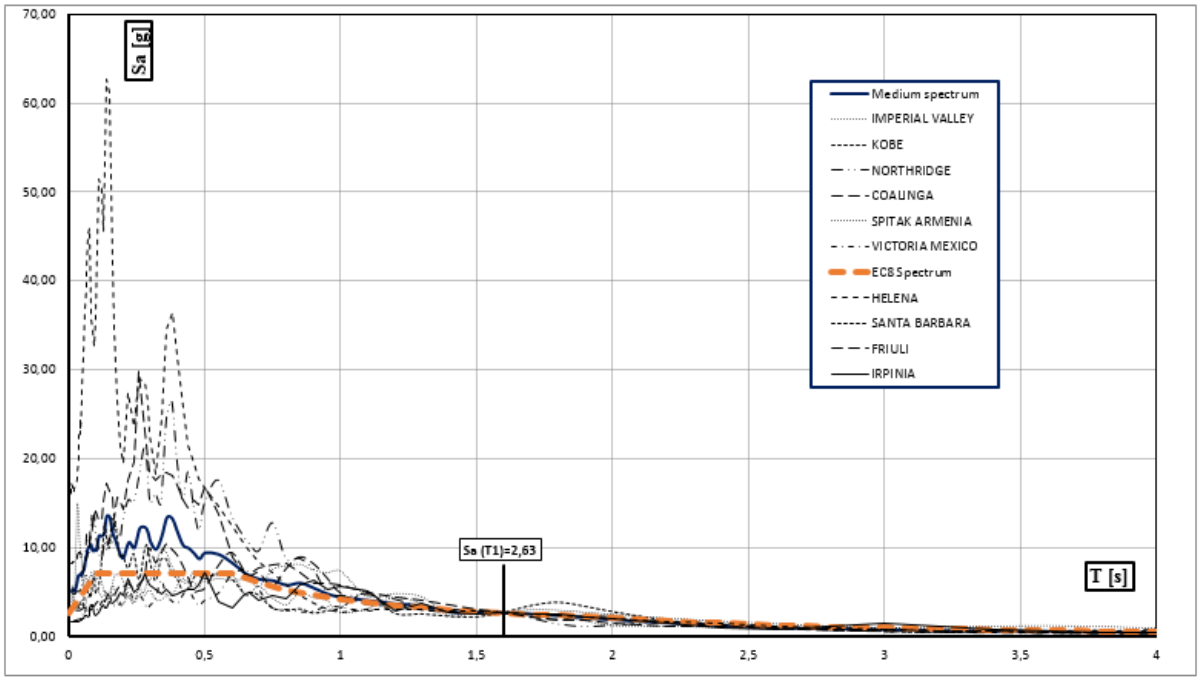

Figure 5.12- Response spectra for the considered ground motion [for the specimen TS-M1-460-CYC 08]

The typology of the beam-to-column connection is the one described in the sub-chapter 3.2 in Figure 3.10, so the ultimate design stroke in this case is 0.013m (0.04x330mm). Concerning the hysteretic behaviour of the specimen, is the one reported in Figure 4.14 of the sub-chapter 4.4.

In Figure 5.13 is reported the required damper stroke for the friction damper in the beam-to-column connections for a certain spectral acceleration. From the results, it is possible to see that this friction damper allows the structure to withstand values of the spectral acceleration between 0,3g to 1,5g, depending on the ground motion. Moreover, for the medium spectrum, the damper achieved the ultimate stroke for a spectral acceleration equal to 1.05g.

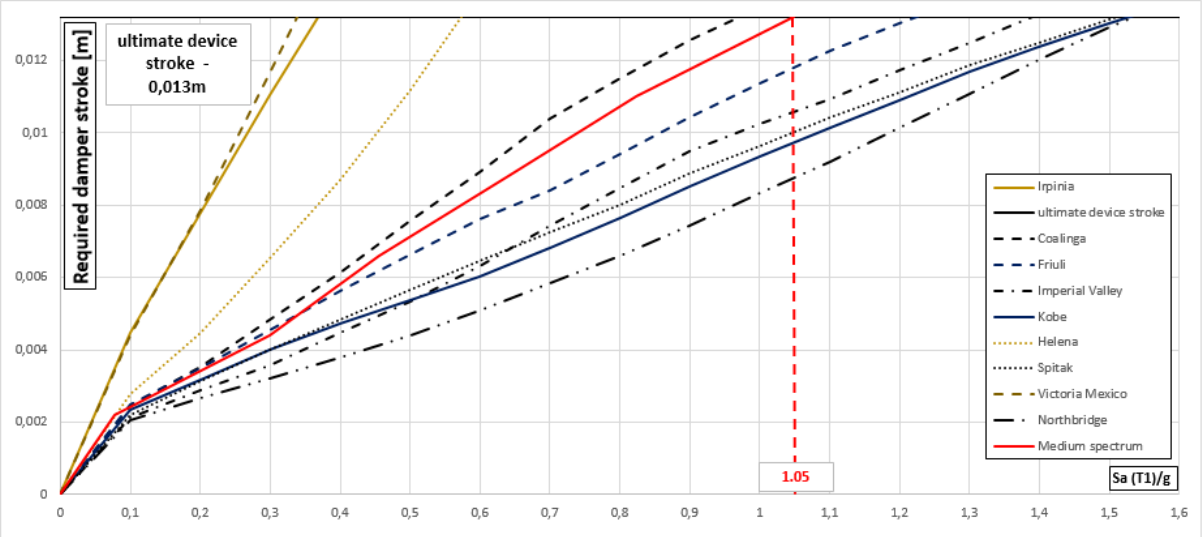

Figure 5.13-Required damper stroke vs spectral acceleration for the friction damper in beam-to-column connections [for the specimen TS-M1-460-CYC 08]

In Figure 5.14 is reported the maximum interstorey drift ratio, which is achieved concerning the medium spectrum, for a spectral acceleration equal to 1.37g.

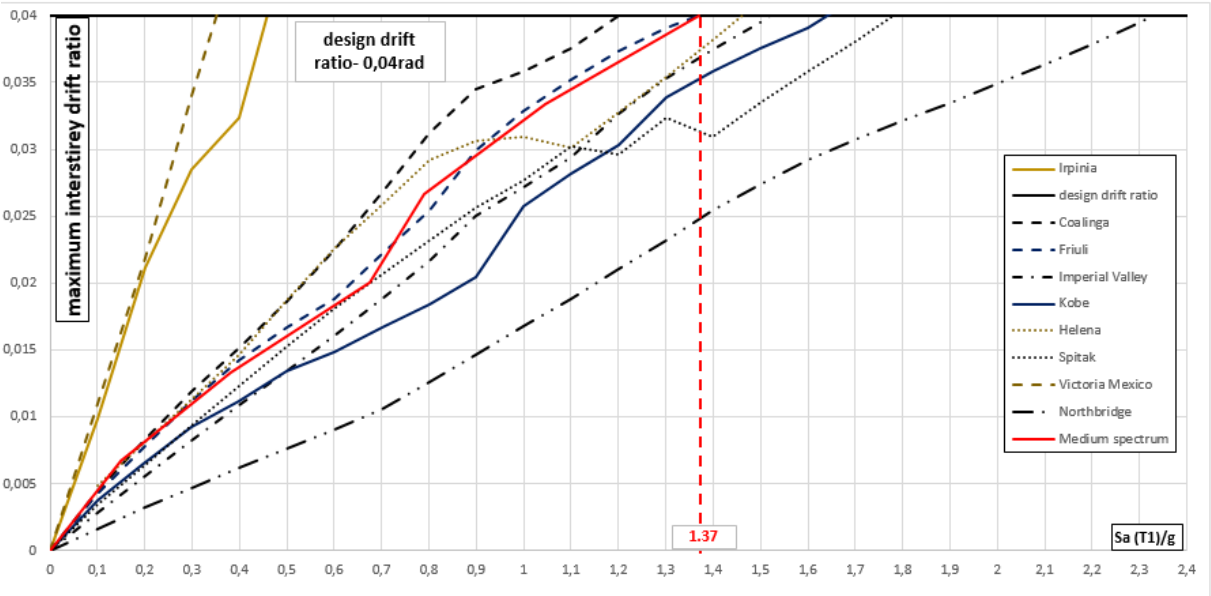

Figure 5.14-Maximum interstorey drift ratio vs spectral acceleration [for the specimen TS-M1-460-CYC 08]

5.2.5. IDA analyses for the MRF with EEP-DB-CYC03

By carrying out an eigenvalue analysis on *SeismoStruct* on the MRF with the EEP-DB-CYC03 specimen, it has showed that the MRF presents a fundamental period equal to 1.24s. In is reported the main data of the considered accelerograms.

Table 5-6-Main data of the considered accelerograms [for the specimen EEP-DB-CYC03]

Earthquake	Date	Component	PGA (g)	Length [s]	Sa (T1=1,2s)
Helena	31-10-1935	N-S	0,15	39,99	0,03
Friuli	15-09-1976	N-S	0,11	26,39	0,09
Imperial Valley	15-10-1979	N-S	0,37	28,35	0,44
Irpinia	23-11-1980	N-S	0,13	35,80	0,22
Victoria Mexico	09-06-1980	N-S	0,15	26,91	0,30
Coalinga	02-05-1983	N-S	0,17	29,99	0,20
Spitak America	12-07-1988	N-S	0,20	19,89	0,29
Northridge	17-01-1994	N-S	0,23	39,90	0,22
Kobe	16-01-1995	N-S	0,25	40,95	0,19

In Figure 5.15 is reported the response spectra of the considered ground motion, as well as the elastic spectra given by the EC8-1 and the medium spectrum. It is clear by observing the graph that the behaviour of the spectra of the considered ground motions have been scaled in order to have a similar behaviour around all have the same spectral acceleration at the fundamental period of the structure.

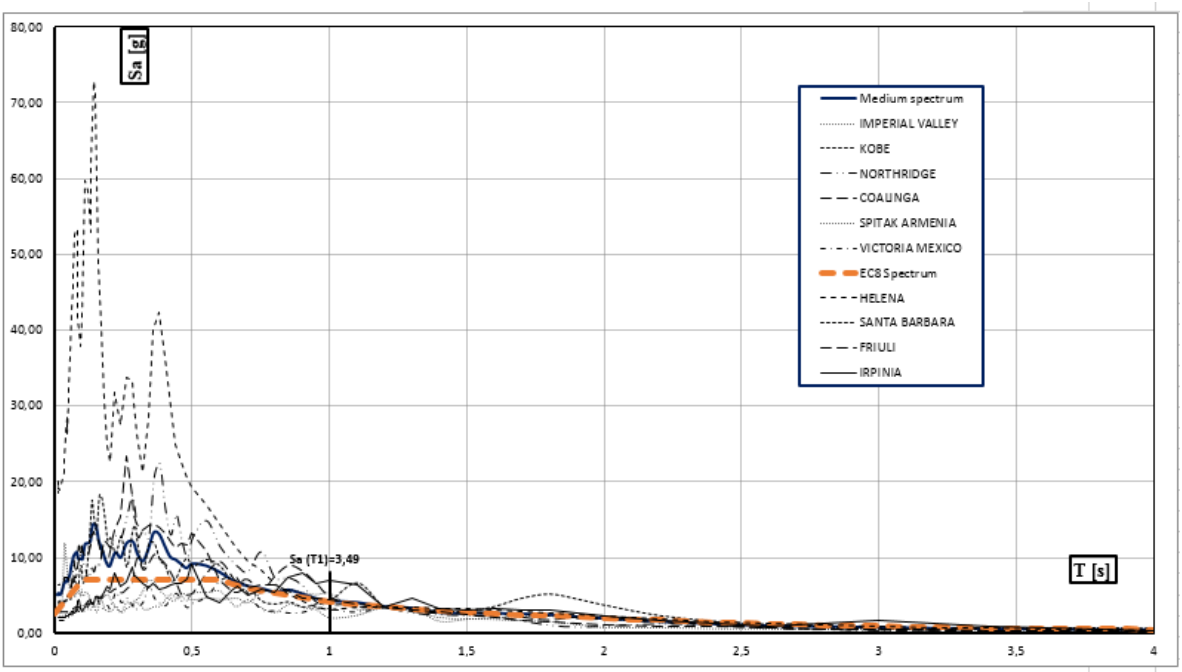

Figure 5.15-Response spectra for the considered ground motion [for the specimen EEP-DB-CYC03]

In this case, the beam-to-column connection is full strength so the IDA analyses have been stopped when at least one of the beam-to-column achieved the design ultimate plastic rotation (0.04 rad). The connection typology and it hysteretic behaviour is reported in the Figure 4.22 of the chapter 4.4.

In Figure 5.16 is reported the required ultimate plastic rotation for a certain spectral acceleration. The graph shows that the MRF with this full strength can withstand spectral accelerations for values between 0.3g to 1.8g, depending on the ground motion, and for the

medium spectra the ultimate rotation is achieved for a spectral acceleration equal to 1.05g. However, in this case, this is not possible without the damage of the beams ends, more specifically, in the dog bone area since it is the responsible for the energy dissipation.

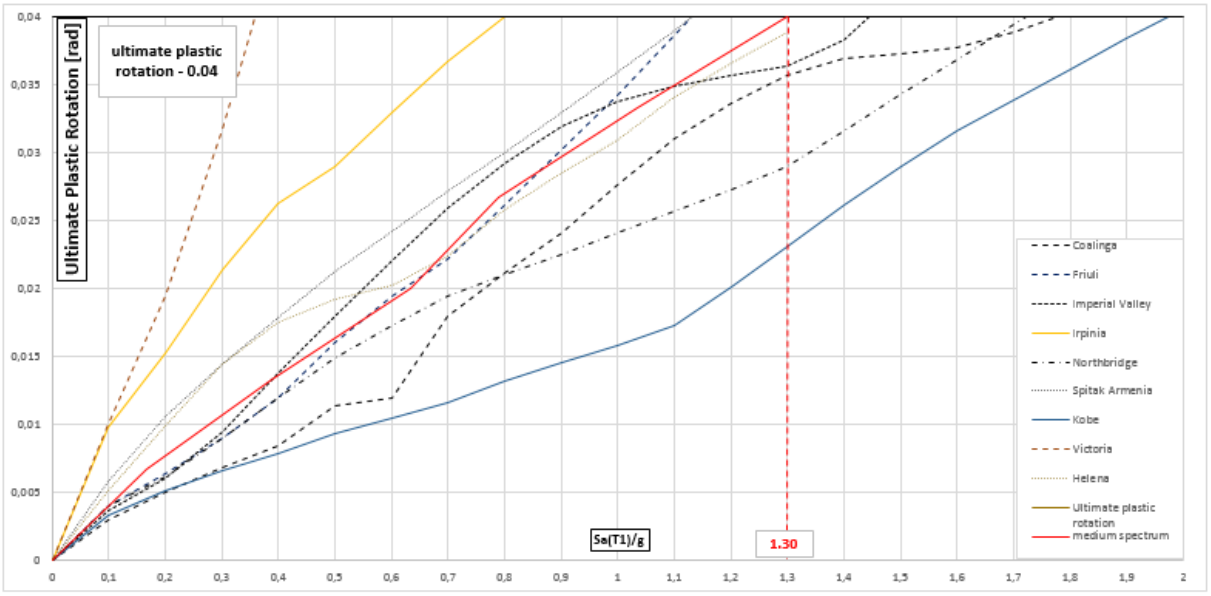

Figure 5.16-Ultimate plastic rotation vs spectral acceleration for the full strength beam-to-column connections [for the specimen EEP-DB-CYC03]

Regarding the maximum interstorey drift ratio, the MRF with this specimen achieved the maximum interstorey drift ratio for an average spectral acceleration equal to 1.15g. At this point it is evident that is the lowest value registered for all the IDA analyses made for the MRF with the different specimens.

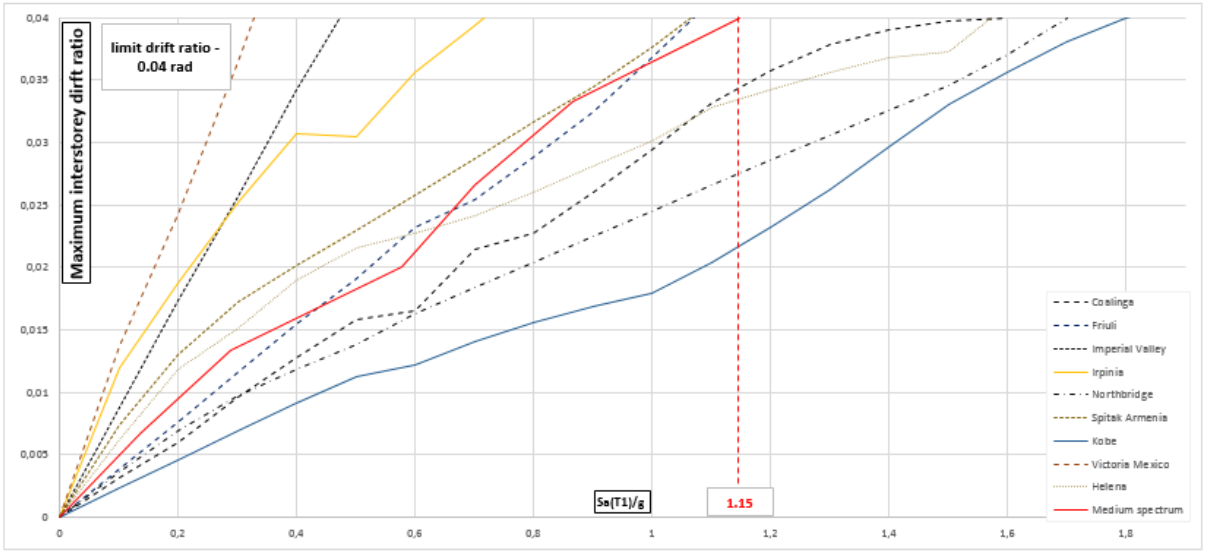

Figure 5.17-Maximum interstorey drift ratio vs spectral acceleration [for the specimen EEP-DB-CYC03]

6. Conclusions and further investigations

In this dissertation work, the influence of innovative beam-to-columns connections on the seismic behaviour of a steel MRF frame has been analysed. These innovative beam-to-column connections are constituted by friction dampers device at the beams flange or in an additional haunch welded to the beam that is responsible for the dissipation of the input seismic energy.

A rigours design procedure based on the second-order rigid plastic analysis has been adopted for the preliminary design of the steel MRF preventing not only the formation of soft storeys but also assuring the formation of a global collapse mechanism. Then, knowing the cyclic behaviour of the connections, the seismic behaviour of the MRF was analysed with each one of the selected connections. The seismic behaviour of the MRF has been made by means of a static nonlinear analysis (for validation of the design procedure and localization of the plastic hinges) and incremental dynamic analyses in order to see the amount of seismic input energy that the friction dampers are able to dissipate. The cyclic behaviour of the connections has been modelled by means of link elements in *SeismoStruct* with a smooth curve, whose parameters have been calibrated until obtaining a good agreement between experimental and modelled behaviour.

Furthermore, the behaviour of the MRF with the dissipative friction joints has been compared to the behaviour of the MRF with a full strength joint.

In the following tables (Table 6-1 and Table 6-2) are reported a summary of the IDA analyses that have been done in the chapter 5.2. In the first table (Table 6-1) is reported, for the MRF with each specimen, the spectra acceleration achieved when the beam-to-column connections have achieved the ultimate device stroke. In the second table (Table 6-2) is reported the spectra acceleration achieved when the structure reach the design drift ratio.

Table 6-1- Required ultimate damper stroke/plastic rotation for the MRF with all the considered specimens

Earthquake	SA (T1)/g *ultimate damper stroke*			
	TSJ-H-SA300-260-CYC13	TSJ-SA300-320-	TS-M2-460-CYC09	TS-M1-460-CYC 08
Helena	0,99	0,83	0,98	0,57
Friuli	0,98	0,92	1,05	1,22
Imperial Valley	1,67	2,37	1,24	1,39
Irpinia	0,45	0,42	0,44	0,37
Victoria Mexico	0,45	0,45	0,3	0,34
Coalinga	1,08	0,82	1,48	0,97
Spitak America	0,77	1,71	1,1	1,51
Northridge	1,57	1,93	1,83	1,54
Kobe	2,4	2,02	1,72	1,53
Medium spectrum	**1,15**	**1,27**	**1,13**	**1,05**

Table 6-2- Maximum interstorey drift ratio (MIDR) for the MRF with all the considered specimens

Earthquake	SA (T1)/g *interstorey drift ratio*				
	TSJ-H-SA300-260-CYC13	TSJ-SA300-320-CYC12	TS-M2-460-CYC09	TS-M1-460-CYC 08	EEP-DB-CYC03
Helena	0,95	0,97	1,43	1,4	1,57
Friuli	0,93	0,3	1,16	1,47	1,07
Imperial Valley	1,71	2,34	0,52	1,62	0,47
Irpinia	0,45	0,42	0,5	0,46	0,71
Victoria Mexico	1,15	0,41	0,31	0,35	0,33
Coalinga	1,08	1,02	1,49	1,2	1,6
Spitak America	1,06	1,72	1,33	1,78	1,06
Northridge	1,48	1,94	2,24	2,33	1,7
Kobe	2,3	2,03	1,69	1,64	1,8
Medium spectrum	**1,23**	**1,24**	**1,19**	**1,36**	**1,15**

Concerning the two specimens with the sprayed aluminium friction damper, the experimental results reported in the chapter 3 showed that the hysteretic behaviour of both specimens are very stable with no significant degradation or pinching. However, due to the additional haunch, the specimen *TSJ-H-SA300-260-CYC13* has a higher resistance, leading to a higher stiffness of the MRF since it has a fundamental period equal to 1.17s with the specimen *TSJ-H-SA300-260-CYC13* and a fundamental period equal to 1.36s with the specimen without the additional haunch.

Regarding the IDA results, the specimen *TSJ-H-SA300-260-CYC13* allows the structure to withstand spectral accelerations values between 0.45g and 2.4g and the specimen *TSJ-SA300-320-CYC12* values between 0.43g to 2g. Regarding the medium spectrum the MRF with the specimen *TSJ-H-SA300-260-CYC13* achieves the ultimate damper stroke a bit earlier than the MRF with the specimen *TSJ-SA300-320-CYC12*. However, this difference is not significant in terms of seismic behaviour of the MRF.

Furthermore, the IDA analyses regarding the maximum interstorey drift ratio, shows that the MRF with both specimens can withstand spectral acceleration between 0.4g to 2.3g and the achievement of the maximum interstorey drift ratio for the medium spectrum is achieved for the same spectral acceleration, 1.23g. Nevertheless it can not be neglected the fact that as the period of the MRF with the connection *TSJ-H-SA300-260-CYC13* is considerably higher than with the connection *TSJ-SA300-320-CYC12*, the spectral acceleration that the structure has been subjected has a higher value for the structure with the connection with the haunch than without it. In fact, this can explained the reason why the structure, even if more rigid, does not achieved the maximum interstorey drift ratio or the damper stroke device, for a higher spectral acceleration than the MRF with the connection without the haunch.

Regarding the specimen with the M_2 friction damper, the experimental results, reported in the chapter 3, showed that this specimen presents a stable hysteretic curves during the analysis, showing just a slight strength and stiffness degradation for high rotation amplitudes due to the consumption of the friction pads. None the less, the resistance of the connection is significantly lower when comparing with the resistance of the connections with the sprayed aluminium friction damper. This fact, as can be seen in the Table 6-1, leads to the achievement of the ultimate damper stroke for a lower spectral acceleration when compared to the specimens with the sprayed aluminium friction damper. In fact, the IDA curves showed that the calibration of the friction dampers allows the structure to withstand values of the spectral acceleration between 0.3g and 1.83g with a value of 1.13g for the medium spectrum, less than the ones

founded for the structure with the specimens with the sprayed aluminium friction damper. Concerning the maximum interstorey drift ratio (Table 6-2), the structure with this specimen achieved the maximum interstorey drift ratio for a spectral acceleration lower than for both the MRF with specimen *TSJ-H-SA300-260-CYC13* and the connection *TSJ-SA300-320-CYC12*.

The last connection with friction damper is the specimen *TS-M1-460-CYC 08*. Observing the IDA results for the MRF with this connection it is clear that, comparing to the other specimens, this one is the one that presents the worse behaviour. In particular, the calibration of the friction damper allows the structure withstand spectral acceleration between 0.3g and 1.8g and the medium spectrum registered a spectral acceleration equal to 1.05g when the ultimate device stroke is reached. However, when looking for the IDA results concerning the maximum interstorey drift ratio, it appears that the structure achieved the maximum interstorey drift ratio for the highest value between all the specimens. This happens because the spectral acceleration that the MRF with this specimen has been subject were the lowest of all the IDA analyses made for the MRF with the other specimens due to the fundamental period of the MRF with the *TS-M1-460-CYC 08* is much higher (T_1 = 1.6s) than the fundamental period of the structure with the others specimen. In others words, the structure with the connection *TS-M1-460-CYC 08* is significantly less affected by the seismic forces than the structure with the other connections and this is the reason why it can achieved the maximum interstorey drift ratio for a higher spectral acceleration.

Regarding the MRF with the full strength connection, it has been compared to the MRF with innovative connections by means of the achievement of the maximum interstorey drift ratio, showing that this connection allows the structure to withstand for a lower value of spectral acceleration. This is due to the fact that, in dissipative friction joints the rotational capacity of the joints can be designed for the required ultimate drift by calibrating the length of the bolted holes.

Regarding the different friction joints, the structure with both the specimen with sprayed aluminium friction damper, *TSJ-H-SA300-260-CYC13* and *TSJ-SA300-320-CYC12*, and the specimen *TS-M2-460-CYC 09* can withstand high spectral accelerations without damage any of the structural elements because all of the input energy is dissipated by the friction dampers. On the other hand, the structure with the *TS-M1-460-CYC 08* specimen presents the poorest behaviour of them all. In fact, this result meet the experimental results reported in chapter 3.2 concerning the connection with the rubber M_1.

In addition, the study made by "*scaling"* the connection with the friction damper M2 for a higher section of the beam showed that the increase of the beam section can also increase the resistance of the structure at a global scale. However, this study should have been made for more earthquakes and for the other friction joints by adopting a more criterions scaling process.

As a conclusion, both static and dynamic nonlinear analyses have confirmed the fulfilment of this dissertation work, the development of free from damage structures even for seismic events with high intensities, due to the ability of the friction dampers to dissipate the input seismic energy.

However, although without structural damage, after a seismic event permanent lateral displacements occurred. Therefore, the problem of re-centring the structure has to be

investigated in forthcomings researches on the subject of free from damages structures. In addition, also the non-structural components are not free from damage, which is a problem to be solved in furthers investigations.

REFERENCES

CEN, 2009. CEN.Eurocódigo1-Acções em estruturas Parte 1-1: Acções gerais.

CEN, 2010, 2010a. CEN. Eurocode 3: design of steel structures – Part 1–1: general rules and rules for buildings; 2005b.

CEN, 2010, 2010b. CEN. Eurocode 8: design of structures for earthquake resistance – Part 1: general rules, seismic actions and rules for buildings; 2005a.

En, N.P., 2009. CEN. Eurocode 0: Basis of strutural design.

En, N.P., 2010. CEN. Eurocode 3: design of steel structures – Part 1–8: design of joints; 2005c.

Gowda, K.K. & Kiran, K.K., 2013. Earthquake resistance of structures using dampers - a review. *International Journal of Advanced Structures and Geotechnical Engineering*, 02(01), pp.31–35.

Inoue, K. et al., 2006. Seismic-Resistant Weld-Free Steel Frame Buildings with Mechanical Joints and Hysteretic Dampers. *Journal of Structural Engineering*, 132(6), pp.864–872.

Kim, K.D. & Engelhardt, M.D., 2002. *Monotonic and cyclic loading models for panel zones in steel moment frames*,

Kishiki, S. et al., 2006. New Ductile Moment-Resisting Connections Limiting Damage To Specific Elements At the Bottom Flange. *Construction*, (852).

Latour, M., 2011. Experimental analysis of innovative dissipative bolted double split tee beam-to-column connections. , 4, pp.53–64.

Latour, M., Piluso, V. & Rizzano, G., 2014. Experimental analysis on friction materials for supplemental damping devices. *Construction and Building Materials*, Volume 65, pp.159–176.

Latour, M., Piluso, V. & Rizzano, G., 2015a. Free from damage beam-to-column joints: Testing and design of DST connections with friction pads. *Engineering Structures*, 85, pp.219–233.

Latour, M., Piluso, V. & Rizzano, G., 2015b. Free from damage beam-to-column joints: Testing and design of DST connections with friction pads. *Engineering Structures*, 85, pp.219–233. Available at: http://linkinghub.elsevier.com/retrieve/pii/S0141029614007603.

Latour, M., Piluso, V. & Rizzano, G., 2014. Friction joints equipped with sprayed aluminium dampers. *EUROSTEEL*.

Latour, M. & Rizzano, G., 2014. Experimental Analysis on the Cyclic Response of Beam to Column Joints : State-of-the-Art at Salerno University. , pp.227–247.

Mazzolani, F.M. & Piluso, V., 1997. Plastic Design of Seismic resistante steel Frames. *Journal of Earthquake Engineering*, 26(January 1996), pp.167–191.

Mountori, R., Nastri, El. & Piluso, V., 2015. Advances in theory of plastic mechanism control: closed form solution for MR-Frames. *Earthquake Engineering & Structural Dynamics*, 44(October 2014), pp.1035–1054.

Mualla, I. & Nielsen, L.O., Enhanced response through supplementary friction damper devices. *Civil Engineering*.

Mualla, I.H. & Belev, B., 2002. Performance of steel frames with a new friction damper device under earthquake excitation. *Engineering Structures*, 24, pp.365–371.

Oh, S.-H., Kim, Y.-J. & Ryu, H.-S., 2009. Seismic performance of steel structures with slit dampers. *Engineering Structures*, 31(9), pp.1997–2008.

Piluso, V., Montuori, R. & Troisi, M., 2014. Innovative structural details in MR-frames for free from damage structures. *Mechanics Research Communications*, 58, pp.146–156.

Seismosoft, 2014. SeismoStruct v7.0 – A computer program for static and dynamic nonlinear analysis of framed structures.

Sivaselvan, M. V. & Reinhorn, A.M., 2000. Hysteretic Models for Deteriorating Inelastic Structures. *Journal of Engineering Mechanics*, 126(June), pp.633–640.

Symans, M.D. & Constantinou, M.C., 1999. Semi-active control systems for seismic protection of structures: a state-of-the-art review. *Engineering Structures*, 21, pp.469–487.

Yeung, S. et al., 2013. Sliding shear capacities of the Asymmetric Friction Connection. , 1997, pp.1–9.